博士論文

Theoretical Studies on the Cosmological Problems via the Electroweak Symmetry Breaking

電弱対称性の自発的破れによる宇宙論的諸問題の研究

Toshinori Matsui [1]

Department of Physics, University of Toyama,
3190 Gofuku, Toyama 930-8555, Japan

富山大学大学院理工学教育部新エネルギー科学専攻

理論物理学研究室

[1]E-mail: matsui@jodo.sci.u-toyama.ac.jp

ACKNOWLEDGMENTS

I would like to express my sincere gratitude to my supervisor, Prof. Shinya Kanemura for providing me much instruction in particle physics and its philosophy. I am very grateful to Prof. Mitsuru Kakizaki, Dr. Hiroaki Sugiyama, Dr. Takehiro Nabeshimai and Mr. Norihito Mok for the fruitful collaborations. I am also grateful to the other faculty members of the laboratory, Prof. Takeshi Kurimoto for useful discussions. I would like to thank Prof. Kazunori Kohri, Prof. Yoshiki Moriwaki and Prof. Takashi Tayama for careful reading of this thesis. Special thanks are also given to the secretary of our group, Ms. Asami Takagi for her kind cooperations and helps. I would also like to thank all the members in my laboratory, Dr. Makoto Nakamura, Dr. Hiroshi Yokoya, Dr. Kei Yagyu, Mr. Hiroyuki Taniguchi, Ms. Mariko Kikuchi, Mr. Naoki Machida, Mr. Akiteru Santa, Mr. Ryo Amai, Mr. Katsuya Hashino, Mr. Shota Nakatani, Mr. Shinya Odori, Mr. Kodai Sakurai, Mr. Yoshiaki Ishigure and Mr. Koichi Ishida for their hospitality.

Abstract

The standard model of particle physics (SM) consists of two important pillars; i.e., the gauge principle and the electroweak symmetry breaking. The SM have been established by the discoveries of the weak gauge bosons in 1980s and the Higgs boson in 2012. However, still we cannot explain the phenomena such as dark matter (DM), neutrino oscillation, cosmic inflation and baryon asymmetry of the Universe (BAU), etc. These problems must be solved by new physics beyond the SM.

On the other hand, the SM has the minimal Higgs sector with one doublet field, though there is no principle to explain such a shape of the Higgs sector. The new physics may be described by introducing an extended Higgs sector. In this case, by exploring the Higgs sector, it is possible to approach not only the nature of electroweak symmetry breaking but also new physics. As the experiment at CERN Large Hadron Collider (LHC) is running today, it has become an urgent task to study Higgs physics.

In this thesis, we focus on the possibility that Higgs physics is related to the cosmological problems. In addition to current and future collider experiments, we consider testability of some Higgs-related new physics scenarios by using various space experiments such as observation of gravitational waves, observation of the cosmic microwave background, direct detection of DM, etc. This thesis consists of the following three subjects.

In Part III, we discuss two new physics models with extended Higgs sectors, which can explain tiny neutrino masses and DM at the same time at the TeV scale. We call these models as "radiative seesaw" models. In radiative seesaw models, a new symmetry imposed to the model forbids generating neutrino masses at the tree level and explains the stability of DM. First, we study the scalar sector of the neutrinophilic two Higgs doublet model (νTHDM), where the neutrinophilic scalar doublet has a small vacuum expectation value (VEV) v_ν and give Dirac masses of neutrinos. We consider a possibility that we can explain naturally small masses of neutrinos by the idea that a small v_ν is generated at the higher order of perturbation. In addition to right-handed neutrinos ν_{iR} and the second $\mathrm{SU}(2)_L$-doublet scalar field Φ_ν which exist in the original νTHDM, we introduce scalars (η and s_2^0) which do not have VEVs and a scalar s_1^0, and we impose the global $\mathrm{U}(1)_X$ symmetry. Although the global $\mathrm{U}(1)_X$ symmetry imposed to the model is broken spontaneously by a new VEV of the singlet field s_1^0, there remains a residual Z_2 symmetry. The lightest Z_2-odd scalar boson in the model can be a dark matter candidate. We clarify that our model can explain neutrino data and DM data. We briefly discuss a possible signature of our model at the LHC.

Second, we consider a radiative seesaw model where the Dirac mass term for neutrinos, the Majorana mass term for right-handed neutrinos, and the other new fermion masses arise via the spontaneous breakdown of the $\mathrm{U}(1)_{\mathrm{B-L}}$ gauge symmetry. We propose the scenario which is an improved version of the previous work from the view point of the anomaly cancellation. With appropriate $\mathrm{U}(1)_{\mathrm{B-L}}$ charge assignments, there exists an unbroken global U(1) symmetry even after spontaneous breaking of the $\mathrm{U}(1)_{\mathrm{B-L}}$ symmetry. The global U(1) symmetry stabilizes the DM, so that we hereafter call it $\mathrm{U}(1)_{\mathrm{DM}}$. The Dirac mass term of neutrinos is radiatively generated at the one-loop level due to the quantum effect of the new particles. Tiny neutrino masses are then explained by the two-loop diagrams with a Type-I-Seesaw-like mechanism. We find that the model can satisfy current data from the neutrino oscillation, the lepton flavor violation, the relic abundance and the direct search for the DM, and the LHC experiment.

In Part IV, we investigate a simple model to explain inflation, neutrino masses and DM simultaneously. We propose a Higgs inflation scenario in a radiative seesaw model with an inert doublet, which originally has been proposed to explain dark matter and neutrino masses. We study the possibility that the Higgs boson as well as neutral components of the Z_2-odd scalar doublet field can satisfy conditions from slow-roll inflation and vacuum stability up to the inflation scale. We study this model under the constraints from the current data, and find parameter regions where additional scalar bosons can play a role of inflatons. They satisfy the current data from neutrino experiments, the dark matter searches and also from LEP and LHC. A unique phenomenological prediction appears in the mass spectrum of inert scalar bosons. We show that this scenario is challenging to be tested at the LHC, but would be well testable at the International Liner Collider by measuring endpoints of energy distribution of a two jet system from decay processes of the inert scalar fields produced via pair production.

In Part V, we discuss spectra of gravitational waves which are originated by the strongly first order phase transition at the electroweak symmetry breaking, which is required for a successful scenario of electroweak baryogenesis. Such spectra are numerically evaluated without high temperature expansion in a set of extended scalar sectors with additional N isospin-singlet fields as a concrete example of renormalizable theories. We find that the produced gravitational waves can be significant, so that they are detectable at future gravitational wave interferometers such as DECIGO and BBO. Furthermore, since the spectra strongly depend on N and the mass of the singlet fields, our results indicate that future detailed observation of gravitational waves can be in general a useful probe of extended scalar sectors with the first order phase transition.

Contents

Part I

Introduction

Overview

In July 2012, the new particle was discovered at the LHC [1, 2]. It is consistent with the Higgs boson of the standard model of particle physics (SM) within the error. However, we cannot explain dark matter (DM) [3, 4], neutrino oscillation [5–13], cosmic inflation [14] and baryon asymmetry of the Universe (BAU) [3, 4, 15, 16]. To solve these problems, we need a new physics model beyond the SM.

On the other hand, the SM has the minimal Higgs sector with one doublet field, though there is no principle to explain such a shape of the Higgs sector. The new physics may be described by introducing an extended Higgs sector. In this case, by exploring the Higgs sector, it is possible to approach not only the nature of electroweak symmetry breaking but also new physics. In this thesis, we focus on the possibility that Higgs physics is related to the cosmological problems.

One of the valuable scenario which can explain DM is known as weakly interactive massive particle (WIMP). In this scenario, typical scale of DM mass is required $\mathcal{O}(100)$GeV. Because collider experiments explore such scale, WIMP scenario is known for testable. This scale is also the scale which explained by Higgs physics.

Standard cosmology is very successful to explain the observations. Additionally, to solve horizon problem and flatness problem, we need to explain cosmic inflation [14] by introducing scalar boson so-called inflaton [17]. The paper [18] proposed the model which the Higgs boson works as an inflaton by introducing the non-minimal coupling ξ so-called Higgs inflation. The advantage of Higgs inflation is testability via Higgs physics. Cosmic microwave background (CMB) observation [4] shows us the scenario of Higgs inflation is not excluded.

Among various scenarios of BAU, electroweak baryogenesis (EWBG) [19] is directly connected with physics of the Higgs sector, requiring a strongly first order phase transition (1stOPT) at the electroweak symmetry breaking (EWSB) and also additional CP violating phases. It is known that new physics beyond the SM is necessary for EWBG. Such a scenario can be tested by experimental determination of the property of the Higgs sector. For instance, the condition of the strongly 1stOPT can predict a significant deviation (order of several tens percent) in the triple Higgs boson coupling (the hhh coupling) from the SM prediction [20], and the required CP violating phases lead to appearance of electric dipole moments, etc. At the LHC experiment and its high luminosity one, the measurement of the hhh coupling seems to be challenging. There is still a hope that in future the hhh coupling could be measured by 13% accuracy [21] at the upgraded version of the International Linear Collider (ILC).

As the experiment at CERN Large Hadron Collider (LHC) is running today, it has become an urgent task to study Higgs physics. In addition to current and future collider experiments, we consider some Higgs-related new physics scenarios by using various space experiments such as observation of gravitational waves, observation of the cosmic microwave background, direct detection of DM, etc.

Solving neutrino mass problem in radiative seesaw models

In order to generate tiny masses of neutrinos, various kinds of models have been proposed. The simplest scenario is so called the seesaw mechanism, where the tiny neutrino masses are generated at the tree level by introducing very heavy particles, such as right-handed neutrinos [22], a complex triplet scalar field [23], or a complex triplet fermion field [24]. There are new physics models with extended Higgs sectors, which can explain tiny neutrino masses and

DM at the same time at the TeV scale, so-called "radiative seesaw" models. In radiative seesaw models, a new symmetry imposed to the model forbids generating neutrino masses at the tree level and explains the stability of DM [25–27]. Such radiative seesaw models are explained by multi-Higgs structure.

We can constrain radiative seesaw models by using experimental data from the neutrino oscillation, the lepton flavor violation, the relic abundance and the direct search for the DM, and the LHC experiment. Furthermore, we can derive predictions of models.

Higgs inflation and a radiative seesaw model

There are some theoretical problems in the simplest Higgs inflation model. When we calculate the running coupling constant of the Higgs self-coupling, the critical energy scale is around 10^{10} GeV due to the contribution of the top quark [28]. The vacuum is difficult to be stable up to the inflation scale $\Lambda_{\rm I}$. This problem can be solved in two Higgs doublet models [29], because the loop effect of additional scalar bosons weakens the top-loop contribution in the running coupling constants [30]. Perturbative unitarity is also violated at the energy scale $\Lambda_{\rm U} = \frac{M_P}{\xi}$ by the Higgs-gauge scattering processes [31]. This problem is solved by a heavy additional real singlet scalar boson which does not interact with gauge fields as shown by [32].

On the other hand, such Higgs inflation models with extended Higgs sector are also testable. Because we can obtain the prediction for mass spectrum at the TeV scale by analyzing the renormalization group equations of running coupling constants which satisfying data of CMB observation. The prediction at the TeV scale would be testable at current and future collider experiments.

Gravitational waves from electroweak phase transition

As a possible alternative method to test the strongly 1stOPT, we may be able to utilize future observation of gravitational waves (GWs) [33]. On February 11th, the first direct detection of GWs emitted by the merger of black holes at Advanced LIGO [34] was reported [35]. Furthermore, a number of observatories such as KAGRA [36], Advanced VIRGO [37] are trying to detect them. The target frequencies of GWs correspond to those from astronomical phenomena such as the binary of neutron stars, black holes, etc. Once the GWs will be detected in the near future, the era of GW astronomy will come true. Spectroscopy of GWs will make it possible to explore phenomena at the very early stage of the Universe, such as a strongly 1stOPT, cosmic inflation, topological defects like cosmic strings, domain wall, etc.

GWs originated from the strongly 1stOPT have been discussed in a model independent way in Refs. [33, 38–45]. In the effective theory approach with higher order operators the possibility of detecting such GWs was studied by Delaunay et al. [46]. Apreda et al. evaluated spectra of GWs from the strongly 1stOPT due to thermal loop effects in the minimal supersymmetric SM (MSSM) [47], although such a scenario was already excluded by the LHC data. Espinosa et al. studied spectra of GWs in extended scalar sectors with the $O(N)$ symmetry [48, 49]. GWs from the non-thermal 1stOPT were investigated in singlet extensions of the SM [50] and the MSSM [47] and in the left-right symmetric model [51].

Organization

This thesis is organized as follows. In Part II, we first review about the Higgs physics in the SM, and problems in the SM. We then discuss phenomena of DM, neutrino oscillation, cosmic

inflation and BAU. In Part III, we discuss radiative seesaw models that can explain tiny neutrino masses and DM at the same time. In Part IV, we investigate a model to explain inflation in a framework of radiative seesaw model. In Part V, we discuss spectra of gravitational waves which are originated by the strongly first order phase transition at the electroweak symmetry breaking, which is required for a successful scenario of electroweak baryogenesis. We show that future detailed observation of gravitational waves can be in general a useful probe of extended scalar sectors with the first order phase transition.

Part II

Beyond the standard model phenomena

Chapter 1

Higgs physics in the standard model

In this chapter, we review the SM. In particular, we focus on the Higgs sector in the SM. We first discuss how all the masses of the SM particles are generated. Second, the bounds of the Higgs boson mass are discussed. Third, how to calculate the decay rates of the Higgs boson is shown. Finally, the production of the Higgs boson at LHC is shown.

1.1 The standard model

After the spontaneous breaking of the $SU(2)_L \times U(1)_Y$ gauge symmetry, the Higgs boson, weak gauge bosons and fermions obtain their masses in the Higgs potential, the kinetic term of the Higgs doublet field and the Yukawa interactions, respectively. The charge assignments for the SM particles under the $SU(3)_c \times SU(2)_L \times U(1)_Y$ gauge symmetry is shown in Fig. 1.1. The Lagrangian of the standard model is given by

$$\mathscr{L}_{SM} = \mathscr{L}_{\rm YM} + \mathscr{L}_{\rm f} + \mathscr{L}_{\rm Higgs} + \mathscr{L}_{\rm Y}. \tag{1.1}$$

1.1.1 The Yang-Mills sector

The Lagrangian of a gauge-invariant kinetic energy term for G^α_ν ($\alpha = 1-8$), W^a_ν ($a = 1-3$) and B_ν is

$$\mathscr{L}_{\rm YM} = -\frac{1}{4} G^\alpha_{\mu\nu} G^{\mu\nu}_\alpha - \frac{1}{4} W^a_{\mu\nu} W^{\mu\nu}_a - \frac{1}{4} B_{\mu\nu} B^{\mu\nu}, \tag{1.2}$$

where

$$G^\alpha_{\mu\nu} = \partial_\mu G^\alpha_\nu - \partial_\nu G^\alpha_\mu - g_s f_{\alpha\beta\gamma} G^\beta_\mu G^\gamma_\nu, \tag{1.3}$$
$$W^a_{\mu\nu} = \partial_\mu W^a_\nu - \partial_\nu W^a_\mu - g \varepsilon_{abc} W^b_\mu W^c_\nu, \tag{1.4}$$
$$B_{\mu\nu} = \partial_\mu B_\nu - \partial_\nu B_\mu. \tag{1.5}$$

	Q_{iL}	u_{iR}	d_{iR}	L_{iL}	ℓ_{iR}	Φ
$\mathrm{SU(3)_C}$	**3**	**3**	**3**	**1**	**1**	**1**
$\mathrm{SU(2)_L}$	**2**	**1**	**1**	**2**	**1**	**2**
$\mathrm{U(1)_Y}$	$\frac{1}{6}$	$\frac{2}{3}$	$-\frac{1}{3}$	$-\frac{1}{2}$	-1	$\frac{1}{2}$

Table 1.1: Particle contents and its charge assignments in the SM.

We define G^α_ν, W^a_ν and B_ν as $\mathrm{SU(3)_C}$, $\mathrm{SU(2)_I}$ and $\mathrm{U(1)_Y}$ gauge fields, respectively. In this basis, the covariant derivative is

$$D_\mu = \partial_\mu + ig_S T^\alpha G^\alpha_\mu + igT^a W^a_\mu + ig'\frac{Y}{2}B_\mu. \tag{1.6}$$

1.1.2 The fermion sector

The Lagrangian of fermion sector is given by

$$\mathscr{L}_\mathrm{f} = \begin{pmatrix}\overline{Q_{iL}} & \overline{u_{iR}} & \overline{d_{iR}} & \overline{L_{iL}} & \overline{\ell_{iR}}\end{pmatrix}\gamma^\mu \begin{pmatrix} (i\partial_\mu - g_s T^\alpha G^\alpha_\mu)\begin{pmatrix}Q_{iL}\\ u_{iR}\\ d_{iR}\end{pmatrix} \\ (i\partial_\mu - gT^a W^a_\mu - g'\frac{Y}{2}B_\mu)L_{iL} \\ (i\partial_\mu - g'\frac{Y}{2}B_\mu)\ell_{iR}\end{pmatrix}, \tag{1.7}$$

where $Q_{iL} \equiv \begin{pmatrix}u_{iL}\\ d_{iL}\end{pmatrix}$, $L_{iL} \equiv \begin{pmatrix}\nu_{iL}\\ \ell_{iL}\end{pmatrix}$.

1.1.3 The Higgs sector

The SM has the minimal Higgs sector with one $\mathrm{SU(2)_L}$ doublet field. The Lagrangian of Higgs sector is

$$\mathscr{L}_\mathrm{Higgs} = |D^\mu \Phi|^2 - V_\mathrm{SM}(\Phi), \tag{1.8}$$

with the Higgs potential in the standard model given by

$$V_\mathrm{SM}(\Phi) = -\mu^2(\Phi^\dagger\Phi) + \frac{1}{2}\lambda(\Phi^\dagger\Phi)^2, \tag{1.9}$$

where the Higgs doublet field Φ can be parametrized as

$$\Phi = \begin{pmatrix} w^+ \\ \frac{1}{\sqrt{2}}(v + h + iz)\end{pmatrix} \tag{1.10}$$

with $w^\pm$ and z are the NG bosons which are absorbed by longitudinal components of W^+ boson and Z boson, respectively, and $v \simeq 246$ GeV is VEV of Φ. By imposing the vacuum condition

$$\left.\frac{\partial V_\mathrm{SM}}{\partial h}\right|_{h\to 0} = 0, \tag{1.11}$$

we obtain

$$\mu^2 = \frac{\lambda}{2}v^2. \tag{1.12}$$

Then, the mass of the physical neutral Higgs boson h is obtained as

$$m_h^2 = \lambda v^2. \tag{1.13}$$

By electroweak symmetry breaking, the mass terms of the weak gauge bosons are derived as

$$
\begin{aligned}
|D^\mu\Phi|^2 &\rightarrow \left|\left(-ig\frac{\sigma^a}{2}W_\mu^a - ig'\frac{1}{2}B_\mu\right)\Phi\right|^2 && (1.14)\\
&= \frac{1}{8}\left|\begin{pmatrix} gW_\mu^3 + g'B_\mu & g(W_\mu^1 - iW_\mu^2) \\ g(W_\mu^1 + iW_\mu^2) & -gW_\mu^3 + g'B_\mu \end{pmatrix}\begin{pmatrix} 0 \\ v \end{pmatrix}\right|^2 && (1.15)\\
&= \frac{1}{8}v^2g^2\left[(W_\mu^1)^2 + (W_\mu^2)^2\right] && (1.16)\\
&+ \frac{1}{8}v^2(g'B_\mu - gW_\mu^3)(g'B^\mu - gW^{3\mu}) && (1.17)\\
&= \left(\frac{1}{2}vg\right)^2 W_\mu^+W^{-\mu} + \frac{1}{8}v^2(W_\mu^3, B_\mu)\begin{pmatrix} g^2 & -gg' \\ -gg' & g'^2 \end{pmatrix}\begin{pmatrix} W^{3\mu} \\ B^\mu \end{pmatrix} && (1.18)\\
&= \left(\frac{1}{2}vg\right)^2 W_\mu^+W^{-\mu} + \frac{1}{8}[gW_\mu^3 - g'B_\mu]^2 + 0[g'W_\mu^3 + gB_\mu]^2. && (1.19)
\end{aligned}
$$

The charged gauge bosons $W^\pm$ and the neutral gauge bosons are obtained by $W_\mu^\pm \equiv (W_\mu^1 \mp iW_\mu^2)/$, $Z_\mu = (gW_\mu^3 - g'B_\mu)/\sqrt{g^2+g'^2}$, $A_\mu = (g'W_\mu^3 + gB_\mu)/\sqrt{g^2+g'^2}$. The masses of $W^\pm$ and Z are

$$m_W = \frac{1}{2}vg,\ m_Z = \frac{1}{2}v\sqrt{g^2+g'^2}, \tag{1.20}$$

and the photon A is massless.

1.1.4 The Yukawa interaction

Finally, Yukawa interactions are

$$\mathscr{L}_{\rm Y} \equiv -\begin{pmatrix} Y_u^{ij} & Y_d^{ij} & Y_\ell^{ij} \end{pmatrix}\begin{pmatrix} \overline{Q_{iL}}\tilde{\Phi}u_{jR} + h.c. \\ \overline{Q_{iL}}\Phi d_{jR} + h.c. \\ \overline{L_{iL}}\Phi\ell_{jR} + h.c. \end{pmatrix}, \tag{1.21}$$

where $\tilde{\Phi} \equiv i\sigma^2\Phi^*$. After electroweak symmetry breaking,

$$
\begin{aligned}
\mathscr{L}_{\rm Y} &\rightarrow -\frac{v}{\sqrt{2}}\left(Y_u^{ij}\bar{u}_{iL}u_{jR} + Y_d^{ij}\bar{d}_{iL}d_{jR} + Y_\ell^{ij}\bar{\ell}_{iL}\ell_{jR} + h.c.\right) && (1.22)\\
&\equiv -(m_u\bar{u}u + m_d\bar{d}d + m_\ell\bar{\ell}\ell) && (1.23)
\end{aligned}
$$

The fermion masses are writen as

$$m_f = \frac{1}{\sqrt{2}}vY_f^{ij}. \tag{1.24}$$

1.1.5 Relation between mass and coupling of particles

As shown in above results, we obtain the universal relation between coupling and masses

$$m_i \propto v. \tag{1.25}$$

1.2 Predictions to the Higgs boson from the standard model

1.2.1 Bounds from perturbative unitarity

From the conservation of probability

$$\begin{aligned} < a|a > &= | < b|S|a > |^2 && (1.26)\\ &= < a|S^\dagger|b >< b|S|a > && (1.27)\\ &= < a|S^\dagger S|a >, && (1.28) \end{aligned}$$

we obtain a consequence of the unitarity of the S-matrix $S^\dagger S = 1$. Inserting $S = 1 + iT$ (T is the part due to interactions), we have

$$-i(T - T^\dagger) = T^\dagger T. \tag{1.29}$$

Namely,

$$\begin{aligned} -i < a|(T - T^\dagger)|a > &= < a|T^\dagger T|a >, && (1.30)\\ -i[\mathscr{M} - \mathscr{M}^*] &= \sum_n \int d\prod_n \mathscr{M}^*\mathscr{M}, && (1.31)\\ 2Im\mathscr{M} &= \sum_n \int d\prod_n |\mathscr{M}|^2. && (1.32) \end{aligned}$$

where,

$$\int d\prod_n = \left(\prod_{i=1}^n \int \frac{d^3p_i}{(2\pi)^3}\frac{1}{2E_i}\right)(2\pi)^4\delta^{(4)}(p_A + p_B - \sum_i p_i). \tag{1.33}$$

From the relation

$$\begin{aligned} \int d\sigma &= \frac{1}{2E_A 2E_B|v_A - v_B|}\left(\prod_{i=1}^n \int \frac{d^3p_i}{(2\pi)^3}\frac{1}{2E_i}\right)|\mathscr{M}(p_A, p_B \to \{p_i\})|^2(2\pi)^4\delta^{(4)}(p_A + p_B - \sum_i p_i),\\ \sigma_{tot} &= \frac{1}{4p_{cm}E_{cm}}\int d\prod_n |\mathscr{M}|^2, \end{aligned} \tag{1.34}$$

we obtain

$$Im\mathscr{M} = 2p_{cm}E_{cm}\sigma_{tot}. \tag{1.35}$$

This relation is known as the optical theorem.

For the case of two particles in the final state

$$\left(\frac{d\sigma}{d\Omega}\right)_{cm} = \frac{|\mathscr{M}|^2}{64\pi^2 E_{cm}^2}, \tag{1.36}$$

we obtain

$$\begin{aligned}\sigma_{tot} &> (\sigma =) \int d\Omega \frac{|\mathscr{M}|^2}{64\pi^2 E_{cm}^2} && (1.37)\\ &= \int d(\cos\theta) \frac{2\pi|\mathscr{M}|^2}{4E_{cm}^2 16\pi^2} && (1.38)\\ &= \frac{1}{s}\int d(\cos\theta)\frac{|\mathscr{M}|^2}{8\pi}. && (1.39)\end{aligned}$$

Then, Eq. (1.35) is

$$\begin{aligned}Im\mathscr{M} &\simeq \frac{s}{2}\sigma_{tot} && (1.40)\\ &> \int d(\cos\theta)\frac{|\mathscr{M}|^2}{16\pi}. && (1.41)\end{aligned}$$

On the other hand, we define the partial wave amplitude a_J as

$$\mathscr{M}(s,t) = 16\pi \sum_J (2J+1) a_J(s) P_J(\cos\theta). \tag{1.42}$$

Then, Eq. (1.41) is

$$\begin{aligned}16\pi\sum_J (2J+1)\mathrm{Im}a_J P_J(\cos\theta) &> 16\pi \sum_{J,J'}(2J+1)(2J'+1)a_J^\dagger a_{J'} \int d(\cos\theta) P_J^\dagger(\cos\theta) P_{J'}(\cos\theta)\\ &= 16\pi\sum_J (2J+1)^2 |a_J|^2 \frac{2\delta_{J,J'}}{2J+1},\\ \mathrm{Im}a_J P_J(\cos\theta) &> 2|a_J|^2,\\ \mathrm{Re}(a_J)^2 + \left(\mathrm{Im}(a_J) - \frac{1}{2}\right)^2 &< \left(\frac{1}{2}\right)^2. \end{aligned} \tag{1.43}$$

In order keep perturbativity, we require that the absolute value of the eigenvalues of the s-wave amplitudes are at most of the order of the unity:

$$|a_J| < a_{\max}. \tag{1.44}$$

We take $a_{\max} = 1$ in this section.

By calculating the partial wave amplitude for elastic scattering of longitudinally polarized gauge bosons, perturbativity condition (Eq. (1.44)) give the prediction of the upper bound of Higgs mass as shown in Fig. 1.1.

1.2.2 Bounds from triviality and vacuum stability

The renormalization group equation of Higgs self coupling is approximately given by

$$\beta_\lambda \equiv \frac{d\lambda(\mu)}{d\mu} \simeq \frac{12\lambda^2}{16\pi^2}. \tag{1.45}$$

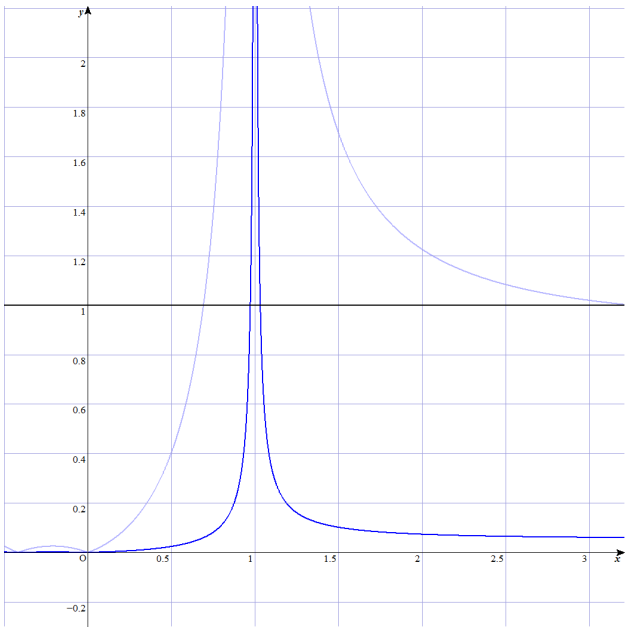

Figure 1.1: A sketch of the energy (s/m_h^2) dependence of the partial wave amplitude for elastic scattering of longitudinally polarized $W^{\pm}$ bosons $|a_0(W_L^+W_L^- \to W_L^+W_L^-)|$ for two choice of the Higgs boson mass ($m_h \simeq 1$TeV (above), 300GeV (below)). The Higgs boson mass is constrained by perturbative unitarity.

When we fix the scale at $v = 246$GeV, we obtain energy dependence of Higgs self coupling,

$$\lambda(\mu) = \frac{\lambda(v)}{1 - \frac{3\lambda(v)}{4\pi^2} \ln\left(\frac{\mu}{v}\right)}. \tag{1.46}$$

In the limit of $\mu \ll v$,

$$\lambda(\mu) = \frac{\lambda(v)}{\ln\left(\frac{e}{(\mu/v)^{3\lambda(v)/4\pi^2}}\right)} \simeq \frac{\lambda(v)}{\ln\infty} \to 0_+. \tag{1.47}$$

On the other hand, in the limit of $\mu \gg v$, we obtain the energy scale Λ, which satisfy

$$\lambda(\Lambda) = \infty. \tag{1.48}$$

Then, we obtain

$$\begin{aligned} 1 - \frac{3\lambda(v)}{4\pi^2} \ln\left(\frac{\Lambda}{v}\right) &= 0, \\ \Lambda &= v \exp\left(\frac{4\pi^2}{3\lambda}\right), \\ &= v \exp\left(\frac{4\pi^2 v^2}{3m_H^2}\right). \end{aligned} \tag{1.49}$$

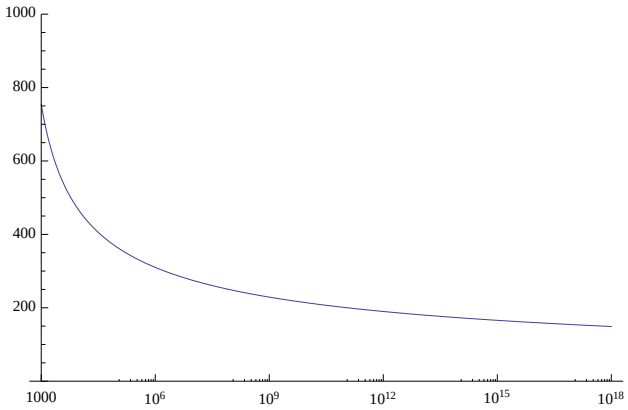

Figure 1.2: The triviality bound: Cutoff scale Λ [GeV] depends on Higgs boson mass m_h [GeV] from Eq. (1.45).

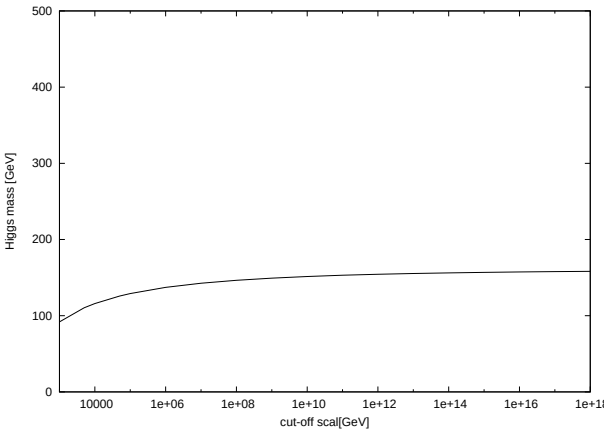

Figure 1.3: Vacuum stability bound: Cutoff scale Λ [GeV] depends on Higgs boson mass m_h [GeV].

The cutoff scale in the SM is determined by Higgs boson mass as shown in Fig. 1.2.

The one-loop renormalization group equations involving the contribution of fermions and gauge bosons are given by [52]

$$\begin{aligned}
\beta(\lambda) &= \frac{1}{16\pi^2}[12\lambda^2 - 12y_t^4 + 12y_t^2\lambda + \frac{9}{4}g^4 + \frac{6}{4}g^2g'^2 + \frac{3}{4}g'^4 - 9\lambda g^2 - 3\lambda g'^2], \\
\beta(g_s) &= 6\frac{-7g_s^3}{16\pi^2}, \quad \beta(g) = \frac{-3g^3}{16\pi^2}, \quad \beta(g') = \frac{7g'^3}{16\pi^2}, \quad \beta(y_t) = \frac{y_t}{16\pi^2}\left[\frac{9}{2}y_t^2 - 8g_s^2 - \frac{9}{4}g^2 - \frac{17}{12}g'^2\right],
\end{aligned}$$

The cutoff scale satisfying $\lambda(\Lambda) = 0$ is calculated by above conditions Eq. (1.50). The condition of vacuum stability

$$\lambda(\mu) > 0 \tag{1.50}$$

give the lower bound of Higgs mass as shown in Fig. 1.3.

1.2.3 Decays of the Higgs boson

We calculate the decay rates of the Higgs boson. There are various decay modes of the Higgs boson; $h \to f\bar{f}(f = t, b, c, s, \mu, \tau)$; $h \to VV, V^*V(V = W, Z)$; $h \to \gamma\gamma, gg$; $h \to Z\gamma$. We define functions

$$\begin{aligned}
f(\tau_i) &= \begin{cases} \arcsin^2\sqrt{\frac{1}{\tau_i}} & (\tau_i \geq 1) \\ -\frac{1}{4}\left[\ln\frac{1+\sqrt{1-\tau_i}}{1-\sqrt{1-\tau_i}} - i\pi\right]^2 & (\tau_i < 1) \end{cases}, \\
g(\tau_i) &= \begin{cases} \sqrt{\tau_i - 1}\arcsin\sqrt{\frac{1}{\tau_i}} & (\tau_i \geq 1) \\ \frac{1}{2}\sqrt{1-\tau_i}\left[\ln\frac{1+\sqrt{1-\tau_i}}{1-\sqrt{1-\tau_i}} - i\pi\right] & (\tau_i < 1) \end{cases}
\end{aligned}$$

f	t	b	c	s	μ	τ
N_{cf}	3	3	3	3	1	1
e_f	$\frac{2}{3}$	$-\frac{1}{3}$	$\frac{2}{3}$	$-\frac{1}{3}$	-1	-1
T_f^{3L}	$\frac{1}{2}$	-$\frac{1}{2}$	$\frac{1}{2}$	$-\frac{1}{2}$	$-\frac{1}{2}$	$-\frac{1}{2}$

Table 1.2: Fermion charge assignments.

where $\tau_i \equiv (2m_i/m_h)^2$, $\lambda_i \equiv (2m_i/m_z)^2$. In Table. 1.2, we show the color factor N_{cf}, the electromagnetic charge of the final state fermion e_f and the third component of the isospin T_f^{3L}. The decay rates of the Higgs boson decaying into the fermion pair $h \to f\bar{f}$ are given by

$$\Gamma(h \to f\bar{f}) = \frac{N_{cf}g^2}{32\pi}\frac{m_f^2 m_H}{m_w^2}(1-\tau_f)^{\frac{3}{2}}. \tag{1.51}$$

The decay rates of the Higgs boson decaying into the gauge boson pair $h \to W^+W^-$ or $h \to ZZ$ are given by

$$\Gamma(h \to W^+W^-) = \frac{g^2}{64\pi}\frac{m_H^3}{m_w^2}\sqrt{1-\tau_w}(1-\tau_w+\frac{3}{4}\tau_w^2), \tag{1.52}$$

$$\Gamma(h \to ZZ) = \frac{g^2}{128\pi}\frac{m_H^3}{m_w^2}\sqrt{1-\tau_z}(1-\tau_z+\frac{3}{4}\tau_z^2). \tag{1.53}$$

On the other hand, the decay modes of $h \to W^*W$ or $h \to Z^*Z$ is given by

$$\Gamma(h \to W^*W) = \frac{g^4 m_H}{512\pi^3}F\left(\frac{m_w}{m_H}\right)\begin{cases}3\ W^* \to tb \text{ not allowed},\\ 4\ W^* \to tb \text{ allowed},\end{cases} \tag{1.54}$$

$$\Gamma(h \to Z^*Z) = \frac{g^4 m_H}{2048\pi^3}\frac{7-\frac{40}{3}\sin^2\theta_w+\frac{160}{9}\sin^4\theta_w}{\cos^4\theta_w}F\left(\frac{m_z}{m_H}\right), \tag{1.55}$$

where

$$\begin{aligned}F(x) &= -|1-x^2|\left(\frac{47}{2}x^2-\frac{13}{2}+\frac{1}{x^2}\right)+3(1-6x^2+4x^4)|\ln x| \\ &\quad +\frac{3(1-8x^2+20x^4)}{\sqrt{4x^2-1}}\cos^{-1}\left(\frac{3x^2-1}{2x^3}\right).\end{aligned} \tag{1.56}$$

There re one-loop induced decay processes, such as $h \to \gamma\gamma$, $h \to gg$ and $h \to Z\gamma$. These decay rates can be given by

$$\Gamma(h \to \gamma\gamma) = \frac{\alpha^2 g^2}{1024\pi^3}\frac{m_H^3}{m_w^2}\left|\sum_f N_{cf}e_f^2 F_f + F_w\right|^2, \tag{1.57}$$

$$\Gamma(h \to gg) = \frac{\alpha_s^2 g^2}{512\pi^3}\frac{m_H^3}{m_w^2}\left|\sum_f F_f\right|^2, \tag{1.58}$$

$$\Gamma(h \to Z\gamma) = \frac{\alpha^2 g^2}{512\pi^3}\frac{m_H^3}{m_w^2}\left|\sum_f A_f + A_w\right|^2\left(1-\frac{m_z^2}{m_H^2}\right), \tag{1.59}$$

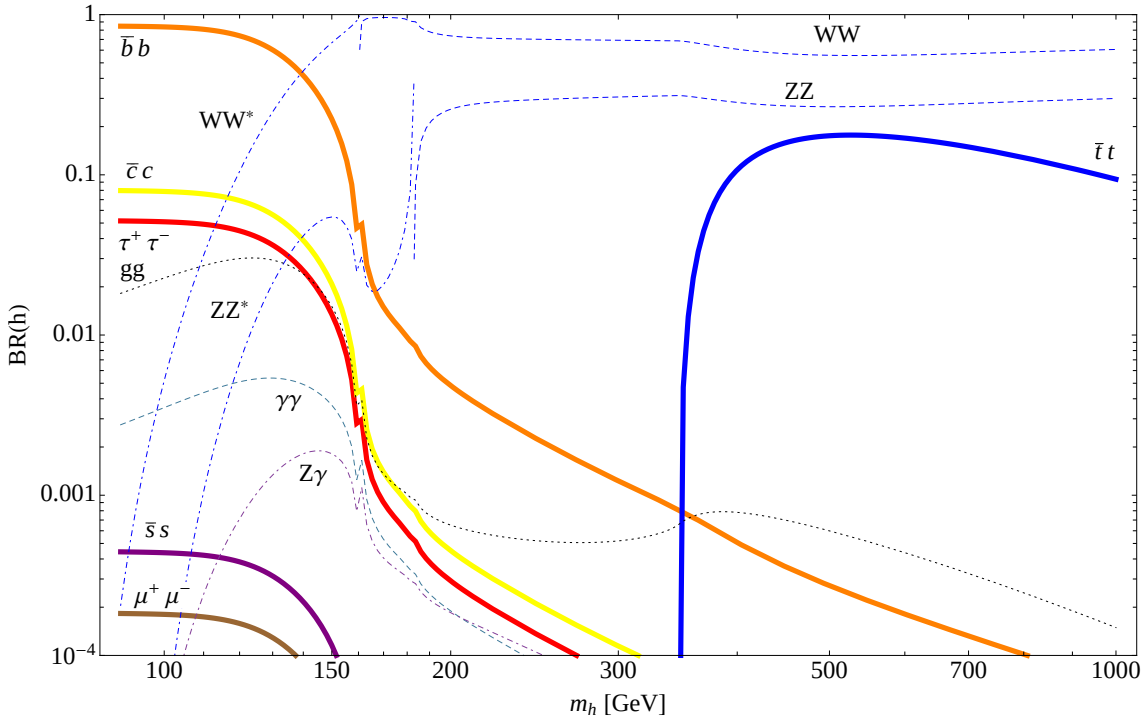

Figure 1.4: The decay branching ratio of the SM Higgs boson as a function of SM Higgs mass.

where $F_s = \tau_s[1 - \tau_s f(\tau_s)], F_f = -2\tau_f[1 + (1 - \tau_f)f(\tau_f)], F_V = 2 + 3\tau_V + 3\tau_V(2 - \tau_V)f(\tau_V)$,

$$
\begin{aligned}
A_f &= \frac{-2N_{cf}e_f(T_f^{3L} - 2e_f \sin^2\theta_w)}{\sin\theta_w \cos\theta_w}[I_1(\tau_f, \lambda_f) - I_2(\tau_f, \lambda_f)], \\
A_w &= -\cot\theta_w \left\{ 4(3 - \tan^2\theta_w) I_2(\tau_w, \lambda_w) + \left[\left(1 + \frac{2}{\tau_w}\right) \tan^2\theta_w - \left(5 + \frac{2}{\tau_w}\right) \right] I_1(\tau_w, \lambda_w) \right\}, \\
I_1(\tau_i, \lambda_i) &= \frac{\tau_i \lambda_i}{2(\tau_i - \lambda_i)} + \frac{\tau_i^2 \lambda_i^2}{2(\tau_i - \lambda_i)^2}[f(\tau_i) - f(\lambda_i)] + \frac{\tau_i^2 \lambda_i}{(\tau_i - \lambda_i)^2}[g(\tau_i) - g(\lambda_i)], \\
I_2(\tau_i, \lambda_i) &= -\frac{\tau_i - \lambda_i}{2(\tau_i \lambda_i)}[f(\tau_i) - f(\lambda_i)].
\end{aligned}
$$

The result of the decay branching ratio is shown in Fig. 1.4.

1.2.4 Production of the Higgs boson at LHC

The production cross section of SM Higgs boson at 14TeV pp-collider is shown in Fig. 1.5.

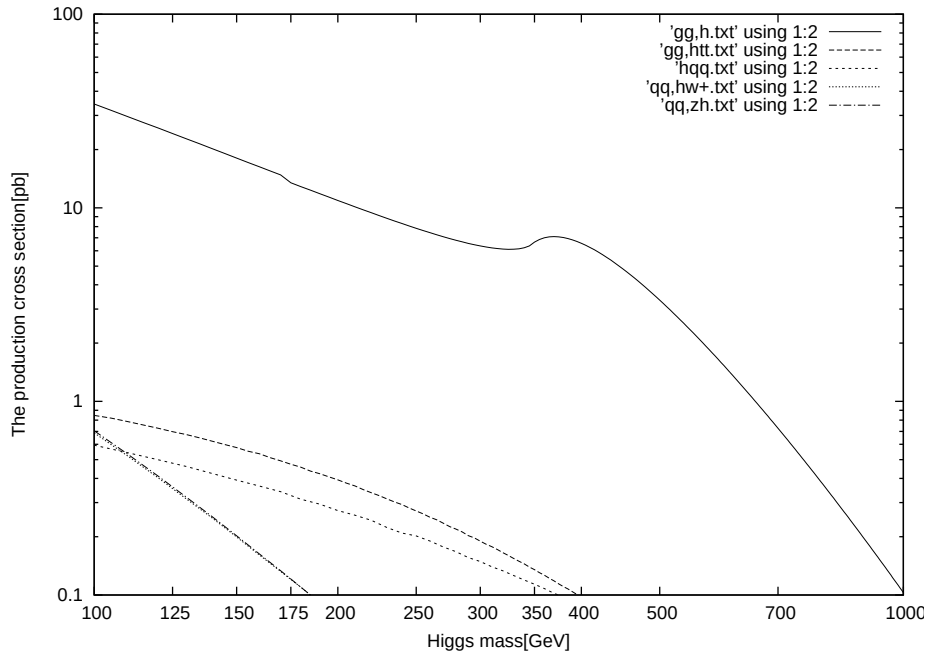

Figure 1.5: The production cross section of SM Higgs boson as a function of Higgs boson mass at 14TeV pp-collider (PDF: mrst2002 nlo).

Chapter 2

Dark matter

2.1 Evidences of DM

We consider an astronomical] object with the orbital velocity v and the mass m which is separated by a distance R from the center of a galaxy with the mass M. The equilibrium of forces of gravity and centripetal force is given by

$$G\frac{mM}{r^2} = \frac{mv^2}{r}. \tag{2.1}$$

We obtain the orbital velocity as $v = \sqrt{GM/r}$.

If we consider the cace that a galaxy is uniform density ρ and the size R_0, we obtain the mass of a galaxy as the function of R:

$$M(R) = \begin{cases} \frac{4}{3}\pi R_0^3 \rho \equiv M_0 \text{ (for } R > R_0), \\ \frac{M_0}{R_0^3} R^3 \qquad \text{(for } R < R_0). \end{cases} \tag{2.2}$$

Then, the orbital velocity v of an astronomical] object is predicted by

$$v(R) \propto \begin{cases} \sqrt{\frac{1}{r}} \text{ (for } R > R_0), \\ r \text{ (for } R < R_0). \end{cases} \tag{2.3}$$

This prediction show us that the rotational speed $v(R)$ behave as $\sqrt{1/r}$.

However, this prediction is not consistent with the observation which reported by V. Rubin and K. Ford in 1970. The observed rotational speed is a constant value $v \simeq 230\text{km s}^{-1}$. This observation show us that there are unknown source of gravity, so called dark matter (DM). Furthermore, there are other various observations which suggest the evidence of DM.

2.2 Constraints of primordial black holes as dark matter

The recent estimation of the amount of DM trapped in stars at their birth have shown the best constraints come from white dwarfs or a neutron stars in globular clusters which exclude the DM consisting entirely of primordial black holes (PBHs) in the mass range $10^{16} - 3 \times 10^{22}$g, with the strongest constraint on the fraction $\Omega_{\rm PBH} = \Omega_{\rm DM} \gtrsim 10^{-2}$ being in the range of PBH masses $10^{17} - 10^{18}$g [53]. Furthermore, Ref. [54] have shown the constraint of the PBH DM

with masses in the range of $2 \times 10^{-9} M_\odot - 10^{-7} M_\odot$. They claim that PBHs in these mass ranges cannot make up the entirety of the DM, thus closing a full order of magnitude in the allowed mass range for PBH DM.

2.3 WIMP hypothesis

We understand the properties of DM as

- almost no interacting with the photon, DM itself and other fermions,
- non-relativistic,
- relic abundance is observed as $\Omega_{\rm DM} = 0.1198 \pm 0.0026$.

In the hypothesis of weakly interacting massive particles (WIMPs), DMs are explained as particles with no electric charge, stable and DM masses are $\mathscr{O}(100)$GeV.

Dark matter stability by new symmetries In this thesis, we consider three scenarios of dark matter stability which explained by discrete symmetry, global U(1) symmetry and gauge symmetry.

2.4 The calculation of relic abundance of dark matter

We review the calculation of relic abundance of dark matter. This section is based on [55–58].

The Boltzmann equation The Boltzmann equation is given by

$$\frac{dn}{dt} + 3H\ n = -\left\langle \sigma_{\rm eff} v \right\rangle (n^2 - n_{\rm EQ}^2). \tag{2.4}$$

By the definition $Y \equiv n/s$, we obtain

$$s\ \frac{dY}{dt} = n^2 - n_{\rm EQ} = s^2 (Y^2 - Y_{\rm EQ}^2). \tag{2.5}$$

During the radiation dominated epoch, the energy density is given by $\rho_{\rm R} = (\pi^2/30) g_* T^4$. By the definition of the scaled inverse temperature $x \equiv m/T$, the Friedmann equation for flat Universe $H^2 = (8\pi/3m_P^2)\rho$ gives

$$t = H^{-1} = 0.301\ g_*^{-1/2} \frac{m_P}{T^2} = 0.301\ g_*^{-1/2} \frac{m_P}{m^2}\ x^2. \tag{2.6}$$

Then, the Boltzmann equation is written by

$$\frac{dY(x)}{dx} = \frac{-x\ \left\langle \sigma_{\rm eff} v \right\rangle (x)\ s}{1.67\ g_*^{1/2}\ \frac{m^2}{m_P}} (Y(x)^2 - Y_{\rm EQ}(x)^2). \tag{2.7}$$

For the case of relativistic particles $s = (2\pi^2/45) g_{*s} T^3$, we obtain

$$\frac{dY(x)}{dx} = \frac{-g_{*s} m\ m_P\ \left\langle \sigma_{\rm eff} v \right\rangle (x)}{3.807\ g_*^{1/2} x^2} (Y(x)^2 - Y_{\rm EQ}(x)^2). \tag{2.8}$$

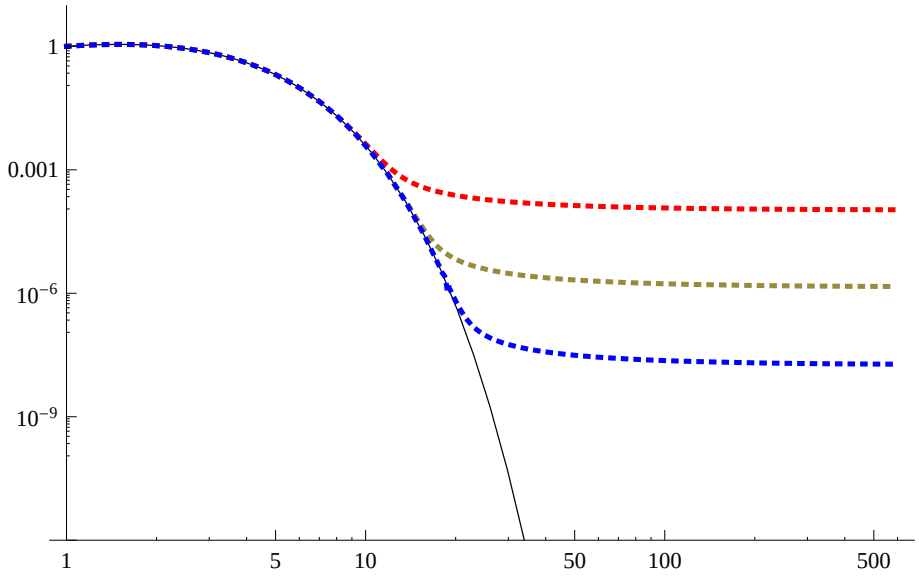

Figure 2.1: The freeze out of a massive particle species. The dashed line is the actual abundance $Y(x)$, and the solid line is the equilibrium abundance $Y_{\rm EQ}(x)$. Each curbs are normalized by $Y(x=1)$.

Freeze out In the non-relativistic regimes ($x \gg 3$), the Boltzmann equation is written by approximately

$$\frac{dY}{dx} = -\lambda x^{-n-2}(Y^2 - Y_{\rm EQ}^2), \tag{2.9}$$

where

$$\lambda = 0.264 \frac{g_{*s}}{g_*^{1/2}} m_P m_{DM} \sigma_0, \tag{2.10}$$

$$Y_{\rm EQ} = 0.145 \frac{g_*}{g_{*s}} x^{\frac{3}{2}} e^{-x} (\text{for } x \gg 3). \tag{2.11}$$

By solving this equation, we obtain the behavior which is shown in Fig. 2.1.

Relic abundance The freeze out point is given in terms of x:

$$x_f = \ln \frac{0.038\ g\ m_P\ m_{DM}\ \langle \sigma_{\rm eff} v \rangle (x_f)}{g_*^{1/2}\ x_f^{1/2}}, \tag{2.12}$$

where $m_p = 1.22 \times 10^{19}$GeV and g_* is total number of effectively relativistic degrees of freedom at the time of freeze out. Eq. (2.12) is usually solved iteratively. By the definition of

$$J(x_f) = \int_{x_f}^{\infty} \frac{\langle \sigma_{\rm eff} v \rangle (x)}{x^2} dx, \tag{2.13}$$

we obtain the relic abundance

$$\Omega h^2 \simeq \frac{1.07 \times 10^9\ {\rm GeV}^{-1}}{g_*^{1/2} m_P J(x_f)}. \tag{2.14}$$

The thermally-averaged annihilation cross section tomes velocity We write the thermal average of the annihilation cross section as

$$\langle \sigma_{\rm eff} v \rangle = \frac{A}{n_{EQ}^2}, \tag{2.15}$$

where

$$n_{EQ} = \sum_i \frac{g_i}{(2\pi)^3} \int d^3 p_i \exp\left(-\frac{E_i}{T}\right) = \frac{T}{2\pi^2} \sum_i g_i \; m_i^2 \; K_2\left(\frac{m_i}{T}\right), \tag{2.16}$$

$$A = \frac{T}{32\pi^4} \sum_{i,\; j} \int_{(m_i+m_j)^2}^{\infty} ds \; g_i \; g_j \; p_{ij} \; W_{ij\to kl} \; K_1\left(\frac{\sqrt{s}}{T}\right). \tag{2.17}$$

where m_i $(i = 1, \cdots, N)$ is masses, g_i is internal degrees of freedom (statistical weights), K_a is the modified Bessel function of the second kind of order a and

$$p_{ij} = \frac{\sqrt{s-(m_i+m_j)^2}\sqrt{s-(m_i-m_j)^2}}{2\sqrt{s}} \tag{2.18}$$

is the momentum of i-th (or j-th) particle in the center-of-mass frame of i-th and j-th particles pair. A dimensionless Lorents invariant, related to the (unpolarized) cross section is given by $W_{ij\to kl}$, $p_{i/j}$. In particular, the contribution of a two-body final state can be written as

$$W_{ij\to kl} = \frac{p_{kl}}{16\pi^2 \; g_i \; g_j \; S_{kl} \; \sqrt{s}} \sum_{\rm internalDF} \int \mid \mathscr{M}(ij \to kl) \mid^2 d\Omega, \tag{2.19}$$

where p_{kl} is the final center-of-mass momentum, S_{kl} is a symmetry factor equal to 2 for identical final particles and to 1 otherwise, and the integration is over the outgoing directions of one of the final particles.

By using

$$\sigma_{ij\to kl} = \frac{1}{64\pi^2 s} \frac{p_{kl}}{p_{ij}} \sum_{\rm internalDF} \int \mid \mathscr{M}(ij \to kl) \mid^2 d\Omega, \tag{2.20}$$

We obtain

$$\begin{aligned} \langle \sigma_{\rm eff} v \rangle &= \frac{T}{32\pi^4 n_{EQ}^2} \sum_{i,j} \int_{(m_i+m_j)^2}^{\infty} ds \frac{[s-(m_i+m_j)^2][s-(m_i-m_j)^2] \; \sigma_{ij\to kl}}{S_{kl}\sqrt{s}} \\ &= \frac{1}{8 \; T \left[\sum_i m_i^2 \; K_2\left(\frac{m_i}{T}\right)\right]^2} \sum_{i,j} \int_{(m_i+m_j)^2}^{\infty} ds \frac{[s-(m_i+m_j)^2][s-(m_i-m_j)^2] \; \sigma_{ij\to kl}}{S_{kl}\sqrt{s}} K_1\left(\frac{\sqrt{s}}{T}\right). \end{aligned}$$

When we determine a model, we can calculate the relic abundance.

Chapter 3

Neutrino oscillation

3.1 Experimental data of neutrino masses and mixing

It has been well established that neutrinos have nonzero masses as shown in the neutrino oscillation measurements [5–13] although they are massless particles in the standard model (SM) of particle physics. Experimental data of neutrino oscillation is measured as

$$\begin{aligned} \Delta m^2_{21} &= 7.46 \times 10^{-5}\mathrm{eV}^2, \quad |\Delta m^2_{32}| = 2.51 \times 10^{-3}\mathrm{eV}^2, \\ \sin^2\theta_{23} &= 1, \quad \sin^2\theta_{13} = 0.09, \quad \tan^2\theta_{12} = 0.427. \end{aligned} \tag{3.1}$$

We cannot explain these data in the framework of the SM. We review the models which can explain the origin of neutrino masses.

3.2 Mechanisms of neutrino mass generation

To explain neutrino masses, we introduce right-handed neutrinos ν_R as shown in Table. 3.1. There are two possible mass terms for neutrinos the Dirac type $\bar{\nu_L}\nu_R$ and the Majorana type $(\bar{\nu_R})^c\nu_R$. As shown in the following, we consider each cases.

	ν_R
$\mathrm{SU(2)_L}$	**1**
$\mathrm{U(1)_Y}$	0

Table 3.1: The right-handed neutrino.

3.2.1 Dirac neutrino

Dirac mass term of the neutrinos is given by

$$\begin{aligned} \mathcal{L}_{\nu\text{-Yukawa}} &= -y_\nu \overline{L}\, i\sigma_2\, \Phi^*\, \nu_R + \mathrm{h.c.} && (3.2)\\ &= -y_\nu(\overline{\nu_L}, \overline{\ell_L}) \begin{pmatrix} 0 & 1 \\ -1 & 0 \end{pmatrix} \begin{pmatrix} \phi^- \\ \phi^0 \end{pmatrix} \nu_R + \mathrm{h.c.} && (3.3)\\ &= -y_\nu \left(\overline{\nu_L}\phi^0_\nu \nu_R - \overline{\ell_L}\phi^-_\nu \nu_R\right) + \mathrm{h.c.} && (3.4)\\ &= -\frac{v}{\sqrt{2}}\, y_\nu\, \overline{\nu_L}\, \nu_R + \mathrm{h.c.} && (3.5)\\ &\equiv -m_D(\overline{\nu_L}\nu_R + \overline{\nu_R}\nu_L). && (3.6) \end{aligned}$$

To explain observed tiny neutrino masses, this case require unnatural tiny Yukawa couplings.

3.2.2 Type-I seesaw with Majorana neutrino

Since the scale of neutrino masses is much different from that of the other fermion masses, they might be generated by a different mechanism from the one for the other fermions. In addition, neutrinos are unique fermions, because these are neutral. Therefore, we can consider the case satisfying $\nu_R = \nu_R^c$. Then, Majorana mass term which violates lepton number is given by

$$\frac{1}{2} m_M \overline{(\nu_R)^c} \nu_R. \tag{3.7}$$

Usually, the possibility that neutrinos are Majorana fermions is utilized as a characteristic feature of the neutrino masses. The most popular example is the seesaw mechanism [59] where very heavy right-handed Majorana neutrinos are introduced:

$$\begin{aligned}
\mathcal{L}_{\nu\text{-Yukawa}} &= -\frac{1}{2}\left(m_D\,\overline{\nu_L}\,\nu_R + m_D\,\overline{\nu_L^c}\,\nu_R^c + m_M\overline{\nu_L^c}\,\nu_R\right) - \frac{1}{2}\left(m_D\,\overline{\nu_R^c}\,\nu_L^c + m_D\,\overline{\nu_R}\,\nu_L + m_M\overline{\nu_R}\,\nu_L^c\right) \\
&= -\frac{1}{2}\begin{pmatrix}\overline{\nu_L} & \overline{\nu_L^c}\end{pmatrix}\begin{pmatrix}0 & m_D \\ m_D & m_M\end{pmatrix}\begin{pmatrix}\nu_R^c \\ \nu_R\end{pmatrix} - \frac{1}{2}\begin{pmatrix}\overline{\nu_R^c} & \overline{\nu_R}\end{pmatrix}\begin{pmatrix}0 & m_D \\ m_D & m_M\end{pmatrix}\begin{pmatrix}\nu_L \\ \nu_L^c\end{pmatrix} \\
&= -\frac{1}{2}\,\overline{L}\,M\,R^c - \frac{1}{2}\,\overline{R^c}\,M\,L,
\end{aligned} \tag{3.8}$$

where $L \equiv \begin{pmatrix}\nu_L \\ \nu_L^c\end{pmatrix}$, $R \equiv \begin{pmatrix}\nu_R \\ \nu_R^c\end{pmatrix}$ and $M \equiv \begin{pmatrix}0 & m_D \\ m_D & m_M\end{pmatrix}$. (From definitions $\nu_{L(R)} \equiv P_{L(R)}\,\nu$, $\nu^c \equiv C\,\overline{\nu}^T$, we obtain the relation $(\nu_{L(R)})^c = \nu^c_{R(L)}$.) By diagonarizing Eq. (3.8), neutrino masses are given by

$$m_\nu \simeq \frac{m_D^2}{m_M}, \quad m_N \simeq m_M. \tag{3.9}$$

By the hierarchy of $m_M >> m_D$, we can explain tiny neutrino masses. Therefore, this model predict very heavy Majorana neutrinos. If these particles have the masses $m_N \simeq 10^{-14}$GeV to explain $m_\nu \simeq 0.1$eV, we can explain Yukawa coupling as natural scale as $y_\nu \simeq 1$. However, it may be difficult to test such heavy ν_R.

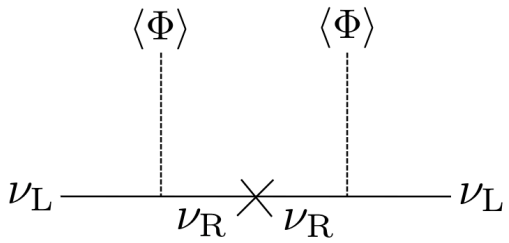

Figure 3.1: Type-I seesaw model.

3.2.3 The neutrinophilic two Higgs doublet model

The neutrinophilic two Higgs doublet model (νTHDM) is a new physics model where neutrinos are regarded as Dirac fermions. The second $\mathrm{SU}(2)_L$-doublet scalar field Φ_ν which couples only with right-handed neutrinos ν_R was first introduced in Ref. [60] for Majorana neutrinos. Phenomenology in the model of Majorana neutrinos is discussed in Ref. [61, 62].

The neutrinophilic doublet field is also utilized for Dirac neutrinos [63] where a spontaneously broken Z_2 parity is introduced in order to achieve the neutrinophilic property. Smallness of neutrino masses are explained by a tiny vacuum expectation value (VEV) $\langle\Phi_\nu\rangle = v_\nu$ of the neutrinophilic scalar without extremely small Yukawa coupling constant for neutrinos. Instead of the Z_2 parity, the model in Ref. [64] uses a global $\mathrm{U}(1)_X$ symmetry that is softly broken in the scalar potential. The $\mathrm{U}(1)_X$ symmetry forbids Majorana mass terms of ν_R, and then neutrinos are Dirac fermions[1]. We refer to the model in Ref. [64] as the νTHDM.

In the most simplest νTHDM, we introduce the Dirac right-handed neutrino ν_R and the neutrinophilic scalar doublet Φ_ν, as shown in Table. 3.2. A global $\mathrm{U}(1)_X$ symmetry is introduced, under which Φ_ν and ν_{iR} have the same nonzero charge while the SM particles have no charge.

	ν_R	$\Phi_\nu = \begin{pmatrix}\phi_\nu^+ \\ \phi_\nu^0\end{pmatrix}$
$\mathrm{SU}(2)_\mathrm{L}$	**1**	**2**
$\mathrm{U}(1)_\mathrm{Y}$	0	$\frac{1}{2}$
Global $\mathrm{U}(1)_\mathrm{X}$	1	1

Table 3.2: Particle contents and its charge assignments in the νTHDM.

The Yukawa interaction Yukawa interaction is given by

$$\begin{aligned}
\mathcal{L}_{\nu\text{-Yukawa}} &= -(y_\nu)_{\ell i}\overline{L_\ell}\, i\sigma_2\, \Phi_\nu^*\, \nu_{iR} + \text{h.c.} && (3.10)\\
&= -(y_\nu)_{\ell i}(\overline{\nu_{\ell L}}, \overline{\ell_{\ell L}}) \begin{pmatrix} 0 & 1 \\ -1 & 0 \end{pmatrix} \begin{pmatrix} \phi_\nu^- \\ \phi_\nu^0 \end{pmatrix} \nu_{iR} + \text{h.c.} && (3.11)\\
&= -(y_\nu)_{\ell i}\left(\overline{\nu_{\ell L}}\phi_\nu^0\nu_{iR} - \overline{\ell_{\ell L}}\phi_\nu^-\nu_{iR}\right) + \text{h.c.} && (3.12)\\
&= -\frac{v_\nu}{\sqrt{2}}(y_\nu)_{\ell i}\,\overline{\nu_{\ell L}}\,\nu_{iR} + \text{h.c.}, && (3.13)
\end{aligned}$$

where $\ell(= e, \mu, \tau)$ denotes the lepton flavor and σ_i (i = 1-3) are the Pauli matrices. Since Majorana mass terms $\overline{(\nu_{iR})^c}\,\nu_{iR}$ are forbidden by the global $\mathrm{U}(1)_\mathrm{X}$ symmetry, there appears an accidental conservation of the lepton number where lepton numbers of Φ_ν and ν_{iR} are 0 and 1, respectively.

Then, neutrino mass matrix in the lepton flavor basis ($\ell = e, \mu, \nu$) is defined by

$$(m_\nu)_{\ell i} = \frac{v_\nu}{\sqrt{2}}(y_\nu)_{\ell i}. \quad (3.14)$$

[1]Since the Majorana mass terms of ν_R can also be acceptable as soft breaking terms of the $\mathrm{U}(1)_X$, the lepton number conservation may be imposed to the Lagrangian.

By diagonalizing, we obtain

$$U_{\rm MNS}^{\dagger} m_\nu = {\rm diag}(m_1, m_2, m_3), \tag{3.15}$$

where Maki-Nakagawa-Sakata (MNS) matrix [65] is given by

$$U_{\rm MNS} = \begin{pmatrix} 1 & 0 & 0 \\ 0 & c_{23} & s_{23} \\ 0 & -s_{23} & c_{23} \end{pmatrix} \begin{pmatrix} c_{13} & 0 & s_{13}e^{-i\delta} \\ 0 & 1 & 0 \\ -s_{13}e^{i\delta} & 0 & c_{13} \end{pmatrix} \begin{pmatrix} c_{12} & s_{12} & 0 \\ -s_{12} & c_{12} & 0 \\ 0 & 0 & 1 \end{pmatrix}. \tag{3.16}$$

In the mass eigenstate (i=1,2,3): $\mathcal{L}_{\nu\text{-Yukawa}} = -m_i \overline{(U^{\dagger}_{MNS})_{i\ell}\nu_{\ell L}}\, \nu_{iR} + \text{h.c.}$, we can construct Dirac neutrinos $\nu_i = \begin{pmatrix} \nu_{iR} \\ (U^{\dagger}_{MNS})_{i\ell}\nu_{\ell L} \end{pmatrix}$.

We can see from Eq. (3.14) that smallness of m_i is explained by the smallness of $v_\nu (\ll v)$. This is the scenario of νTHDM.

The scalar potential If the VEV v_ν is generated spontaneously, a CP-odd scalar $\phi^0_{\nu i}$ becomes massless as a Nambu-Goldstone boson with respect to the breaking of $\mathrm{U}(1)_X$, where $\phi^0_\nu = (v_\nu + \phi^0_{\nu r} + i\phi^0_{\nu i})/\sqrt{2}$. In addition, a CP-even neutral scalar $\phi^0_{\nu r}$ has a small mass ($\propto v_\nu \ll v$). Therefore, the scenario of the spontaneous breaking of $\mathrm{U}(1)_X$ is not allowed by the measurement of the invisible decay of the Z boson. The scalar potential is given by [2]

$$\begin{aligned} V^{(\nu\text{THDM})} &= -\mu^2_{\Phi 1}\Phi^\dagger\Phi + \mu^2_{\Phi 2}\Phi^\dagger_\nu\Phi_\nu - \left(\mu^2_{\Phi 12}\Phi^\dagger_\nu\Phi + \text{h.c.}\right) \\ &\quad + \lambda_{\Phi 1}(\Phi^\dagger\Phi)^2 + \lambda_{\Phi 2}(\Phi^\dagger_\nu\Phi_\nu)^2 + \lambda_{\Phi 12}(\Phi^\dagger\Phi)(\Phi^\dagger_\nu\Phi_\nu) + \lambda'_{\Phi 12}(\Phi^\dagger\Phi_\nu)(\Phi^\dagger_\nu\Phi). \end{aligned} \tag{3.19}$$

We can take $\mu^2_{\Phi 12}$ positive and real without loss of generality by the rephasing of Φ_ν. Here, we take $\mu^2_{\Phi 1} > 0$, $\mu^2_{\Phi 2} > 0$.

The VEV of ϕ^0_ν is induced by $\mu^2_{\Phi 12}$ which break $\mathrm{U}(1)_{\rm X}$ softly. Since the term does not breaks the lepton number conservation, neutrinos are still Dirac particles. When we take $v_\nu \ll v$, we obtain two VEVs

$$v \simeq \frac{\mu_{\Phi 1}}{\sqrt{\lambda_{\Phi 1}}}, \quad v_\nu \simeq \frac{2v\,\mu^2_{\Phi 12}}{2\mu^2_{\Phi 2} + (\lambda_{\Phi 12} + \lambda'_{\Phi 12})v^2}. \tag{3.20}$$

When we take $\mu_{\Phi 2} \simeq v$, we obtain $v_\nu \simeq \mu^2_{\Phi 12}/v$. Then, $\mu_{\Phi 12}/v \simeq 10^{-6}$ is required by taking $y_\nu \simeq and m_\nu \simeq 0.1$eV. In such a simplest model, parameter tuning is required. Stability of the tiny v_ν is discussed in Refs. [62, 66]. In our model presented in Chap. 6, $\mu_{\Phi 12}/v$ becomes small because $\mu^2_{\Phi 12}$ is generated at the one-loop level.

[2] In general 2HDM, we can write terms

$$V^{(\text{THDM})} \to \left(\lambda_5(\Phi^\dagger\Phi_\nu)^2 + \text{h.c.}\right) \tag{3.17}$$

$$+ \left(\lambda_6(\Phi^\dagger\Phi)(\Phi^\dagger\Phi_\nu) + \text{h.c.}\right) + \left(\lambda_7(\Phi^\dagger_\nu\Phi_\nu)(\Phi^\dagger\Phi_\nu) + \text{h.c.}\right). \tag{3.18}$$

However, these terms are forbidden by the global $\mathrm{U}(1)_{\rm X}$ symmetry.

3.3 Loop suppression scenarios

We consider loop suppression scenario which explained by m-loop induced dimension $(5+2n)$ operator $(n \geqq 0)$

$$\mathscr{L}_{\text{eff}} = \frac{c_{ij}}{\Lambda^{2n+1}} \nu_L^i \nu_L^j (\phi^0 \phi^0)^{n+1} \tag{3.21}$$

which are induced by quantum effect. In such scenarios, the size of neutrino masses from the operator with the mass dimension $(2n+1)$, which arises from a m-loop diagram, can be estimated as [67]

$$(m_\nu)_{ij} = c'_{ij} \left\langle \phi^0 \right\rangle \left(\frac{1}{16\pi} \right)^m \left(\frac{\langle \phi^0 \rangle}{\Lambda} \right)^{2n+1}. \tag{3.22}$$

We can explain loop suppressed neutrino masses.

The radiative seesaw scenario is an alternative way to explain tiny neutrino masses, where they are radiatively induced at the one loop level or at the three loop level by introducing Z_2-odd scalar fields and Z_2-odd right-handed neutrinos [25–27]. For radiative seesaw models which are invariant under the unbroken discrete Z_2 symmetry, we can explain DM and neutrino masses at the same time.

3.4 The Ma model

Especially, we consider a minimal model which proposed by the paper [26]. In this model, we introduce Z_2-odd scalar doublet Φ_2 and right handed neutrinos $(\nu_R)_i$ $(i = 1-3)$. The Z_2-odd lightest neutral particle can be a dark matter candidate.

The Higgs potential which is same as IDM is given by

$$\begin{aligned} V_{\text{IDM}}(\Phi_1, \Phi_2) &= \mu_1^2 |\Phi_1|^2 + \mu_2^2 |\Phi_2|^2 + \frac{1}{2}\lambda_1 |\Phi_1|^4 + \frac{1}{2}\lambda_2 |\Phi_2|^4 + \lambda_3 |\Phi_1|^2 |\Phi_2|^2 \\ &\quad + \lambda_4 (\Phi_1^\dagger \Phi_2)(\Phi_2^\dagger \Phi_1) + \frac{1}{2}\lambda_5 [(\Phi_1^\dagger \Phi_2)^2 + h.c.]. \end{aligned} \tag{3.23}$$

When we assume $\mu_1^2 < 0$ and $\mu_2^2 > 0$, Φ_1 obtains the vacuum expectation value (VEV) v $(= \sqrt{-2\mu_1^2/\lambda_1})$, while Φ_2, which has the odd-quantum number of the Z_2 symmetry, cannot get the VEV. Mass eigenstates of the scalar bosons are the SM-like Z_2-even Higgs scalar boson h, the Z_2-odd CP-even scalar boson H, the Z_2-odd CP-odd scalar boson A and Z_2-odd charged scalar bosons $H^\pm$. Masses of these scalar bosons are given by

$$m_h^2 = \lambda_1 v^2, \quad m_{H^\pm}^2 = \mu_2^2 + \frac{1}{2}\lambda_3 v^2, \quad m_{H,A}^2 = \mu_2^2 + \frac{1}{2}(\lambda_3 + \lambda_4 \pm \lambda_5) v^2. \tag{3.24}$$

The constraints of vacuum stability is given by

$$\lambda_1 > 0, \lambda_2 > 0, \sqrt{\lambda_1 \lambda_2} + \lambda_3 + \lambda_4 + \lambda_5 > 0, \tag{3.25}$$

and we here impose the conditions of triviality

$$\lambda_i < 2\pi. \tag{3.26}$$

The Yukawa interaction for leptons and the Majorana mass term are given by

$$\mathcal{L}_{\rm Ma-Yukawa} = \mathcal{L}_{\rm SM-Yukawa} + h_{ij}\,\overline{(L_L)_i}\,\Phi_2^c\,(\nu_R)_j + h.c., \tag{3.27}$$

$$\mathcal{L}_{\rm Majorana} = \frac{1}{2}\,M_i\,\overline{(\nu_R)_i^c}\,(\nu_R)_i + h.c.\,, \tag{3.28}$$

where the superscript c denotes the charge conjugation. Neutrino masses are generated at the loop level by

$$(m_\nu)_{ij} = \sum_k \frac{h_{ik}h_{jk}M_k}{16\,\pi^2}\left[\frac{m_H^2}{m_H^2-M_k^2}\ln\frac{m_H^2}{M_k^2} - \frac{m_A^2}{m_A^2-M_k^2}\ln\frac{m_A^2}{M_k^2}\right] \tag{3.29}$$

$$= \frac{\lambda_5 v^2}{8\pi^2}\sum_k \frac{h_{ik}h_{jk}M_k}{m_0^2-M_k^2}\left[1 - \frac{M_k^2}{m_0^2-M_k^2}\ln\frac{m_0^2}{M_k^2}\right], \tag{3.30}$$

where $m_0^2 = (m_H^2 + m_A^2)/2$.

The neutrino oscillation data Eq. (3.1) is explained by neutrino Yukawa coupling constants h_{ik} in this model. Neutrino mass of the flavor basis $(m_\nu)_{ij}$ is diagonalized by MNS matrix $U_{\rm MNS}$ as $U_{\rm MNS}^\dagger\, m_\nu\, U_{\rm MNS}^* = {\rm diag}(m_1 e^{i\alpha_1},\, m_2 e^{i\alpha_2},\, m_3 e^{i\alpha_3})$. Here, we impose normal hierarchy and $m_1 = 0, \delta = 0, \alpha_{1-3} = 0$ as input parameter.

Chapter 4

Inflation

The standard cosmology is a very successful model to explain the expansion of the Universe, the abundances of the light elements and the cosmic microwave background. However, we need inflation to solve horizon problem and flatness problem. In general, the inflation is explained by the exponential expansion [14]. But, we do not know the detail of the inflation. The scenario of slow-roll inflation [17] can be realized by a scalar particle, so-called the inflaton. If the inflation potential is given, parameters for the slow-roll inflation can be calculated.

We consider one possibility of inflation scenarios, the Higgs inflation scenario [18], where Higgs boson plays a role of inflaton. In this model, we introduce the coupling term of the Higgs field Φ with gravity as $\xi\Phi^\dagger\Phi\mathcal{R}$ ($\mathcal{R}$ is the Ricci scalar). Then, its coupling is too large $\xi \simeq 10^5$ from the primordial power spectrum of the curvature perturbation . Slow-roll parameters which are calculated by the inflation potential must satisfy the data from the Planck experiment [4]. The inflation scale ($\Lambda_{\rm I} = M_P/\sqrt{\xi}$ for the Higgs inflation scenario) is also calculated from the inflation potential. Constraints of the slow-roll inflation scenario can be satisfied with experiments. Especially, the data from the Planck experiment [4] support the Higgs inflation scenario.

4.1 Inconsistency between big-bang cosmology and observations

The Friedmann equation is given by

$$H^2 = \frac{8\pi G}{3}\rho - \frac{k}{R^2} \tag{4.1}$$

where $H \equiv \dot{R}/R$ is Hubble parameter. By introducing density parameter $\Omega \equiv \rho/\rho_c$ ($\rho_c \equiv 3H^2/8\pi G$ is the critical density), we obtain

$$\frac{k}{H^2R^2} = \Omega - 1. \tag{4.2}$$

The flat Universe satisfy $\Omega = 1$. Observed data of flatness show

$$|\Omega_0 - 1| \leq 0.2. \tag{4.3}$$

When we take $\Omega = \Omega_r + \Omega_m + \Omega_\Lambda (\Omega_r \equiv \rho_r/\rho_c \ , \ \Omega_m \equiv \rho_m/\rho_c \ , \ \Omega_\Lambda \equiv \rho_\Lambda/\rho_c)$ and $\rho = \rho_r + \rho_m + \rho_\Lambda (\rho_r \equiv \rho_{r,0}/R^4 \ , \ \rho_m \equiv \rho_{m,0}R^3 \ , \ \rho_\Lambda \equiv \rho_{\Lambda,0})$, we obtain

$$\frac{H^2}{H_0^2} = \frac{\Omega_{r,0}}{R^4} + \frac{\Omega_{m,0}}{R^3} + \frac{1-\Omega_0}{R^2} + \Omega_{\Lambda,0} \tag{4.4}$$

$$\Omega - 1 = \frac{R^2(\Omega_0 - 1)}{\Omega_{r,0} + \Omega_{m,0}R + (1-\Omega_0)R^2 + \Omega_{\Lambda,0}R^4} \tag{4.5}$$

by using $R_0 \equiv 1$. At Planck time $t_P = 5.391 \times 10^{-44}$sec $(R(t_P) = 2 \times 10^{-32})$,

$$\Omega_P - 1 \simeq \frac{R^2(\Omega_0-1)}{\Omega_{r,0}} \tag{4.6}$$

$$\leq \frac{(2\times 10^{-32})^2 \times 0.2}{8.4 \times 10^{-5}} \tag{4.7}$$

$$\leq \mathscr{O}(10^{-60}). \tag{4.8}$$

In the standard cosmology, we cannot explain this flatness naturally.

On the other hand, we define temperature fluctuation of the cosmic microwave background:

$$\left(\frac{\delta T}{T}\right)^2 \equiv \frac{l(l+1)}{2\pi} C_l. \tag{4.9}$$

where l $(\sim 180^\circ/\theta)$ is multipole, C_l is defined as partial wave expansion of temperature correlation function of two points

$$C(\theta) \equiv \frac{1}{4\pi} \sum_{l=0}^{\infty} (2l+1) C_l P_l(\cos\theta), \tag{4.10}$$

where C_l is partial wave amplitude and $P_l(\cos\theta)$ is Legendre polynomial. CMB temperature fluctuation $\delta T/T$ is observed at each l (namely, θ). In the region $l < 100$ $(\theta > 2^\circ)$, we observed

$$\frac{\delta T}{T} \simeq 10^{-5} (\theta > 2^\circ). \tag{4.11}$$

At the last scattering period, two points A and B are separated by the distance $d_H(t_{ls})$. At present, we observe as the distance $(1+z_{ls})d_H(t_{ls})$ where $z_{ls} \simeq 1000$ and $1 + z_{ls} = R(t_0)/R(t_{ls})$. When we observe two points of the distance $d_p(t_{ls} \to t_{t_0})$, the casual region θ is explained as

$$AB = (1+z_{ls}) d_H(t_{ls}) > d_p(t_{ls} \to t_{t_0})\theta, \tag{4.12}$$

$$\theta < \frac{(1+z_{ls})d_H(t_{ls})}{d_p(t_{ls} \to t_{t_0})}. \tag{4.13}$$

The relation

$$d_p(t_{ls} \to t_{t_0}) = 0.98 d_H(t_0) \tag{4.14}$$

show us

$$\theta < \frac{(1+z_{ls})d_H(t_{ls})}{d_H(t_0)} \tag{4.15}$$

$$< \frac{1000 \times 0.4 Mpc}{14000 Mps} \tag{4.16}$$

$$< 2^\circ. \tag{4.17}$$

In the standard cosmology, we cannot explain why two points are almost same property outside casual region.

To solve flatness problem and horizon problem, we need to explain inflation [14].

4.2 Slow-roll inflation

Models of inflation are explained by introducing scalar boson so-called inflaton [17] In the models of slow-roll inflation, the homogeneous evolution of the inflaton field φ is governed by the equation of motion

$$\ddot{\varphi} + 3H\dot{\varphi} + V(\varphi) = 0, \tag{4.18}$$

and the Friedmann equation

$$H^2 = \frac{1}{3M_P^2}, \tag{4.19}$$

where $H = \dot{a}/a$ is the Hubble parameter, $M_P^2 = (8\pi G)^{-1/2}$ is the reduced Planck mass, and $V(\varphi)$ is the scalar potential. On the other hand, the slow-roll parameters are defined by

$$\epsilon \equiv \frac{M_P^2}{2}\left(\frac{dV/d\varphi}{V}\right)^2, \tag{4.20}$$

$$\eta \equiv M_P^2\frac{d^2V/d\varphi^2}{V}. \tag{4.21}$$

Necessary conditions for the slow-roll scenario are $\epsilon \ll 1$ and $|\eta| \ll 1$.

4.3 Constraints from the cosmic microwave background data

It is convenient to expand the power spectra of curvature and tensor perturbations around a pivot scale k_0 as

$$\mathscr{P}_{\mathscr{R}} = A_s\left(\frac{k}{k_0}\right)^{n_s-1+\frac{1}{2}\frac{dn_s}{d\ln k}\ln\frac{k}{k_0}+\frac{1}{3!}\frac{d^2n_s}{d\ln k^2}(\ln kk_0)^2+\cdots}, \quad \mathscr{P}_t = A_t\left(\frac{k}{k_0}\right)^{n_t+\frac{1}{2}\frac{dn_t}{d\ln k}\ln\frac{k}{k_0}+\cdots}, \tag{4.22}$$

where A_s (A_t) is the scalar (tensor) amplitude and n_s (n_t), $dn_s/d\ln k$ ($dn_t/d\ln k$) and $d^2n_s/d\ln k^2$ are the scalar (tensor) spectral index, the running of the scalar (tensor) spectral index, and the running of the running of the scalar spectral index, respectively. From the scalar potential, the parameters of the scalar and tensor power spectra may be calculated approximately in the framework of the slow-roll approximation by evaluating the following equations at the value of the inflation field φ_0. The number of e-folding before the end of inflation, N_0, at which the

pivot scale k_0 becomes

$$\begin{aligned} N_0 &= \int_{t_0}^{t_{\rm end}} dt\, H && (4.23)\\ &= \int_{\varphi_0}^{\varphi_{\rm end}} \frac{d\varphi}{\dot\varphi} H && (4.24)\\ &= \frac{1}{M_P^2}\int_{\varphi_{\rm end}}^{\varphi_0} V V_\varphi d\varphi && (4.25)\\ &= \frac{1}{M_P}\int_{\varphi_{\rm end}}^{\varphi_0} \frac{d\varphi}{\sqrt{2\epsilon}}, && (4.26) \end{aligned}$$

where the field value at the end of inflation $\varphi_{\rm end}$ is given by

$$\max\{\epsilon(\varphi_{\rm end}), |\eta(\varphi_{\rm end})|\} = 1. \tag{4.27}$$

From the e-folding number $50 < N_0 < 60$ constrained by the Planck experiment [4], the field value at the initial of inflation φ_0 is determined. Then, we can calculate n_s, r and A_s, as

$$A_s \equiv \frac{V(\varphi_0)}{24\pi M_P^4 \epsilon(\varphi_0)}, \tag{4.28}$$

$$n_s \equiv 1 - 6\epsilon + 2\eta, \quad r \equiv 16\epsilon. \tag{4.29}$$

At the pivot scale $k_0 = 0.05{\rm Mpc}^{-1}$, the scalar amplitude A_s and the spectral index n_s of the base ΛCDM model are constrained by the Planck 2015 data as [4]

$$A_s = 2.196^{+0.080}_{-0.078}) \times 10^{-9}, \quad n_s = 0.9655 \pm 0.0062 \quad (68\%\ {\rm CL, Planck\ TT+lowP}), \tag{4.30}$$

assuming $dn_s/d\ln k = d^2 n_s/d\ln k^2 = r = 0$. The Planck 2015 have shown upper bound on the r for the ΛCDM+r model as [4]

$$\begin{aligned} &r_{0.002} < 0.10 (95\%\ {\rm CL, Planck\ TT+lowP}), && (4.31)\\ &r_{0.002} < 0.11 (95\%\ {\rm CL, Planck\ TT+lowP+lensing}), && (4.32)\\ &r_{0.002} < 0.11 (95\%\ {\rm CL, Planck\ TT+lowP+BAO}), && (4.33)\\ &r_{0.002} < 0.10 (95\%\ {\rm CL, Planck\ TT,TE,EE+lowP}). && (4.34) \end{aligned}$$

4.4 Higgs inflation

Higgs inflation is realized by introducing the non-minimal gravitational coupling ξ [18]. The scalar sector of SM, coupled to gravity is given by

$$\begin{aligned} \frac{\mathcal{L}_J}{\sqrt{-g^J}} &= |D_\mu H|^2 - \mu^2 H^\dagger H - \lambda (H^\dagger H)^2 - \frac{M_P^2}{2}\mathcal{R} - \xi H^\dagger H \mathcal{R} && (4.35)\\ &= \frac{1}{2}(\partial_\mu h)^2 - \frac{\lambda}{4}(h^2 - v^2)^2 - \frac{M_P^2}{2}\mathcal{R} - \frac{1}{2}\xi h^2 \mathcal{R}. && (4.36) \end{aligned}$$

where Higgs field is unitary gauge $H = (1/\sqrt{2})\begin{pmatrix} 0 & h+v \end{pmatrix}^T$ and $\mathcal{R}$ is Ricci scalar.

By making conformal transformation from Jordan frame to the Einstein frame $g^E_{\mu\nu} = \Omega^2 g^J_{\mu\nu}$; $\Omega^2 = 1 + \xi h^2/M_P^2$, it is possible to get rid of non-minimal coupling

$$\begin{aligned}\frac{\mathcal{L}_E}{\sqrt{-g^E}} &\rightarrow \frac{1}{\Omega^2}\frac{1}{2}(\partial_\mu h)^2 + \frac{1}{\Omega^4}\frac{3\xi^2 h^2}{M_P^2}(\partial_\mu h)^2 - \frac{1}{\Omega^4}\frac{\lambda}{4}(h^2 - v^2)^2 \\ &+ \frac{1}{\Omega^2}\frac{1}{8}\left[2g^2(v+h)^2 W^+_\mu W^{-\mu} + (g^2 + g'^2)(v+h)^2 Z_\mu Z^\mu\right] - \frac{M_P^2}{2}\hat{\mathcal{R}}. \end{aligned} \tag{4.37}$$

where $\mathcal{R} = \Omega^{-2}\hat{\mathcal{R}} + 6\Omega^{-3}\Omega_{;\mu\nu}g^{E\mu\nu}$. Then, we define each part of this Lagrangian as

$$\mathcal{L}_{\rm kin} \equiv \frac{1}{\Omega^2}\frac{1}{2}(\partial_\mu h)^2 + \frac{1}{\Omega^4}\frac{3\xi^2 h^2}{M_P^2}(\partial_\mu h)^2, \;\; \mathcal{L}_{\rm scalar}(\equiv -V) \equiv -\frac{1}{\Omega^4}\frac{\lambda}{4}(h^2 - v^2)^2,$$
$$\mathcal{L}_{\rm gauge} \equiv \frac{1}{\Omega^2}\frac{1}{8}\left[2g^2(v+h)^2 W^+_\mu W^{-\mu} + (g^2 + g'^2)(v+h)^2 Z_\mu Z^\mu\right], \;\; \mathcal{L}_{\rm grav} \equiv -\frac{M_P^2}{2}\hat{\mathcal{R}}.$$

With the redefinition of the field

$$\frac{d\chi}{dh} = \sqrt{\frac{\Omega^2 + \frac{6\xi^2 h^2}{M_P^2}}{\Omega^4}}, \tag{4.38}$$

the kinetic term is canonically normalized $\mathcal{L}_{\rm kin} = (\partial_\mu \chi)^2/2$. At the electro-weak scale ($\Omega^2 \simeq 1$, $h \simeq \chi$), it is same as Higgs potential of SM

$$V(\chi) = \frac{\lambda}{4}(\chi^2 - v^2)^2. \tag{4.39}$$

In the limit of $h \gg M_P/\sqrt{\xi}$ $\left(h \simeq (M_P/\sqrt{\xi})\exp(\chi/\sqrt{6}M_P)\right)$, the scalar potential is given by

$$V(\chi) \quad = \frac{\lambda M_P^4}{4\xi^2}\left(1 + \exp\left(-\frac{2\chi}{\sqrt{6}M_P}\right)\right)^{-2} \tag{4.40}$$

This potential is behave as $V(\chi \rightarrow \infty) = \lambda M_P^4/4\xi^2$.

To explain observation of CMB, we evaluate slow-roll parameter

$$\epsilon = \frac{M_P^2}{2}\left(\frac{dV/d\chi}{V}\right)^2 \simeq \frac{4M_P^4}{3\xi^2 h^4}, \quad \eta = M_P^2\frac{d^2V/d\chi^2}{V} \simeq -\frac{4M_P^2}{3\xi h^2}. \tag{4.41}$$

Slow-roll end $\epsilon_{\rm end} \simeq 1$ gives the field value at the end of inflation

$$h_{\rm end} \simeq \left(\frac{4}{3}\right)^{\frac{1}{4}}\frac{M_P}{\sqrt{\xi}} \simeq 1.07\frac{M_P}{\sqrt{\xi}}. \tag{4.42}$$

The e-folding number is given by

$$N_0 \quad \equiv \int_{h_{end}}^{h_0}\frac{1}{M_P^2}\frac{V}{dV/dh}\left(\frac{d\chi}{dh}\right)^2 dh \tag{4.43}$$
$$\simeq \frac{6}{8}\frac{h_0^2 - h_{end}^2}{M_P^2/\xi}. \tag{4.44}$$

When the value of $50 < N < 60$, initial value of the field is given by

$$h_0 \simeq 9.4\frac{M_P}{\sqrt{\xi}}. \tag{4.45}$$

On the other hand, the scalar amplitude (4.29) satisfying the constraint of Planck (4.30) give

$$\xi \simeq 49000\sqrt{\lambda}. \tag{4.46}$$

In this relation, observable parameter is given by

$$n_s \equiv 1 + 2\eta - 6\epsilon \simeq 0.97, \quad r \equiv 16\epsilon \simeq 0.0033. \tag{4.47}$$

Chapter 5

Baryon asymmetry of the Universe

Baryon asymmetry of the Universe [68] is known as one of the beyond the SM phenomena. Among various scenarios of BAU, electroweak baryogenesis (EWBG) [19] is directly connected with physics of the Higgs sector, requiring a strongly first order phase transition (1stOPT) at the electroweak symmetry breaking (EWSB) and also additional CP violating phases. Such a scenario can be tested by experimental determination of the property of the Higgs sector. For instance, the condition of the strongly 1stOPT can predict a significant deviation (order of several tens percent) in the triple Higgs boson coupling (the hhh coupling) from the SM prediction [20], and the required CP violating phases lead to appearance of electric dipole moments, etc. At the LHC experiment and its high luminosity one, the measurement of the hhh coupling seems to be challenging. There is still a hope that in future the hhh coupling could be measured by 13% accuracy [21] at the upgraded version of the International Linear Collider (ILC).

5.1 Baryon number

5.1.1 Definition of baryon asymmetry

The baryon asymmetry is characterized by the ratio of the baryon number to entropy

$$\frac{n_B}{s} \equiv \frac{n_b - n_{\bar{b}}}{s} \tag{5.1}$$

where s is the entropy density and n_b ($n_{\bar{b}}$) is the (anti)baryon number density. The photon density n_γ is related to s by $s = 7.04 n_\gamma$ at present. We can determine Eq. (5.1) by the value of $\eta \equiv n_B/n_\gamma$.

5.1.2 Observations

When the ratio of proton and neutron is freezeout $(n_n/n_p)_{\text{freezeout}} \simeq 1/7$, ^{4}He mass fraction $Y_p \equiv \rho_{^4He}/\rho_B$ is fixed as

$$\begin{aligned} Y_p &\simeq \frac{4 m_N n_{^4He}}{m_N (n_n + n_p)} && (5.2) \\ &\simeq \frac{2\left(\frac{n_n}{n_p}\right)_{\text{freezeout}}}{\left(\frac{n_n}{n_p}\right)_{\text{freezeout}} + 1} \quad \text{(We take } n_{^4He} = \frac{n_n}{2} \text{ and } m_N \simeq m_p \simeq m_n\text{)} && (5.3) \\ &\simeq 0.25. && (5.4) \end{aligned}$$

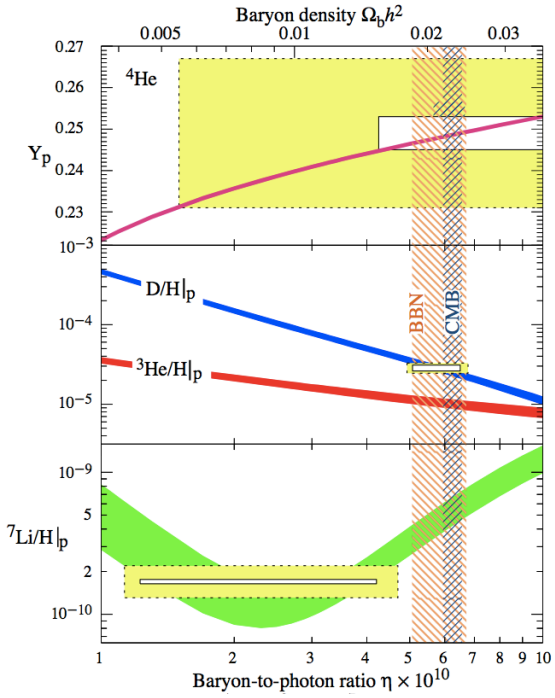

Figure 5.1: The abundances of ^{4}He, D, ^{3}He and ^{7}Li as predicted by the standard model of Big-Bang nucleosynthesis. The narrow vertical band indicates the CMB measure of the cosmic baryon density, while the wider band indicates the BBN concordance range (both at 95% CL). This figure is quoted by [68].

The abundances of ^{4}He, D, ^{3}He and ^{7}Li as predicted by the standard model of Big-Bang nucleosynthesis is shown in Fig. 5.1. To explain the light-elements abundances within the framework of the standard big-bang nucleosynthesis, it is required that $\eta \simeq 10^{-10}$. Thus, we obtain [68]

$$\frac{n_B}{s} \simeq \mathscr{O}(10^{-10}). \tag{5.5}$$

5.2 Sakharov's three condition

To explain the BAU, Sakharov's three conditions [15] must be satisfied:

- baryon number violation,
- C and CP violation,
- departure from equilibrium.

In the framework of the SM, the observed Higgs mass cannot satisfy these conditions. Therefore, we need new physics by the extension from SM.

5.3 Scenarios for baryogenesis

There are some scenarios to solve this problem. For example, Leptogenesis, EWBG, etc.

5.3.1 Leptogenesis

A scenario of Leptogenesis [69] is realized by the seesaw mechanism. Indeed, the seesaw mechanism requires that violated lepton number provides in general new CP violating phases in the neutrino Yukawa interactions and decay out of equilibrium. Thus, all three Sakharov's conditions are naturally fulfilled in this scenario. A review paper of Leptogenesis is [70].

5.3.2 Electroweak baryogenesis

For a scenario of EWBG [19], Sakharov's three conditions are satisfied sphaleron process, CP violating phases and strongly first order phase transition (1stOPT) [71]. One of the necessary conditions [15] to generate BAU is the departure from thermal equilibrium. To satisfy this condition (the so-called sphaleron decoupling condition), the baryon number changing sphaleron interaction must quickly decouple in the broken phase, which is described by

$$\Gamma_{\rm sph}(T) \lesssim H(T), \tag{5.6}$$

where $\Gamma_{\rm sph}(T)$ is the reaction rate of the sphaleron process and $H(T)$ is the Hubble parameter at T. $\Gamma_{\rm sph}(T)$ can be obtained by demanding that the baryon number changing rate in the broken phase [72]

$$\Gamma(T)_{\rm sph} \equiv -\frac{1}{B}\frac{dB}{dt} \simeq \frac{13N_f}{4\cdot 32\pi^2}\frac{\omega_-}{\alpha_W^3}\mathcal{N}e^{-E_{\rm sph}/T}, \tag{5.7}$$

where N_f is number of generation, $\alpha_W = \alpha_{\rm em}/\sin^2\theta(m_Z)$, ω_- is the negative mode of the fluctuations around sphaleron, $\mathcal{N}$ represents the translational and rotational zero-mode factors of the fluctuations about the sphaleron, and the sphaleron energy is denoted as $E_{\rm sph} = 4\pi\varphi(T)\mathcal{E}(T)/g_2$. Then, Eq. (5.6) can be translated into the condition of a strongly 1stOPT

$$\frac{\varphi_c}{T_c} > \zeta_{\rm sph}(T_c), \tag{5.8}$$

where φ_c gives the broken phase minimum at the critical temperature T_c, and $\zeta_{\rm sph}$ is given by [73]

$$\zeta_{\rm sph}(T) \equiv \frac{g_2}{4\pi\mathcal{E}(T)}\left[42.97 + \ln\mathcal{N} + \ln\left(\frac{\omega_-}{m_W}\right) - \frac{1}{2}\ln\left(\frac{g_*}{106.75}\right) - 2\ln\left(\frac{T}{100\ {\rm GeV}}\right)\right]. \tag{5.9}$$

As an example, $\zeta_{\rm sph} \simeq 1.24$ in the SM [73], 0.9 in the MSSM [73] and 1.1-1.2 in the real singlet-extended standard model [74]. As shown in these results, we can take typically $\zeta_{\rm sph} \simeq 1$.

5.4 First order electroweak phase transition

5.4.1 Electroweak phase transition

For the case of 1stOPT, the effective potential of finite temperature have degenerate vacuum $\phi = 0(\equiv \phi_S), \phi_c(\equiv \phi_B)$ at the critical temperature $T = T_c$, as shown in Fig. 5.2. The true vacuum depending on the temperature is the non-continuous behavior in this case. For the case of second order phase transition, the true vacuum depending on the temperature is continuous behavior.

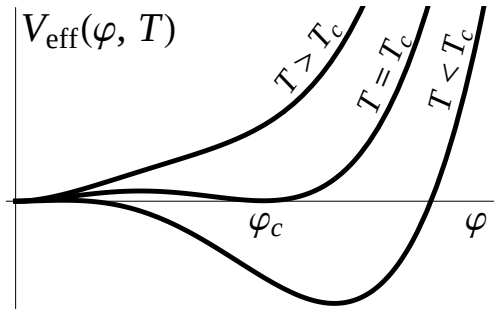

Figure 5.2: Behavior of EWPT for the case of 1stOPT. The effective potential of finite temperature depends on the temperature vs order parameter.

5.4.2 First order electroweak phase transition for two Higgs doublet model

The condition of strongly 1st order EWPT is realized by the non-decoupling effect due to the additional scalar. Furthermore, we can test such scenario by measuring the deviation of the triple Higgs boson coupling. In this section, we consider the two Higgs doublet model (2HDM) as the example, based on [20, 75–77].

Effective potential at zero temperature

The Higgs potential of the 2HDM is given by

$$\begin{aligned} V_{\rm tree}^{\rm 2HDM} &= m_1^2|\Phi_1|^2 + m_2^2|\Phi_2|^2 - (m_3^2\Phi_1^\dagger\Phi_2 + h.c.) \\ &+ \frac{1}{2}\lambda_1|\Phi_1|^4 + \frac{1}{2}\lambda_2|\Phi_2|^4 + \lambda_3|\Phi_1|^2|\Phi_2|^2 + \lambda_4(\Phi_1^\dagger\Phi_2)(\Phi_2^\dagger\Phi_1) + \left[\frac{1}{2}\lambda_5(\Phi_1^\dagger\Phi_2)^2 + h.c.\right]. \end{aligned}$$

where m_{1-3}^2 are parameters with its mass dimension two, and λ_{1-5} is the self-coupling constants of the scalar bosons. After the EWSB, the Higgs doublets are parametrized as

$$\Phi_1 = \begin{pmatrix} w^\pm \\ \frac{1}{\sqrt{2}}(v_1 + h + i\,z_1) \end{pmatrix}, \quad \Phi_2 = \begin{pmatrix} H^+ \\ \frac{1}{\sqrt{2}}(v_2 + H^0 + iA^0) \end{pmatrix} \tag{5.10}$$

where $\omega^\pm$ and z are Nambu-Goldstone bosons and v ($\simeq 246$ GeV) is the vacuum expectation value (VEV). The mass of h is set as $m_h = 125$ GeV.

One-loop effective potential at zero temperature We parametrize m_3^2 and the Higgs VEVs as

$$M^2 \equiv \frac{m_3^2}{\sin\beta\cos\beta}, \quad \langle\Phi_1\rangle = \begin{pmatrix} 0 \\ \frac{1}{\sqrt{2}}\varphi_1 \end{pmatrix} = \begin{pmatrix} 0 \\ \frac{1}{\sqrt{2}}\varphi\cos\beta \end{pmatrix}, \quad \langle\Phi_2\rangle = \begin{pmatrix} 0 \\ \frac{1}{\sqrt{2}}\varphi_2 \end{pmatrix} = \begin{pmatrix} 0 \\ \frac{1}{\sqrt{2}}\varphi\sin\beta \end{pmatrix} \tag{5.11}$$

and we take $\sin(\beta-\alpha) = -1, \tan\beta = 1$, then

$$M^2 = 2m_3^2, \quad \langle\Phi_1\rangle = \langle\Phi_2\rangle = \begin{pmatrix} 0 \\ \frac{1}{2}\varphi \end{pmatrix}. \tag{5.12}$$

For simplicity, we assume

$$\lambda_1 = \lambda_2 \equiv \lambda, \quad m_1 = m_2 \equiv m. \tag{5.13}$$

The mass formula of additional scalar bosons are given by

$$m_H^2 = M^2 + \frac{1}{2}(\lambda - (\lambda_3 + \lambda_4 + \lambda_5))v^2 = M^2 + m_h^2 - (\lambda_3 + \lambda_4 + \lambda_5)v^2, \tag{5.14}$$

$$m_A^2 = M^2 - \lambda_5 v^2, \quad m_{H^\pm}^2 = M^2 - \frac{1}{2}(\lambda_4 + \lambda_5)v^2. \tag{5.15}$$

We consider the case of degenerate additional scalar bosons $m_\Phi = m_H = m_A = m_H^\pm$.

The one-loop effective potential at zero temperature is given by

$$V_{\rm eff}(\varphi, T=0) = V_0(\varphi) + \Delta V_1(\varphi) + V^{\rm c.t.}(\varphi). \tag{5.16}$$

The tree level potential $V_0(\varphi)$ and the one-loop potential $\Delta V_1(\varphi)$ are given by

$$V_0(\varphi) = -\frac{\mu^2}{2}\varphi^2 + \frac{\lambda}{8}\varphi^4, \tag{5.17}$$

$$\Delta V_1(\varphi) = \sum_i \frac{n_i}{64\,\pi^2} M_i^4(\varphi) \left\{ \ln \frac{M_i^2(\varphi)}{Q^2} - c_i - \Delta \right\}, \tag{5.18}$$

where c_i=3/2, $\Delta = \frac{1}{\epsilon} - \gamma + \ln 4\pi$, $M_i(\varphi)$ and n_i are the field-dependent mass and the degrees of freedom for each particles F_i, respectively

$$n_{W_L^\pm} = 4, \quad n_{Z_L} = 2, \quad n_{\gamma_L} = 2, \quad n_{W_T^\pm} = 2, \quad n_{Z_T} = 1, \quad n_{\gamma_T} = 1, \quad n_t = -12, \quad n_b = -12, \tag{5.19}$$

and Q is the renormalization scale. The counter term of the dimension full parameter μ^2 is given by

$$V^{\rm c.t.}(\varphi) = -\frac{1}{2}\delta\mu^2\varphi^2. \tag{5.20}$$

If we define the renormalized vacuum expectation value v, the renormalized mass of the Higgs boson m_h at the one loop level by the following three conditions ($\overline{\rm DR}$ renormalization scheme),

$$0 \equiv \left.\frac{\partial V_{\rm eff}(\varphi, T=0)}{\partial \varphi}\right|_{\varphi=v}, \quad m_h^2 \equiv \left.\frac{\partial^2 V_{\rm eff}(\varphi, T=0)}{\partial \varphi^2}\right|_{\varphi=v},$$

we obtain

$$\ln Q^2 = \frac{\sum_i n_i \left(\left.\frac{\partial M_i^2(\varphi)}{\partial \varphi}\right|_{\varphi=v}\right)^2 \ln m_i^2}{\sum_i n_i \left(\left.\frac{\partial M_i^2(\varphi)}{\partial \varphi}\right|_{\varphi=v}\right)^2}, \quad \delta\mu^2 = \sum_i \frac{n_i m_i^2}{32\pi^2 v} \left.\frac{\partial M_i^2(\varphi)}{\partial \varphi}\right|_{\varphi=v} \left(\ln \frac{m_i^2}{Q^2} - 1\right),$$

where m_i is the physical mass of the i-th particle running in the loop.

Thus, the tree potential $V_0(\varphi)$ and the renormalized one-loop potential $\Delta V_1(\varphi)$ are obtained as

$$V_0(\varphi) = \frac{m_h^2}{8v^2}(\varphi^2 - v^2)^2, \tag{5.21}$$

$$\begin{aligned}\Delta V_1(\varphi) = &\sum_{i=W^\pm,Z,\gamma,t,b} \frac{n_i}{64\,\pi^2}\left(2m_i^2 M_i^2(\varphi) + M_i^4(\varphi)\left\{\ln\frac{M_i^2(\varphi)}{m_i^2} - \frac{3}{2}\right\} + \{M_i^4(\varphi) - 2m_i^2 M_i^2(\varphi)\}\ln\frac{m_i^2}{Q^2}\right) \\ &+ \sum_{\Phi}\frac{1}{64\,\pi^2}\left(2m_\Phi^2(M_\Phi^2(\varphi) - M^2) + M_\Phi^4(\varphi)\left\{\ln\frac{M_\Phi^2(\varphi)}{m_\Phi^2} - \frac{3}{2}\right\} + \{M_\Phi^4(\varphi) - 2m_\Phi^2(M_\Phi^2(\varphi) - M^2)\}\ln\frac{m_\Phi^2}{Q^2}\right).\end{aligned} \tag{5.22}$$

Here, we have neglected the one loop contribution of the Higgs boson.

The renormalized triple Higgs boson coupling is calculated at the one loop level in SM as

$$\begin{aligned}\lambda_{hhh}^{\rm 2HDM} &\equiv \left.\frac{\partial^3 V_{\rm eff}(\varphi, T=0)}{\partial\varphi^3}\right|_{\varphi=v} \\ &= \frac{3m_h^2}{v}\left\{1 + \frac{m_H^4}{12\pi^2 m_h^2 v^2}\left(1 - \frac{M^2}{m_H^2}\right)^3 + \frac{m_A^4}{12\pi^2 m_h^2 v^2}\left(1 - \frac{M^2}{m_A^2}\right)^3 + \frac{m_{H^\pm}^4}{6\pi^2 m_h^2 v^2}\left(1 - \frac{M^2}{m_{H^\pm}^2}\right)^3 - \frac{N_{c_t} m_t^4}{3\pi^2 m_h^2 v^2}\right\}\end{aligned} \tag{5.23}$$

The triple Higgs boson coupling at one-loop in the SM $\lambda_{hhh}^{\rm SM}$ is approximately given by [75]

$$\lambda_{hhh}^{\rm SM} = \frac{3m_h^2}{v}\left(1 - \frac{m_t^4}{\pi^2 m_h^2 v^2}\right). \tag{5.24}$$

Then, deviation of the triple Higgs boson coupling from the SM is defined by

$$\frac{\Delta\lambda_{hhh}}{\lambda_{hhh}^{\rm SM}} = \frac{\lambda_{hhh}^{\rm 2HDM}}{\lambda_{hhh}^{\rm SM}} - 1. \tag{5.25}$$

The behavior of $\Delta\lambda_{hhh}/\lambda_{hhh}^{\rm SM}$ is shown in Fig. 5.3.

Effective potential at finite temperature

When we consider a ring-improved effective potential by replacing the field-dependent masses in Eq. (9.5) as [78]

$$M_i^2(\varphi) \to M_i^2(\varphi, T) = M_i^2(\varphi) + \Pi_i(T), \tag{5.26}$$

where $\Pi_i(T)$ is the finite temperature contribution to the self-energies, field dependent masses of the gauge bosons in the one-loop contribution at zero temperature are replaced by thermally corrected ones

$$\Delta V_1(\varphi) \to \Delta V_1(\varphi, T). \tag{5.27}$$

The thermally corrected field-dependent masses of the gauge bosons are explained by

$$M_g^{2(L,T)}(\varphi, T) = \frac{\varphi^2}{4}\begin{pmatrix} g^2 & & & \\ & g^2 & & \\ & & g^2 & gg' \\ & & gg' & g'^2 \end{pmatrix} + a_g^{L,T}T^2\begin{pmatrix} g^2 & & & \\ & g^2 & & \\ & & g^2 & \\ & & & g'^2 \end{pmatrix} \tag{5.28}$$

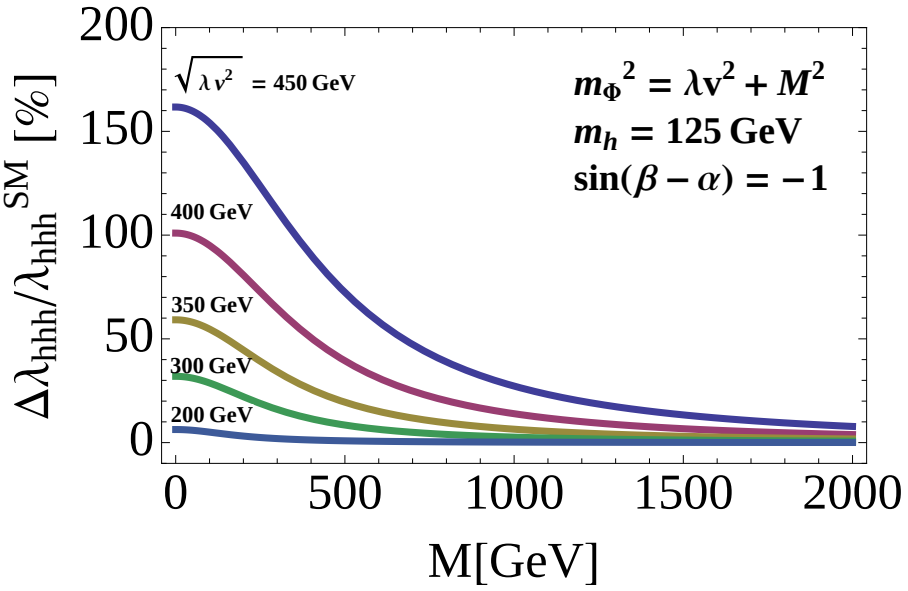

Figure 5.3: The decoupling behavior of $\Delta\lambda_{hhh}/\lambda_{hhh}^{\rm SM}$. The mass of the heavy Higgs bosons $m_\Phi \equiv m_H = m_A = m_{H^\pm}$ is given by $m_\Phi^2 = \lambda v^2 + M^2$. This figure is based on [75, 76].

in the (W^+, W^-, W^3, B) basis with $a_g^L = 2$ (11/6 in the absecce of the second Higgs doublet), $a_g^T = 0$. Notice that only the self-energy for the longitudinal modes of the gauge bosons receive thermal corrections. The field-dependent masses of fermions do not receive thermal corrections,

$$M_{t,b}^2(\varphi) = m_{t,b}^2 \frac{\varphi^2}{v^2}. \tag{5.29}$$

The thermally corrected field-dependent mass of the singlet scalars are explained by

$$M_\Phi^2(\varphi, T) = M^2 - \frac{1}{2}m_h^2 + (m_\Phi^2 - M^2 + \frac{1}{2}m_h^2)\frac{\varphi^2}{v^2}, \tag{5.30}$$

where $\Pi_\Phi(T) = (T^2/12v^2)(6m_{W^\pm}^2 + 3m_Z^2 + 5m_h^2 + 4m_\Phi^2 - M^2 + 6m_t^2 + 6m_b^2)$.

The effective potential at finite temperatures is given at the one-loop level by

$$V_{\rm eff}(\varphi, T) = V_0(\varphi) + \Delta V_1(\varphi, T) + \Delta V_T(\varphi, T). \tag{5.31}$$

The finite-temperature contribution to the effective potential is written as

$$\Delta V_T(\varphi, T) = \frac{T^4}{2\pi^2}\left\{ \sum_{i=W^\pm, Z, \gamma, S} n_i I_{\rm B}(a_i^2) + \sum_{i=t,b} n_i I_{\rm F}(a_i^2) \right\} \tag{5.32}$$

where $I_{\rm B,F}(a_i^2) \equiv \int_0^\infty dx\, x^2 \ln\left(1 \mp \exp\left(-\sqrt{x^2 + a_i^2}\right)\right)$ with $a_i = M_i(\varphi, T)/T$. If we take $a^2 \ll 1$, we can understand the behavior of $I_{\rm B,F}(a_i^2)$ approximately:

$$I_{\rm B}(a^2) = -\frac{\pi^4}{45} + \frac{\pi^2}{12}a^2 - \frac{\pi}{6}(a^2)^{3/2} - \frac{a^4}{32}\left(\ln\frac{a^2}{\alpha_{\rm B}} - \frac{3}{2}\right) + \frac{\zeta(3)}{96(2\pi)^2}a^6 - \frac{\zeta(5)}{256(2\pi)^4}a^8 + \cdots, \tag{5.33}$$

$$I_{\rm F}(a^2) = \frac{7\pi^4}{360} - \frac{\pi^2}{24}a^2 - \frac{a^4}{32}\left(\ln\frac{a^2}{\alpha_{\rm F}} - \frac{3}{2}\right) + \frac{7\zeta(3)}{96(2\pi)^2}a^6 - \frac{31\zeta(5)}{256(2\pi)^4}a^8 + \cdots, \tag{5.34}$$

where, $\ln \alpha_{\rm B} = 2\ln(4\pi) - 2\gamma_{\rm E} \simeq 3.91, \ln \alpha_{\rm F} = 2\ln\pi - 2\gamma_{\rm E} \simeq 1.14$ and $\gamma_{\rm E}$ is Euler constant.

We can calculate ϕ_c/T_c on each (M, m_Φ) from above effective potential as shown in Fig. 5.4.

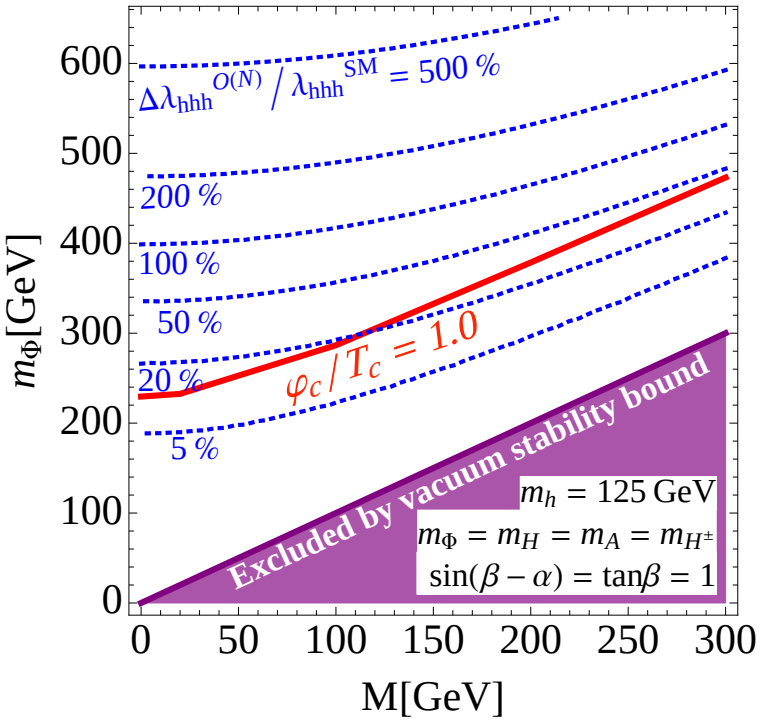

Figure 5.4: The allowed region which satisfy $\varphi_c/T_c > 1$, where EWBG can be viable with the strongly 1stOPT on the plane of m_Φ and M Contours for the deviation in the hhh coupling from the SM prediction are also shown. Bounds from vacuum stability is also shown. This figure is based on [20].

Part III

Radiative seesaw models

Chapter 6

Neutrinophilic two Higgs doublet model

If the neutrinophilic scalars in the νTHDM exist within the experimentally accessible energy scale (namely the TeV-scale), decays of the neutrinophilic charged scalar into leptons can provide direct information on the neutrino mass matrix because it is proportional to the matrix of new Yukawa coupling constants for the neutrinophilic scalar field [64, 79]. In such a case, the smallness of a new VEV which is relevant to Dirac neutrino masses is interpreted by the smallness of a soft-breaking parameter of the global $U(1)_X$ symmetry. Because lepton number violation which is caused by masses of the Majorana neutrinos has not been discovered, it is worth considering the possibility that neutrinos are not Majorana fermions but Dirac fermions similarly to charged fermions. It seems then better to have a suppression mechanism for the soft-breaking parameter by extending the νTHDM with TeV scale particles including a dark matter candidate. The existence of dark matter has also been established in cosmological observations [1, 3], and it is an important guideline for constructing new physics models.

The reason why the neutrino masses are tiny can be explained by a mechanism that the interaction of neutrinos with the SM Higgs boson is generated via a loop diagram involving a dark matter candidate in the loop while the interaction is forbidden at the tree level [25–27, 80–85]. Notice that smallness of neutrino masses in such radiative mechanisms does not require new particles to be very heavy. Similarly, if neutrino masses arise from a new VEV, smallness of neutrino masses can be explained by assuming that the VEV is generated at the loop level by utilizing a dark matter candidate [86]. In this paper, we extend the νTHDM such that the new VEV is generated at the one-loop level (see also Ref. [87]) where a dark matter candidate is involved in the loop.

This chapter is organized as follows. The νTHDM is extended in Sec. 6.1 such that a small VEV is generated via the one-loop diagram which involving a dark matter candidate in the loop. Section 6.2 is devoted to discussion on phenomenology in the extended νTHDM. We conclude in Sec. 6.3. This chapter is based on [88].

6.1 An extension of the νTHDM

Since we try to generate $\mu^2_{\Phi 12}$ in Eq. (3.19) at the loop level, it does not appear in the Lagrangian. Then the $U(1)_X$ symmetry should be broken spontaneously. For the spontaneous breaking, we rely on an additional scalar s_1^0 which is a singlet field under the SM gauge group. Similarly to the singlet Majoron model [89] where a VEV of a singlet field spontaneously breaks the lepton number conservation by two units, the Nambu-Goldstone boson from s_1^0 is

	ν_{iR}	$\Phi_\nu = \begin{pmatrix}\phi_\nu^+ \\ \phi_\nu^0\end{pmatrix}$	$\eta = \begin{pmatrix}\eta^+ \\ \eta^0\end{pmatrix}$	s_1^0	s_2^0
$SU(2)_L$	$\underline{\mathbf{1}}$	$\underline{\mathbf{2}}$	$\underline{\mathbf{2}}$	$\underline{\mathbf{1}}$	$\underline{\mathbf{1}}$
$U(1)_Y$	0	1/2	1/2	0	0
Global $U(1)_X$	3	3	3/2	1	1/2

Table 6.1: New particles which are added to the SM in our model.

acceptable [89]; the Nambu-Goldstone boson couples first with only neutrinos among fermions. If $\mathrm{U}(1)_X$-charges of Φ_ν and s_1^0 are 3 and 1, respectively, a dimension-5 operator $(s_1^0)^3\Phi_\nu^\dagger\Phi$ is allowed by the $\mathrm{U}(1)_X$ symmetry although $\Phi_\nu^\dagger\Phi$ is forbidden. Then, $\mu_{\Phi 12}^2$ is generated from the dimension-5 operator with the VEV of s_1^0. In this paper, we show the simplest realization of the dimension-5 operator at the one-loop level where dark matter candidates are involved in the loop.

Table 6.1 is the list of new particles added to the SM. In the table, ν_{iR} and Φ_ν are the particles which exist in the νTHDM. The $\mathrm{U}(1)_X$ symmetry is spontaneously broken by the VEV of s_1^0. We take a scenario where η and s_2^0 do not have VEVs. Since their $\mathrm{U}(1)_X$-charges are half-integers while the one for s_1^0 is an integer, a Z_2 symmetry remains unbroken after the $\mathrm{U}(1)_X$ breaking. Here, η and s_2^0 are Z_2-odd particles. The Z_2 symmetry stabilizes the lightest Z_2-odd particle which can be a dark matter candidate.

The Yukawa interaction in this model is identical to those in the νTHDM (see Eq. (3.13)). The scalar potential in this model is expressed as

$$\begin{aligned} V &= -\mu_{s1}^2|s_1^0|^2 + \mu_{s2}^2|s_2^0|^2 - \mu_{\Phi 1}^2\Phi^\dagger\Phi + \mu_{\Phi 2}^2\Phi_\nu^\dagger\Phi_\nu + \mu_\eta^2\eta^\dagger\eta \\ &\quad - \left(\mu\, s_1^{0*}(s_2^0)^2 + \text{h.c.}\right) \\ &\quad + \left(\lambda_{s\Phi 1\eta}\, s_1^{0*}(s_2^0)^*\Phi^\dagger\eta + \text{h.c.}\right) + \left(\lambda_{s\Phi 2\eta}\, s_1^0 s_2^0\Phi_\nu^\dagger\eta + \text{h.c.}\right) + \cdots . \end{aligned} \tag{6.1}$$

Only the relevant parts to our discussion are presented in Eq. (6.1). The other terms are shown in Appendix. Parameters μ, $\lambda_{s\Phi 1\eta}$, and $\lambda_{s\Phi 2\eta}$ are taken to be real and positive values by rephasing of scalar fields without loss of generality. At the tree level, v_ν, v, and v_s ($= \sqrt{2}\langle s_1^0\rangle$) are given by

$$v_\nu = 0, \quad \begin{pmatrix} v^2 \\ v_s^2 \end{pmatrix} = \frac{2}{4\lambda_{s1}\lambda_{\Phi 1} - \lambda_{s1\Phi 1}^2} \begin{pmatrix} 2\lambda_{s1} & -\lambda_{s1\Phi 1} \\ -\lambda_{s1\Phi 1} & 2\lambda_{\Phi 1} \end{pmatrix} \begin{pmatrix} \mu_{\Phi 1}^2 \\ \mu_{s1}^2 \end{pmatrix}. \tag{6.2}$$

The Z_2-odd scalar fields (η and s_2^0) result in the following particles: two CP-even neutral scalars ($\mathcal{H}_1^0$ and $\mathcal{H}_2^0$), two CP-odd neutral ones ($\mathcal{A}_1^0$ and $\mathcal{A}_2^0$), and a pair of charged ones ($\mathcal{H}^\pm$). It is clear that $\mathcal{H}^\pm = \eta^\pm$. When $\mathcal{H}_1^0$ (or $\mathcal{A}_1^0$) is lighter than $\mathcal{H}^\pm$, the neutral one becomes the dark matter candidate. On the other hand, from Z_2-even scalar fields (Φ, Φ_ν, and s_1^0), we have three CP-even particles (h^0, H^0, and H_ν^0), two CP-odd ones (A_ν^0 and a massless z_2^0), and a pair of charged scalars ($H_\nu^\pm$). The mixings between ϕ_ν^0 and others are ignored because we take $v_\nu/v \ll 1$ and $v_\nu/v_s \ll 1$. Then, Φ_ν provides H_ν^0 ($= \phi_{\nu r}^0$), A_ν^0 ($= \phi_{\nu i}^0$), and $H_\nu^\pm$ ($= \phi_\nu^\pm$). It is easy to see that $z_2^0 = s_{1i}^0$, where $s_1^0 = (v_s + s_{1r}^0 + is_{1i}^0)/\sqrt{2}$. The formulae of scalar mixings and scalar masses are presented in Appendix. Hereafter, we assume that scalar fields in Table 6.1

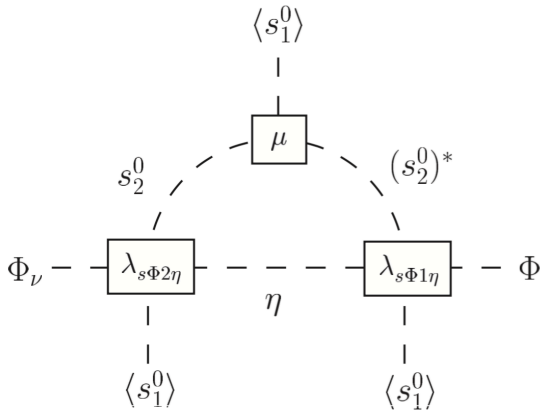

Figure 6.1: The one-loop diagram of the leading contribution to $(\mu^2_{\Phi 12})_{\rm eff}\,[\Phi^\dagger_\nu \Phi]$ with respect to μ, $\lambda_{s\Phi 1\eta}$, and $\lambda_{s\Phi 2\eta}$.

are almost mass eigenstates just for simplicity, which is achieved when $\lambda_{s\Phi 1\eta}$ and $\lambda_{s1\Phi 1}$ are small.

By using cubic and quartic interactions shown in Eq. (6.1), the interaction $\Phi^\dagger_\nu \Phi$ is obtained with the one-loop diagram in Fig. 6.1. The coefficient $(\mu^2_{\Phi 12})_{\rm eff}$ of the interaction is calculated as

$$(\mu^2_{\Phi 12})_{\rm eff} = \frac{\mu\,\lambda_{s\Phi 1\eta}\,\lambda_{s\Phi 2\eta}\,v_s^3}{32\sqrt{2}\,\pi^2(m_\eta^2 - m_{s2}^2)}\left(1 - \frac{m_\eta^2}{m_\eta^2 - m_{s2}^2}\ln\frac{m_\eta^2}{m_{s2}^2}\right), \tag{6.3}$$

where $m_\eta^2 \equiv \mu_\eta^2 + \left\{\left(\lambda_{\Phi 1\eta} + \lambda'_{\Phi 1\eta}\right)v^2 + \lambda_{s1\eta}v_s^2\right\}/2$, $m_{s2}^2 \equiv \mu_{s2}^2 + \left(\lambda_{s2\Phi 1}v^2 + \lambda_{s12}v_s^2\right)/2$. Ignoring loop corrections to terms which exist at the tree-level, we finally arrive at

$$v_\nu = \frac{v\,(\mu^2_{\Phi 12})_{\rm eff}}{m^2_{H^0_\nu}}, \tag{6.4}$$

where $m^2_{H^0_\nu} \equiv \mu^2_{\Phi 2} + (\lambda_{\Phi 12} + \lambda'_{\Phi 12})v^2/2 + \lambda_{s1\Phi 2}v_s^2/2$ which is the mass of H^0_ν $(= \phi^0_{\nu r})$. For example, we have $m_\nu = \mathcal{O}(0.1)\,{\rm eV}$ for $m_{s2} = \mathcal{O}(10)\,{\rm GeV}$ (as the dark matter mass), $v_s \sim m_\eta \sim m_{H_\nu} = \mathcal{O}(100)\,{\rm GeV}$, $\mu = \mathcal{O}(1)\,{\rm GeV}$, $y_\nu = \mathcal{O}(10^{-4})$, and $\lambda_{s\Phi 1\eta} \sim \lambda_{s\Phi 2\eta} = \mathcal{O}(10^{-2})$.

6.2 Phenomenology

Hereafter, we take the following values of parameters as an example:

$$\begin{aligned} &(y_\nu)_{\ell i} \sim 10^{-4}, \quad \lambda_{s\Phi 1\eta} = \lambda_{s\Phi 2\eta} = 10^{-2}, \quad \mu = 1\,{\rm GeV}, \quad v_s = 300\,{\rm GeV}, \\ &m_{H^0_\nu} = m_{A^0_\nu} = m_{H^\pm_\nu} = 300\,{\rm GeV}, \quad m_{\mathcal{H}^0_2} = 230\,{\rm GeV}, \quad m_{\mathcal{H}^0_1} = 60\,{\rm GeV}. \end{aligned} \tag{6.5}$$

These values can satisfy constraints from the ρ parameter, searches of lepton flavor violating processes, the relic abundance of dark matter, and direct searches for dark matter. In order to satisfy $\rho \simeq 1$, particles which come from an SU(2) multiplet have a common mass. If $\mathcal{H}^0_1 \simeq \eta^0_r$ for example, we take $m_{\mathcal{H}^\pm} \sim m_{\mathcal{A}^0_1} \sim m_{\mathcal{H}^0_1}$. Since y_ν is not assumed to be very large, contributions of $H^\pm_\nu$ to lepton flavor violating decays of charged leptons are negligible. For example, the

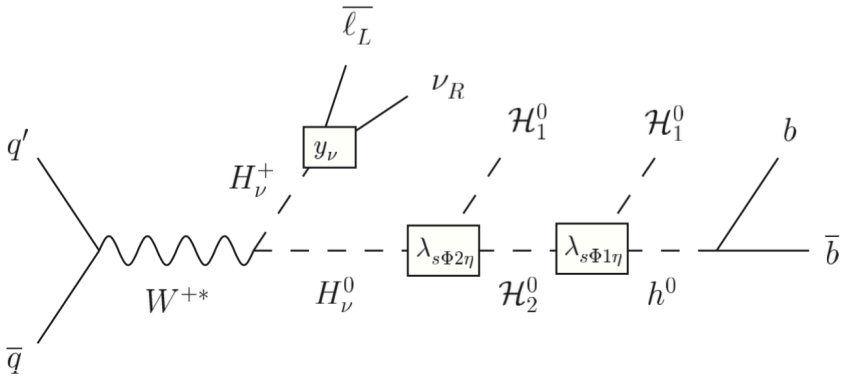

Figure 6.2: A possible signature of our model at the LHC.

branching ratio BR($\mu \to e\gamma$) [64] is proportional to $|(y_\nu y_\nu^\dagger)_{\mu e}|^2$ and becomes about 10^{-22} which is much smaller than the current bound at the MEG experiment [90]: BR($\mu \to e\gamma$) $< 5.7 \times 10^{-13}$ at the 90 % confidence level.

6.2.1 Dark matter

We assume that the mixing between s_2^0 and η^0 is negligible for simplicity, which corresponds to the case $\lambda_{s\Phi 1\eta} \ll 1$. Then, the dark matter candidate $\mathcal{H}_1^0$ is dominantly made from s_{2r}^0 or η_r^0. We also assume that $\lambda_{s12}|s_1^0|^2|s_2^0|^2$ and $\lambda_{s1\eta}|s_1^0|^2(\eta^\dagger\eta)$ are negligible in order to avoid $\mathcal{H}_1^0\mathcal{H}_1^0 \to z_2^0 z_2^0$ which would reduce the dark matter abundance too much. Notice that these coupling constants (λ_{s12} and $\lambda_{s1\eta}$) are not used in the loop diagram in Fig. 6.1. When $\mathcal{H}_1^0 \simeq s_{2r}^0$, the $\mathcal{H}_1^0$ is similar to the real singlet dark matter in Ref. [91]. Experimental constraints on the singlet dark matter can be found e.g. in Ref. [92]. We see that $53\,\mathrm{GeV} \lesssim m_{\mathcal{H}_1^0} \lesssim 64\,\mathrm{GeV}$ and $90\,\mathrm{GeV} \lesssim m_{\mathcal{H}_1^0}$ are allowed. On the other hand, when $\mathcal{H}_1^0 \simeq \eta_r^0$, the dark matter is similar to the one in the so-called inert doublet model [29, 93]. See e.g. Refs. [94, 95] for experimental constraints on the inert doublet model. It is shown that $45\,\mathrm{GeV} \lesssim m_{\mathcal{H}_1^0} \lesssim 80\,\mathrm{GeV}$ is allowed. In order to suppress the scattering of $\mathcal{H}_1^0$ on nuclei mediated by the Z boson, sufficient splitting of $m_{\mathcal{H}_1^0}$ and $m_{\mathcal{A}_1^0}$ is required: $m_{\mathcal{A}_1^0} - m_{\mathcal{H}_1^0} \gtrsim 100\,\mathrm{keV}$ (See e.g. Ref. [95]). Values of $m_{\mathcal{H}_1^0}$ and $m_{\mathcal{H}_2^0}$ in Eq. (6.5) are obtained by using $m_\eta = 60\,\mathrm{GeV}$ and $m_s = 231\,\mathrm{GeV}$ in Eqs. (A.11) and (A.12) in Appendix, and then these values of m_η and m_s give $m_{\mathcal{A}_1^0} - m_{\mathcal{H}_1^0} \simeq 400\,\mathrm{keV}$.

Since we discuss in the next subsection a possible collider signature where H_ν^0 decays into $\mathcal{H}_1^0$, a light dark matter ($m_{\mathcal{H}_1^0} \simeq m_{h^0}/2$) is interesting such that H_ν^0 (and $H_\nu^\pm$) can also be light. We take $m_{\mathcal{H}_1^0} = 60\,\mathrm{GeV}$ as an example for both cases, $\mathcal{H}_1^0 \simeq s_{2r}^0$ and $\mathcal{H}_1^0 \simeq \eta_r^0$.

6.2.2 Collider

In the νTHDM as well as in our model, the neutrino mass matrix m_ν is simply proportional to y_ν. The flavor structure of $H_\nu^+ \to \overline{\ell_L}\nu_R$ (summed over the neutrinos) is predicted [64] by using current information on m_ν obtained by neutrino oscillation measurements. The prediction enables the νTHDM to be tested at collider experiments. Since this advantage should not be spoiled, $H_\nu^\pm \to \mathcal{H}_1^0\mathcal{H}^\pm$ ($\mathcal{H}^\pm\mathcal{H}_2^0$) should be forbidden for $\mathcal{H}_1^0 \simeq s_{2r}^0$ ($\mathcal{H}_1^0 \simeq \eta_r^0$). Therefore, we assume that $m_{\mathcal{H}^\pm}$ satisfies $m_{H_\nu^\pm} \leq m_{\mathcal{H}_1^0} + m_{\mathcal{H}^\pm}$ for $\mathcal{H}_1^0 \simeq s_{2r}^0$ or $m_{H_\nu^\pm} \leq m_{\mathcal{H}^\pm} + m_{\mathcal{H}_2^0}$ for $\mathcal{H}_1^0 \simeq \eta_r^0$;

for example, $m_{\mathcal{H}^\pm} = 250\,\text{GeV}$ (100 GeV) for $\mathcal{H}_1^0 \simeq s_{2r}^0$ (η_r^0).

The process in Fig. 6.2 would be a characteristic collider signature of our model. Notice that the process utilizes two coupling constants ($\lambda_{s\Phi 1\eta}$ and $\lambda_{s\Phi 2\eta}$) which appear also in Fig. 6.1. Thus, the process indicates that $\mu_{\Phi 12}^2 \Phi_\nu^\dagger \Phi$ is radiatively generated with a contribution of dark matter. In the original νTHDM in comparison, H_ν^0 decays into $\nu\overline{\nu}$ for the case with $m_{H_\nu^0} = m_{H_\nu^\pm}$. In order to observe the process in Fig. 6.2, the partial decay width $\Gamma(H_\nu^0 \to \mathcal{H}_1^0\mathcal{H}_2^0)$ should be larger than $\Gamma(H_\nu^0 \to \nu\overline{\nu})$. Using our benchmark values, we have

$$\Gamma(H_\nu^0 \to \nu\overline{\nu}) = \frac{\text{tr}(y_\nu^\dagger y_\nu) m_{H_\nu^0}}{16\pi} \simeq 60\,\text{eV}, \tag{6.6}$$

$$\Gamma(H_\nu^0 \to \mathcal{H}_1^0\mathcal{H}_2^0) = \frac{\lambda_{s\Phi 2\eta}^2 v_s^2}{64\pi m_{H_\nu^0}} \sqrt{1 - \frac{(m_{\mathcal{H}_2^0} + m_{\mathcal{H}_1^0})^2}{m_{H_\nu^0}^2}} \sqrt{1 - \frac{(m_{\mathcal{H}_2^0} - m_{\mathcal{H}_1^0})^2}{m_{H_\nu^0}^2}} \simeq 30\,\text{keV}. \tag{6.7}$$

Then, H_ν^0 decays into $\mathcal{H}_1^0\mathcal{H}_2^0$ dominantly[1]. If y_ν is large enough for $\mu \to e\gamma$ to be discovered in near future, the process in Fig. 6.2 becomes very rare because $H_\nu^0 \to \nu\overline{\nu}$ is the dominant channel. Next, when the mixings between Z_2-odd particles are negligible, $\mathcal{H}_2^0$ can decay only into $\mathcal{H}_1^0 h^0$ via $\lambda_{s\Phi 1\eta}$ because $\mathcal{H}_2^0 \to \mathcal{H}_1^0 H^0$ is kinematically forbidden for the values in Eq. (6.5). Thus, even if $\lambda_{s\Phi 1\eta}$ is rather small, the branching ratio for $\mathcal{H}_2^0 \to \mathcal{H}_1^0 h^0$ can be almost 100 %. As a result, the process in Fig. 6.2 can be free from the one-loop suppression and smallness of coupling constants (y_ν, $\lambda_{s\Phi 1\eta}$, and $\lambda_{s\Phi 2\eta}$) which are used to suppress v_ν. The cross section of $pp \to H_\nu^+ H_\nu^0 + H_\nu^- H_\nu^0$ for the masses in Eq. (6.5) is 7 fb at the LHC with $\sqrt{s} = 14\,\text{TeV}$. The SM background events come from $t\bar{t}$, WZ, and $t\bar{b}$. Cross sections for $pp \to t\bar{t}$, $W^+Z + W^-Z$, and $t\bar{b} + \bar{t}b$ at the LHC with $\sqrt{s} = 14\,\text{TeV}$ are 833 pb [96], 55.4 pb [97], and 3.91 pb [98], respectively. Detailed analysis on kinematic cuts of the background events is beyond the scope of this paper.

If Nature chooses a parameter set for which the process in Fig. 6.2 is not possible, the deviation from the νTHDM would be the increase of new scalar particles which might be discovered directly and/or change predictions in the νTHDM about e.g. $h^0 \to \gamma\gamma$.

6.3 Conclusions and discussion

The νTHDM is a new physics model where masses of Dirac neutrinos are generated by a VEV (v_ν) of the second $\text{SU}(2)_L$-doublet scalar field Φ_ν which has a Yukawa interaction with only ν_R because of a global $\text{U}(1)_X$ symmetry in the Lagrangian. We have presented a simple extension of the νTHDM by introducing the third $\text{SU}(2)_L$-doublet scalar field η and two neutral $\text{SU}(2)_L$ singlet fields (s_1^0 and s_2^0). Although the global $\text{U}(1)_X$ is broken by a VEV of s_1^0, there remains a residual Z_2 symmetry under which η and s_2^0 are Z_2-odd particles. These Z_2-odd particles provide a dark matter candidate. The v_ν for neutrino masses can be suppressed without requiring very heavy particles because the VEV is generated at the one-loop level.

A possible signature of the deviation from the νTHDM at the LHC is $\overline{\ell} j_b j_b \not{E}_T$ via $pp \to H_\nu^+ H_\nu^0$ followed by $H_\nu^+ \to \overline{\ell}\nu$ and $H_\nu^0 \to \mathcal{H}_1^0\mathcal{H}_2^0 \to \mathcal{H}_1^0\mathcal{H}_1^0 h^0 \to \mathcal{H}_1^0\mathcal{H}_1^0 b\overline{b}$. Coupling constants which control $H_\nu^0 \to \mathcal{H}_1^0\mathcal{H}_2^0$ and $\mathcal{H}_2^0 \to \mathcal{H}_1^0 h^0$ are the ones used in the one-loop diagram which is the key to generate v_ν.

[1]Cascade decay of A_ν^0 results in $\mathcal{H}_1^0\mathcal{H}_1^0 z_2^0$ which is invisible similarly to $A_\nu^0 \to \nu\overline{\nu}$.

Chapter 7

Neutrino mass and dark matter from gauged $U(1)_{B-L}$ breaking

If ν_R are introduced to the standard model of particle physics (SM), there are two possible mass terms for neutrinos (See e.g., Ref. [99]), the Dirac type $\overline{\nu_L}\nu_R$ and the Majorana type $\overline{(\nu_R)^c}\nu_R$. In radiative seesaw models (See e.g., Refs. [25–27, 81, 86, 88, 100]), an *ad hoc* unbroken Z_2 symmetry forbids generating neutrino masses at the tree level and explains the dark matter (DM) stability. A model in Ref. [100] was constructed such that the breaking of the $\mathrm{U(1)_{B-L}}$ gauge symmetry gives a residual symmetry for the DM stability and the Majorana neutrino mass of ν_R. However, the anomaly cancelation for the $\mathrm{U(1)_{B-L}}$ gauge symmetry requires to introduce more additional fermions except for particles for the radiative neutrino mass.

In this chapter, we propose a new model which is an improved version of the model in Ref. [100] from the view point of the anomaly cancellation. With appropriate $\mathrm{U(1)_{B-L}}$ charge assignments, there exists an unbroken global U(1) symmetry even after the breakdown of the $\mathrm{U(1)_{B-L}}$ symmetry. The global U(1) symmetry stabilizes the DM, so that we hereafter call it $\mathrm{U(1)_{DM}}$. In our work, the DM candidate is a new scalar boson. Furthermore, the Dirac mass term of neutrinos is radiatively generated at the one-loop level due to the quantum effect of the new particles. Tiny neutrino masses are explained by the two-loop diagrams with a Type-I-Seesaw-like mechanism. We find that the model can satisfy current data from the neutrino oscillation, the lepton flavor violation (LFV), the relic abundance and the direct search for the DM, and the LHC experiment. This chapter is based on [101].

7.1 Model

We introduce new particles which listed in Table 7.1. We determine assignment of $\mathrm{U(1)_{B-L}}$ charges from conditions for cancellation of the $[\mathrm{U(1)_{B-L}}] \times [\mathrm{gravity}]^2$ and $[\mathrm{U(1)_{B-L}}]^3$ anomalies;

$$3 - \frac{1}{3}N_{\nu_R} - \frac{2}{3}N_\psi = 0, \tag{7.1}$$

$$3 - \frac{1}{27}N_{\nu_R} + \left(-2x^2 - \frac{4}{3}x - \frac{8}{27}\right)N_\psi = 0, \tag{7.2}$$

where N_ψ is the number of ψ_{Ri} (the same as the number of ψ_{Li}), and N_{ν_R} is the number of ν_{Ra}.

There are four solutions as presented in Table 7.2. Except for Case III, the $\mathrm{U(1)_{B-L}}$ charges of some new particles are irrational numbers while the $\mathrm{U(1)_{B-L}}$ symmetry is spontaneously

	σ^0	$(\nu_R)_a$	$(\psi_L)_i$	$(\psi_R)_i$	η	s^0
$\mathrm{SU(2)_I}$	**1**	**1**	**1**	**1**	**2**	**1**
$\mathrm{U(1)_Y}$	0	0	0	0	1/2	0
$\mathrm{U(1)}_{B-L}$	2/3	$-1/3$	$x+2/3$	x	$x+1$	$x+1$
Spin	0	1/2	1/2	1/2	0	0

Table 7.1: Particle contents in this model. Indices i and a run from 1 to N_ψ and from 1 to N_{ν_R}, respectively.

	Case I	Case II	Case III	Case IV
N_ψ	1	2	3	4
N_{ν_R}	7	5	3	1
x	$\frac{2\sqrt{3}-1}{3}$	$\frac{\sqrt{6}-1}{3}$	$\frac{1}{3}$	$\frac{\sqrt{3}-1}{3}$

Table 7.2: Sets of N_ψ, N_{ν_R} and x, for which the $\mathrm{U(1)_{B-L}}$ gauge symmetry is free from anomaly.

broken by the vacuum expectation value (VEV) of σ^0 whose $\mathrm{U(1)_{B-L}}$ charge is a rational number. Therefore, the irrational charges are conserved, and the lightest particle with an irrational $\mathrm{U(1)_{B-L}}$ charge becomes stable so that the particle can be regarded as a DM candidate. In this chapter, we take Case IV as an example.

In addition to the SM one, the new Yukawa interactions are given by

$$\mathcal{L}_{\rm Y} = -(y_R)_i\,\overline{(\nu_R)_i}\,(\nu_R)_i^c\,(\sigma^0)^* - (y_\psi)_i\,\overline{(\psi_R)_i}\,(\psi_L)_i\,(\sigma^0)^* - h_{ij}\,\overline{(\psi_L)_i}\,(\nu_R)_j\,s^0 - f_{\ell i}\,\overline{(L_L)_\ell}\,(\psi_R)_i\,\tilde{\eta} + \text{h.c.}, \tag{7.3}$$

where $\tilde{\eta} \equiv i\sigma_2\,\eta^*$. The scalar potential in our model is the same as that in the previous model [100]:

$$\begin{aligned} V(\Phi,\sigma,\eta,s) &= -\mu_\phi^2\Phi^\dagger\Phi + \mu_s^2|s^0|^2 + \mu_\eta^2\eta^\dagger\eta - \mu_\sigma^2|\sigma^0|^2 + \mu_3\,(s^0\,\eta^\dagger\,\Phi + \text{h.c.}) \\ &+ \lambda_\phi\left(\Phi^\dagger\Phi\right)^2 + \lambda_s|s^0|^4 + \lambda_\eta\left(\eta^\dagger\eta\right)^2 + \lambda_\sigma|\sigma^0|^4 + \lambda_{s\sigma}|s^0|^2|\sigma^0|^2 \\ &+ \lambda_{s\eta}|s^0|^2\eta^\dagger\eta + \lambda_{s\phi}|s^0|^2\Phi^\dagger\Phi + \lambda_{\sigma\eta}|\sigma^0|^2\eta^\dagger\eta + \lambda_{\sigma\phi}|\sigma^0|^2\Phi^\dagger\Phi \\ &+ \lambda_{\phi\phi}(\eta^\dagger\eta)(\Phi^\dagger\Phi) + \lambda_{\eta\phi}(\eta^\dagger\Phi)(\Phi^\dagger\eta). \end{aligned} \tag{7.4}$$

Neutral scalar fields are given by $\phi^0 = \frac{1}{\sqrt{2}}(\phi_r^0 + iz_\phi)$, $\sigma^0 = \frac{1}{\sqrt{2}}(\sigma_r^0 + iz_\sigma)$, $\eta^0 = \frac{1}{\sqrt{2}}(\eta_r^0 + i\eta_i^0)$, $s^0 = \frac{1}{\sqrt{2}}(s_r^0 + is_i^0)$. Two scalar fields ϕ^0 and σ^0 obtain VEVs v_ϕ [$= \sqrt{2}\,\langle\phi^0\rangle = 246\,\text{GeV}$] and v_σ [$= \sqrt{2}\,\langle\sigma^0\rangle$]. The VEV v_σ provides a mass of the $\mathrm{U(1)_{B-L}}$ gauge boson Z' as $m_{Z'} = (2/3)g_{\rm B-L}v_\sigma$, where $g_{\rm B-L}$ is the $\mathrm{U(1)_{B-L}}$ gauge coupling constant. After the gauge symmetry breaking with v_ϕ and v_σ, we can confirm in Eqs. (7.3) and (7.4) that there is a residual global $\mathrm{U(1)_{DM}}$ symmetry, for which irrational $\mathrm{U(1)_{B-L}}$-charged particles (η, s^0, ψ_{Li}, and ψ_{Ri}) have the same $\mathrm{U(1)_{DM}}$-charge while the other particles are neutral.

Two CP-even scalar particles h^0 and H^0 are obtained by ϕ^0-σ^0 mixing as $\sin 2\theta_0 = 2\lambda_{\sigma\phi}v_\phi v_\sigma / (m_{H^0}^2 - m_{h^0}^2)$. Two neutral complex scalars η^0 and s^0 are obtained by η^0-s^0 mixing as $\sin 2\theta_0' =$

$\sqrt{2}\mu_3 v_\phi/(m^2_{\mathcal{H}^0_2} - m^2_{\mathcal{H}^0_1})$. Scalar masses are given by

$$m^2_{h^0,H^0} = \lambda_\phi v_\phi^2 + \lambda_\sigma v_\sigma^2 \mp \sqrt{\left(\lambda_\phi v_\phi^2 - \lambda_\sigma v_\sigma^2\right)^2 + \lambda^2_{\sigma\phi} v_\phi^2 v_\sigma^2}, \tag{7.5}$$

$$m^2_{\mathcal{H}^0_1,\mathcal{H}^0_2} = \frac{1}{2}\left(m_\eta^2 + m_s^2 \mp \sqrt{\left(m_\eta^2 - m_s^2\right)^2 + 2\mu_3^2 v_\phi^2}\right), \tag{7.6}$$

where $m_\eta^2 = \mu_\eta^2 + (\lambda_{\phi\phi} + \lambda_{\eta\phi})\, v_\phi^2/2 + \lambda_{\sigma\eta} v_\sigma^2/2$, $m_s^2 = \mu_s^2 + \lambda_{s\phi} v_\phi^2/2 + \lambda_{s\sigma} v_\sigma^2/2$. The mass of the charged scalar $\eta^\pm$ is $m^2_{\eta^\pm} = m_\eta^2 - \lambda_{\eta\phi}\, v_\sigma^2/2$. Nambu-Goldstone bosons z_ϕ and z_σ are absorbed by Z and Z' bosons, respectively.

7.2 Phenomenology

7.2.1 Neutrino masses

Tiny neutrino masses are generated by two-loop diagrams in Fig. 7.1 [100]. The mass matrix m_ν is expressed in the flavor basis as

$$(m_\nu)_{\ell\ell'} = \left(\frac{1}{16\pi^2}\right)^2 \sum_{i,j,a} f_{\ell i}\, h_{ia}\, (m_R)_a\, (h^T)_{aj}\, (f^T)_{j\ell'} \Big[(I_1)_{ija} + (I_2)_{ija}\Big], \tag{7.7}$$

where explicit formulas of $(I_1)_{ija}$ and $(I_2)_{ija}$ are shown in Ref. [101]. The neutrino mass matrix $(m_\nu)_{\ell\ell'}$ is diagonalized by a unitary matrix $U_{\rm MNS}$, the so-called Maki-Nakagawa-Sakata (MNS) matrix [65], as $U^\dagger_{\rm MNS}\, m_\nu\, U^*_{\rm MNS} = {\rm diag}(m_1 e^{i\alpha_1},\, m_2 e^{i\alpha_2},\, m_3 e^{i\alpha_3})$. We take m_i (i = 1-3) to be real and positive values. Two differences of three phases α_i are physical Majorana phases. In our analysis, the following values [6, 9, 12] obtained by neutrino oscillation measurements are used in order to search for a benchmark point of model parameters:

$$\sin^2 2\theta_{23} = 1, \quad \sin^2 2\theta_{13} = 0.09, \quad \tan^2\theta_{12} = 0.427, \quad \delta = 0, \quad \{\alpha_1,\, \alpha_2,\, \alpha_3\} = \{0,\, 0,\, 0\},$$
$$m_1 = 10^{-4}\,{\rm eV}, \Delta m^2_{21} = 7.46 \times 10^{-5}\,{\rm eV}^2, \Delta m^2_{32} = +2.51 \times 10^{-3}\,{\rm eV}^2, \text{where } \Delta m^2_{ij} \equiv m_i^2 - m_j^2.$$

By using an ansatz [101] for the structure of Yukawa matrix $f_{\ell i}$, we found a benchmark point as

$$f = \begin{pmatrix} 1.79 & -2.49 & -1.97 & 2.56 \\ -1.82 & 1.10 & 1.30 & -0.818 \\ 1.40 & -0.598 & -0.905 & 0.222 \end{pmatrix} \times 10^{-2},\ h = \begin{pmatrix} 0.7 & 0.8 & 0.9 & 1 \end{pmatrix}^T,$$
$$\{g_{\rm B-L},\, m_{Z'}\} = \{0.1,\, 4\,{\rm TeV}\},$$
$$\{m_{h^0},\, m_{H^0},\, \cos\theta_0\} = \{125\,{\rm GeV},\, 1\,{\rm TeV},\, 1\},\ \{m_{\mathcal{H}^0_1},\, m_{\mathcal{H}^0_2},\, \cos\theta_0'\} = \{60\,{\rm GeV},\, 450\,{\rm GeV},\, 0.05\},$$
$$m_{\eta^\pm} = 420\,{\rm GeV},\ (m_R)_1 = 250\,{\rm GeV},$$
$$\{m_{\psi_1},\, m_{\psi_2},\, m_{\psi_3},\, m_{\psi_4}\} = \{650\,{\rm GeV},\, 750\,{\rm GeV},\, 850\,{\rm GeV},\, 950\,{\rm GeV}\}.$$

The values of $\{m_{h^0},\, m_{H^0},\, \cos\theta_0\}$ correspond to $\lambda_\phi \simeq 0.13$, $\lambda_\sigma \simeq 2.8 \times 10^{-4}$ and $\lambda_{\sigma\phi} = 0$. The values of $\{m_{\mathcal{H}^0_1},\, m_{\mathcal{H}^0_2},\, \cos\theta_0'\}$ and $m_{\eta^\pm}$ can be produced by $m_s \simeq 60\,{\rm GeV}$, $m_\eta \simeq 450\,{\rm GeV}$, $\mu_3 \simeq 57\,{\rm GeV}$ and $\lambda_{\eta\phi} \simeq 0.86$.

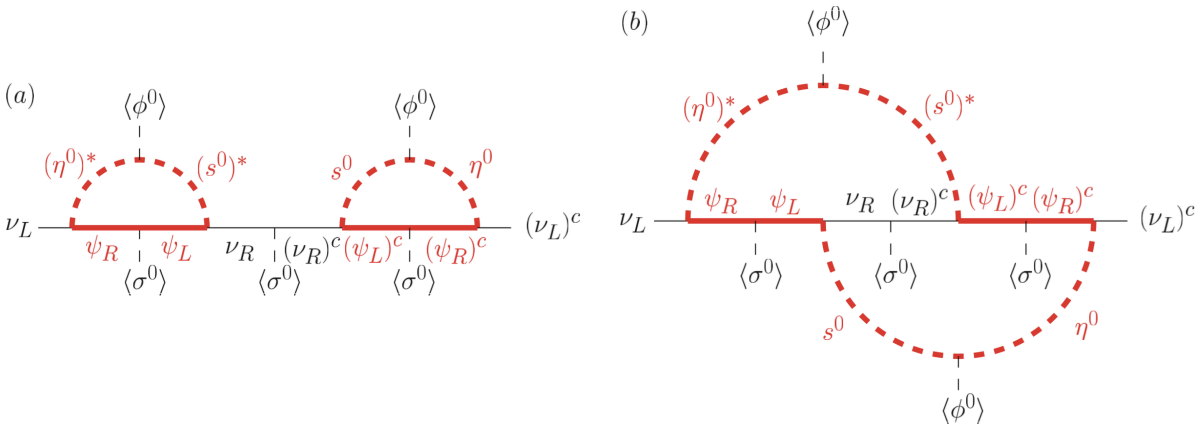

Figure 7.1: Two-loop diagrams for tiny neutrino masses in this model. Bold (red) lines are propagators of particles of irrational $U(1)_{B-L}$ charges.

7.2.2 Lepton flavor violation

We consider the condition of the LFV decays of charged leptons. The charged scalar $\eta^\pm$ contributes to the branching ratio (BR) of $\mu \to e\gamma$ whose formula have been calculated [102]. At the benchmark point, we have $\mathrm{BR}(\mu \to e\gamma) = 6.1 \times 10^{-14}$ which satisfies the current constraint $\mathrm{BR}(\mu \to e\gamma) < 5.7 \times 10^{-13}$ (90% C.L.) [103].

7.2.3 Dark matter

In our model, the scalar $\mathcal{H}_1^0$ turns out to be the DM candidate due to the following reason. If the DM is the fermion ψ_1, it annihilates into a pair of SM particles via the s-channel process mediated by h^0 and H^0. Even for a maximal mixing $\cos\theta_0 = 1/\sqrt{2}$ [104], the observed abundance of the DM [4] requires $v_\sigma \lesssim 10\,\mathrm{TeV}$. The current constraint from direct searches of the DM [105] requires larger v_σ in order to suppress the Z' contribution.

The scalar DM $\mathcal{H}_1^0$ at the benchmark point is dominantly made from s^0 which is a gauge-singlet field under the SM gauge group, because of the tiny mixing $\cos\theta_0' = 0.05$. The annihilation of $\mathcal{H}_1^0$ into a pair of the SM particles is dominantly caused by the s-channel scalar mediation via h^0 [106] because H^0 is assumed to be heavy. The coupling constant $\lambda_{\mathcal{H}_1^0\mathcal{H}_1^0 h^0}$ for the $\lambda_{\mathcal{H}_1^0\mathcal{H}_1^0 h^0}\, v_\phi \mathcal{H}_1^0 \mathcal{H}_1^{0*} h^0$ interaction controls the annihilation cross section, the invisible decay $h^0 \to \mathcal{H}_1^0 \mathcal{H}_1^{0*}$ in the case of kinematically accessible, and the h^0 contribution to the spin-independent scattering cross section σ_{SI} on a nucleon. In Ref. [107], for example, we see that $\mathcal{H}_1^0$ with $m_{\mathcal{H}_1^0} = 60\,\mathrm{GeV}$ and $\lambda_{\mathcal{H}_1^0\mathcal{H}_1^0 h^0} \sim 10^{-3}$ can satisfy constraints from the relic abundance of the DM and the invisible decay of h^0. We see also that the h^0 contribution to σ_{SI} is small enough to satisfy the current constraint $\sigma_{\mathrm{SI}} < 9.2 \times 10^{-46}\,\mathrm{cm}^2$ for $m_{\mathrm{DM}} = 60\,\mathrm{GeV}$ [105]. Although the scattering of $\mathcal{H}_1^0$ on a nucleon is mediated also by the Z' boson in this model, the contribution can be suppressed by taking a large v_σ. The benchmark point corresponds to $v_\sigma = 60\,\mathrm{TeV}$ and gives about $6.6 \times 10^{-47}\,\mathrm{cm}^2$ for the scattering cross section via Z', which is smaller than the current constraint [105] by an order of magnitude. Thus, the constraint from the direct search of the DM is also satisfied at the benchmark point.

$q\overline{q}$	$\ell\overline{\ell}$	$\nu_L\overline{\nu_L}$	$\nu_R\overline{\nu_R}$	$\psi_1\overline{\psi_1}$	$\psi_2\overline{\psi_2}$	$\psi_3\overline{\psi_3}$	$\psi_4\overline{\psi_4}$	$\mathcal{H}_1^0\mathcal{H}_1^{0*}$	$\mathcal{H}_2^0\mathcal{H}_2^{0*}$	$\eta^+\eta^-$
0.21	0.32	0.16	0.0059	0.046	0.045	0.044	0.043	0.041	0.038	0.039

Table 7.3: Branching ratios of Z' decays.

7.2.4 Z' and ν_R search

The LEP-II bound $m_{Z'}/g_{\rm B-L} \gtrsim 7\,{\rm TeV}$ [108] is satisfied at the benchmark point because of $m_{Z'}/g_{\rm B-L} = 40\,{\rm TeV}$ which we take for a sufficient suppression of $\sigma_{\rm SI}$ for the direct search of the DM. The production cross section of Z' with $g_{\rm B-L} = 0.1$ and $m_{Z'} = 4\,{\rm TeV}$ is about 0.3 fb at the LHC with $\sqrt{s} = 14\,{\rm TeV}$ [109]. Notice that the current bound $m_{Z'} \gtrsim 3\,{\rm TeV}$ at the LHC [110] is for the case where the gauge coupling for Z' is the same as the one for Z, namely $g_{\rm B-L} \simeq 0.7$. Decay branching ratios of Z' are shown at the benchmark point in Table 7.3. Decays of ψ_i are dominated by $\psi_i \to \nu_R\mathcal{H}_1^0$ with the Yukawa coupling constants h_{i1} because $y_{\ell i}$ for $\psi_i \to \ell^\pm\eta^\mp$ are small in order to satisfy the $\mu \to e\gamma$ constraint. The $\mathcal{H}_2^0$ ($\simeq \eta^0$) decays into $h^0\mathcal{H}_1^0$ via the trilinear coupling constant μ_3. The main decay mode of $\eta^\pm$ is $\eta^\pm \to W^\pm\mathcal{H}_1^0$ through the mixing θ_0' between η^0 and s^0.

The ν_R decay into H^0 is forbidden because it is heavier than ν_R at the benchmark point. Since the B−L charge of ν_R is rather small, ν_R is not produced directly from Z'. However, ν_R can be produced through the decays of ψ_i. As a result, about 18 % of Z' produces ν_R. For $\nu_R \to W\ell$ (56 %) followed by the hadronic decay of W (68 %), the ν_R would be reconstructed. In this model, an invariant mass of a pair of the reconstructed ν_R is not at $m_{Z'}$ in contrast with a naive model where only three ν_R with B−L = −1 are introduced to the SM. This feature of ν_R also enables us to distinguish this model from the previous model in Ref. [100] where ν_R with B−L = 1 can be directly produced by the Z' decay.

7.3 Conclusions

We have improved the model in Ref. [100] by considering anomaly cancellation of the $U(1)_{\rm B-L}$ gauge symmetry. We have shown that there are four anomaly-free cases of B−L charge assignment, and three of them have an unbroken global $U(1)_{\rm DM}$ symmetry. The $U(1)_{\rm DM}$ guarantees that the lightest $U(1)_{\rm DM}$-charged particle is stable such that it can be regarded as a DM candidate. The spontaneous breaking of the $U(1)_{\rm B-L}$ symmetry generates the Majorana mass term of ν_R and masses of new fermions ψ. In addition, the Dirac mass term of neutrinos is generated at the one-loop level where the DM candidate involved in the loop. Tiny neutrino masses are obtained at the two-loop level.

The case of the fermion DM is excluded, and the lightest $U(1)_{\rm DM}$-charged scalar $\mathcal{H}_1^0$ should be the DM in this model. We have found a benchmark point of model parameters which satisfies current constraints from neutrino oscillation data, lepton flavor violation searches, the relic abundance of the DM, direct searches for the DM, and the LHC experiments. In such radiative seesaw models, ν_R would be produced at the LHC. In our model, ν_R cannot be directly produced by the Z' decay, but can be produced by the cascade decay $Z' \to \psi_i\overline{\psi}_i \to \nu_R\overline{\nu_R}\mathcal{H}_1^0\mathcal{H}_1^{0*}$. By the unusual B−L charge of ν_R, the invariant mass distribution of $\nu_R\overline{\nu_R}$ does not take a peak at $m_{Z'}$, which could be a characteristic signal.

Part IV

Higgs inflation in a radiative seesaw model

Chapter 8

Higgs inflation in a radiative seesaw model

There are some theoretical problems in the simplest Higgs inflation model [18]. When we calculate the running coupling constant of the Higgs self-coupling, the critical energy scale is around 10^{10} GeV due to the contribution of the top quark [28]. The vacuum is difficult to be stable up to the inflation scale $\Lambda_{\rm I}$. This problem can be solved in two Higgs doublet models [29]. Because the loop effect of additional scalar bosons weakens the top-loop contribution in the running coupling constants [30]. Perturbative unitarity is also violated at the energy scale $\Lambda_{\rm U} = M_P/\xi$ by the Higgs-gauge scattering processes [31]. This problem is solved by a heavy additional real singlet scalar boson which does not interact with gauge fields as shown by [32].

In this chapter, we explain not only dark matter, neutrino masses but also inflation. We show a radiative seesaw scenario with the multi-Higgs structure, which was proposed by E. Ma [26], is constrained by the inflation condition. We discuss the testability of the characteristic mass spectrum at the collider experiments. This chapter is based on [111].

8.1 Model

In our model, we introduce the second scalar doublet Φ_2, right handed neutrinos ν_R^i ($i = 1-3$) and real singlet scalar σ and impose quantum numbers under the an unbroken discrete Z_2 symmetry shown in Table 8.1.

The Yukawa interaction for leptons and the Majorana mass term are given by

$$\mathcal{L}_{\rm Yukawa} = Y_\ell \overline{L_L}\Phi_1 \ell_R + Y_\nu \overline{L_L}\Phi_2^c \nu_R + h.c.\,, \qquad \mathcal{L}_{\rm Majorana} = \frac{1}{2} M_R^k \overline{(\nu_R^k)^c}\nu_R^k, \tag{8.1}$$

where the superscript c denotes the charge conjugation. In the Feynman diagram in Fig. 8.1, which is explained by Ref. [26], the extra lightest neutral particle can be a dark matter candidate

	Q_L	u_R	d_R	L_L	ℓ_R	Φ_1	Φ_2	ν_R	σ
$\rm SU(3)_C$	**3**	**3**	**3**	**1**	**1**	**1**	**1**	**1**	**1**
$\rm SU(2)_I$	**2**	**1**	**1**	**2**	**1**	**2**	**2**	**1**	**1**
$\rm U(1)_Y$	$\frac{1}{6}$	$\frac{2}{3}$	$-\frac{1}{3}$	$-\frac{1}{2}$	-1	$\frac{1}{2}$	$\frac{1}{2}$	0	0
Z_2	1	1	1	1	1	1	-1	-1	-1

Table 8.1: Particle contents and their quantum charges.

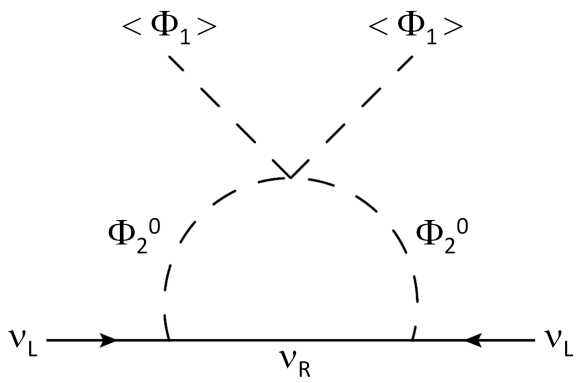

Figure 8.1: The Feynman diagram for tiny neutrino masses.

by Z_2 symmetry. We can explain neutrino masses at the loop level by

$$(m_\nu)_{ij} = \sum_k \frac{(Y_\nu)_i^k (Y_\nu)_j^k M_R^k}{16\pi^2} \left[\frac{m_H^2}{m_H^2 - \left(M_R^k\right)^2} \ln \frac{m_H^2}{\left(M_R^k\right)^2} - \frac{m_A^2}{m_A^2 - \left(M_R^k\right)^2} \ln \frac{m_A^2}{\left(M_R^k\right)^2} \right]. \quad (8.2)$$

The neutrino oscillation data is explained by neutrino Yukawa coupling constants $(Y_\nu)_i^k$, which satisfy $(Y_\nu)_i^k (Y_\nu)_j^k / M_R^k \simeq \mathcal{O}(10^{-7})$ GeV^{-1}.

The Higgs potential is given by

$$\begin{aligned} V_{\rm J} &= \frac{1}{2}\left(1 + \frac{2\xi_1|\Phi_1|^2 + 2\xi_2|\Phi_2|^2 + \zeta\sigma^2}{M_P^2}\right) M_P^2 \mathcal{R} \\ &+ \mu_1^2|\Phi_1|^2 + \mu_2^2|\Phi_2|^2 + \mu_\sigma^2\sigma^2 + \mu_{\sigma\phi}[\sigma(\Phi_1^\dagger\Phi_2)^2 + h.c.] + \frac{1}{2}\lambda_1|\Phi_1|^4 + \frac{1}{2}\lambda_2|\Phi_2|^4 + \lambda_\sigma\sigma^4 \\ &+ \lambda_3|\Phi_1|^2|\Phi_2|^2 + \lambda_4(\Phi_1^\dagger\Phi_2)(\Phi_2^\dagger\Phi_1) + \frac{1}{2}\lambda_5[(\Phi_1^\dagger\Phi_2)^2 + h.c.] + \lambda_{\sigma 1}|\Phi_1|^2\sigma^2 + \lambda_{\sigma 2}|\Phi_2|^2\sigma^2, \quad (8.3) \end{aligned}$$

When we assume $\mu_1^2 < 0$ and $\mu_2^2 > 0$, Φ_1 obtains the vacuum expectation value (VEV) v $(= \sqrt{-2\mu_1^2/\lambda_1})$, while Φ_2, which has the odd-quantum number of the Z_2 symmetry, cannot get the VEV. Mass eigenstates of the scalar bosons are the SM-like Z_2-even Higgs scalar boson h, the Z_2-odd CP-even scalar boson H, the Z_2-odd CP-odd scalar boson A and Z_2-odd charged scalar bosons $H^\pm$. Masses of these scalar bosons are given in Ref. [26]; $m_h^2 = \lambda_1 v^2$, $m_H^2 = \mu_2^2 + (\lambda_3 + \lambda_4 + \lambda_5)v^2/2$, $m_A^2 = \mu_2^2 + (\lambda_3 + \lambda_4 - \lambda_5)v^2/2$, $m_{H^\pm}^2 = \mu_2^2 + \lambda_3 v^2/2$. As the Z_2-odd neutral singlet scalar σ is constrained by perturbative unitarity [112]: $m_\sigma \leq \Lambda_U$, we assume that m_σ is heavy enough, so that it gives an insignificant effect on phenomenology. For simplicity, we take $\mu_{\sigma\phi} = \lambda_{\sigma 1} = \lambda_{\sigma 2} = 0$ and $\xi_1 \simeq \xi_2 \ll \zeta$. We study parameter regions which satisfy the conditions of vacuum stability and perturbative unitarity.

8.2 Constraints on the parameters

The Higgs potential in the Einstein frame is given by

$$V_{\rm E} = \frac{V_{\rm J}}{\Omega^4} = \frac{M_P^4}{8} \frac{\lambda_1 h_1^4 + \lambda_2 h_2^4 + \lambda_\sigma\sigma^4 + 2\{\lambda_3 + \lambda_4 + \lambda_5\cos(2\theta)\}h_1^2 h_2^2 + \lambda_{\sigma 1} h_1^2\sigma^2 + \lambda_{\sigma 2} h_2^2\sigma^2}{(M_P^2 + \xi_1 h_1^2 + \xi_2 h_2^2 + \zeta\sigma^2)^2}, \quad (8.4)$$

where

$$\Omega^2 = 1 + \frac{2\xi_1|\Phi_1|^2 + 2\xi_2|\Phi_2|^2 + \zeta\sigma^2}{M_P^2},\ \Phi_1 = \begin{pmatrix} 0 \\ h_1 \end{pmatrix},\ \Phi_2 = \begin{pmatrix} 0 \\ h_2 e^{i\theta} \end{pmatrix}. \tag{8.5}$$

For small field values $\Omega^2 \simeq 1$, the potential is the same as Jordan frame for the initial Higgs field ($V_{\rm E} \simeq V_{\rm J}$). On the other hand, for large fields values $\Omega^2 \gg 1$, we define $\varphi \equiv \sqrt{3/2}M_P \ln\Omega^2$, $r_2 \equiv h_2/h_1$, $r_\sigma \equiv \sigma/h_1$. For stabilizing r_2, r_σ as a finite value, we need to impose following condition:

$$\lambda_1\lambda_2 - (\lambda_3 + \lambda_4)^2 \ > \ 0. \tag{8.6}$$

This is the constraint from the inflation on our model because the heavy particle σ dominantly plays a role of inflaton.

The CP-odd boson A is assumed to be the lightest Z_2-odd particle; i.e., the dark matter candidate. When we change the sign of the coupling constant λ_5, the similar discussion can be applied for the case of the CP-even boson H to be the lightest. As λ_5 can be sizable which is not constrained from the inflation, the dominant scattering process is $AN \to AN$ (N is a nucleon) where the standard model-like Higgs boson is propagating. We can avoid the process $AN \to HN$ kinematically, and the cross section is consistent with the current direct search results for dark matter. As shown in [113, 114], the cross section of $AN \to AN$ process is

$$\sigma(AN \to AN) \simeq \frac{\lambda_{hAA}^2}{4m_h^4}\frac{m_N^2}{\pi(m_A + m_N)^2}f_N^2, \tag{8.7}$$

where $\lambda_{hAA} \equiv \lambda_3 + \lambda_4 - \lambda_5$, $f_N \equiv \sum_q m_N f_{Tq} + (2/9)m_N f_{TG}$ and m_N is the mass of nucleon, where $f_{Tu} + f_{Td} = 0.056$, $f_{Ts} = 0$ [115] and $f_{TG} = 0.944$ [116]. To satisfy the data of the dark matter relic abundance from the Planck experiment [4] and the data of the upper bound on the scattering cross section for $AN \to AN$ from the experiments $\sigma \simeq 2 \times 10^{-45}{\rm cm}^2$ [117, 118], the coupling constant λ_{hAA} is required to satisfy

$$\lambda_{hAA} \lesssim 0.036, \tag{8.8}$$

at the electroweak scale. When λ_5 is not small, the co-annihilation process $AH \to XX$ via the Z boson does not contribute to the dark matter relic abundance. This case is the same as the singlet scalar dark matter model [107, 119]. On the other hand, to avoid the current invisible decay $h \to AA$ kinematically [120, 121], m_A must be bigger than $m_h/2$. To satisfy these dark matter conditions, we require

$$63\ {\rm GeV} \lesssim m_A \lesssim 66\ {\rm GeV}. \tag{8.9}$$

Take into account the above conditions, the vacuum stability condition

$$\lambda_1 > 0,\ \lambda_2 > 0,\ \sqrt{\lambda_1\lambda_2} + \lambda_3 + \min[0, \lambda_4 + \lambda_5, \lambda_4 - \lambda_5] > 0, \tag{8.10}$$

and the conditions of triviality $\lambda_i \lesssim 2\pi$, we analyze the renormalization group equations [52]. In Fig. 8.2, running of the scalar coupling constants is shown between the electroweak scale and the inflation scale. In Table 8.2, we show the values of the scalar coupling constants at the scales of $\mathcal{O}(10^2)$ GeV and $\mathcal{O}(10^{17})$ GeV, which satisfy the conditions of the dark matter and the inflation. From this parameter set, mass spectrum of the scalar bosons is constrained by

$$m_H \lesssim 100\ {\rm GeV}, 142\ {\rm GeV} \lesssim m_{H^\pm} \lesssim 146\ {\rm GeV}. \tag{8.11}$$

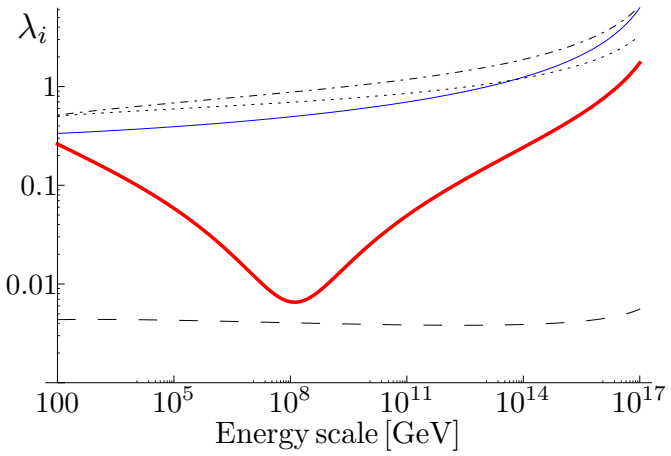

Figure 8.2: Running of the scalar coupling constants. Red (solid), blue (dashed), brown (dot-dashed), green (dotted) and black (long-dashed) curves show λ_1, λ_2, λ_3, $|\lambda_4|$ and λ_5, respectively.

	λ_1	λ_2	λ_3	λ_4	λ_5
10^2 GeV	0.262	0.335	0.514	-0.503	4.35×10^{-3}
10^{17} GeV	1.74	6.28	6.60	-3.30	5.57×10^{-3}

Table 8.2: The possible parameter set which satisfies constraints from the inflation condition and the dark matter data at the scales of 10^2 GeV and 10^{17} GeV.

8.3 Collider Phenomenology

In this scenario, $m_{H^\pm}$ is about 140 GeV. This value satisfies the lower bound from the LEP experiment [122, 123]. From the measurement of the Z boson decay width, $m_H + m_A$ is greater than m_Z [122, 124]. Moreover, the direct detection of dark matter at LEP give a constraint on HA pair production [124]. Because of the constraint from the inflation $m_H \lesssim 100$ GeV, the mass difference between the two inert scalar bosons is allowed only in a narrow region [122,124]:

$$m_H - m_A < 8 \text{ GeV}. \tag{8.12}$$

In Ref. [125], the collider phenomenology in the inert doublet model is discussed at the LHC with $\sqrt{s} = 14$ TeV. According to their work, the process of $q\overline{q} \to Z \to HA \to Z^{(*)}AA \to \ell^+\ell^- AA$ is dominant. They chose the mass difference of inert neutral scalar bosons to be 10, 50 and 70 GeV. As m_A is 65 GeV in our model, if the mass difference becomes large, inflation condition Eq. (8.6) cannot be satisfied. On the contrary, if the mass difference become small, the signal is also small ($S/\sqrt{B} = 0.02$). Therefore, the model is difficult to be tested at the LHC.

Let us discuss the signals of H, A and $H^\pm$ at the ILC with $\sqrt{s} = 500$ GeV. In this analysis, we use Calchep 2.5.6 for numerical evaluation [126]. The detail which contains background analysis

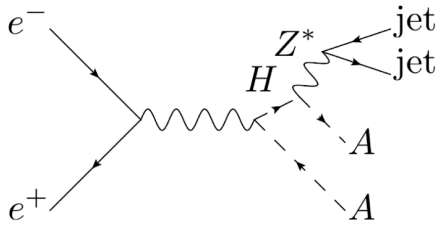

Figure 8.3: The signal of HA production at the ILC.

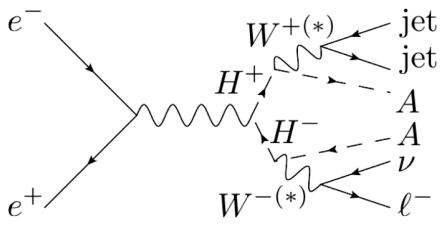

Figure 8.4: The signal of H^+H^- production at the ILC.

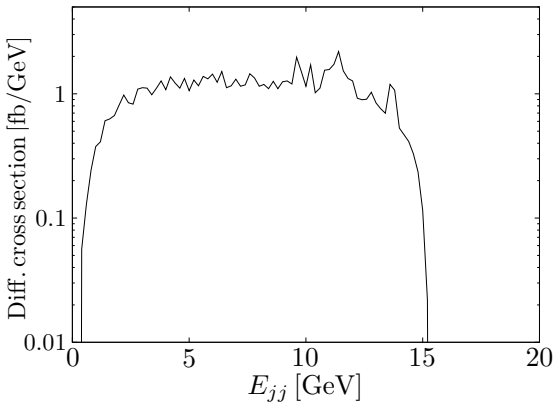

Figure 8.5: The distribution of E_{jj} for the cross section for $e^+e^- \to HA \to AAZ^* \to AAjj$. In our parameter set, the endpoint in the E_{jj} distribution is estimated at 0.28 GeV $< E_{jj} <$ 15 GeV. This value corresponds to $m_H = 67$ GeV, $m_A = 65$ GeV.

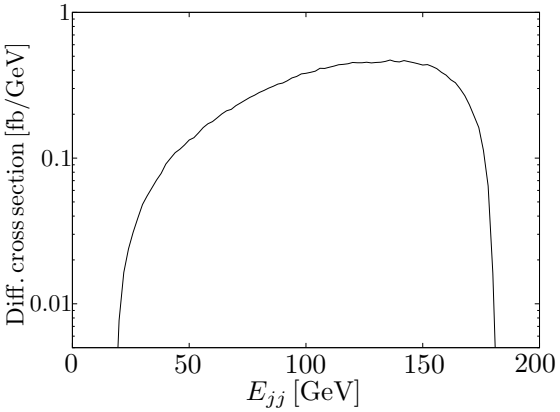

Figure 8.6: The distribution of E_{jj} for the cross section for $e^+e^- \to H^+H^- \to W^{+(*)}W^{-(*)}AA \to jj\ell\nu AA$. In our parameter set, the endpoint in the E_{jj} distribution is estimated at 17 GeV $< E_{jj} <$ 180 GeV. This value corresponds to $m_{H^\pm} = 140$ GeV, $m_A = 65$ GeV.

of inert doublet model is disused in the paper [127] which is applicable to our model. First, the dominant signal of the HA production process is $e^+e^- \to Z^* \to HA \to AAZ^* \to AAjj$ (j: jet, Z^*: off-shell Z boson) shown in Fig. 8.3. The final state is two jets with a missing momentum. The energy of the two-jet system E_{jj} satisfies the following equation because of the kinematical constraint given as

$$\frac{m_H^2 - m_A^2}{4m_H^2}\left(\sqrt{s} - \sqrt{s - 4m_H^2}\right) < E_{jj} < \frac{m_H^2 - m_A^2}{4m_H^2}\left(\sqrt{s} + \sqrt{s - 4m_H^2}\right). \tag{8.13}$$

When the center of mass energy is $\sqrt{s} = 500$ GeV, E_{jj} is evaluated by using our parameter set as 0.28 GeV $< E_{jj} <$ 15 GeV. The distribution of E_{jj} of the cross section for this prosecc is shown in Fig. 8.5. We expect that m_H and m_A can be measured by using the endpoints in the E_{jj} distribution at the ILC after the background reduction.

Next, the dominant signal of the H^+H^- production process is $e^+e^- \to Z^*(\gamma^*) \to H^+H^- \to W^{+(*)}W^{-(*)}AA \to jjl\nu AA$ ($W^{\pm(*)}$ is off-shell W boson) as shown in Fig. 8.4. The final state of this process is a charged lepton and two jets with the missing momentum. From the same discussion, the energy of the two-jet system, E_{jj} is constrained as

$$\frac{m_{H^\pm}^2 - m_A^2}{4m_{H^\pm}^2}\left(\sqrt{s} - \sqrt{s - 4m_{H^\pm}}\right) < E_{jj} < \frac{m_{H^\pm}^2 - m_A^2}{4m_{H^\pm}^2}\left(\sqrt{s} + \sqrt{s - 4m_{H^\pm}}\right). \tag{8.14}$$

When the center of mass energy is $\sqrt{s} = 500$ GeV, E_{jj} is evaluated by using our parameter set as 17 GeV $< E_{jj} <$ 180 GeV. The distribution of E_{jj} of the cross section for this process is shown in Fig. 8.6. We expect that $m_{H^\pm}$ and m_A can be measured by using the endpoints in the E_{jj} distribution at the ILC after the background reduction. Backgrounds could also be reduced by imposing kinematic cuts. We can measure $m_{H^\pm}$ and m_A by observing the endpoints in the E_{jj} distribution at the ILC.

8.4 Conclusion

In the original Higgs inflation scenario, it would be difficult to satisfy perturbative unitarity and vacuum stability. These problems can be solved by considering multi-Higgs models. In the framework of the radiative seesaw scenario with the multi-Higgs structure, we can explain not only dark matter, neutrino masses but also inflation. This scenario would be testable at the ILC by measuring the energy distribution of the inert scalar pair production.

Part V

Gravitational waves from electroweak phase transition

Chapter 9

$O(N)$ scalar singlet model

As a possible alternative method to test the strongly 1stOPT, we may be able to utilize future observation of gravitational waves (GWs) [33]. On February 11th, the first direct detection of GWs emitted by the merger of black holes at Advanced LIGO [34] was reported [35]. Furthermore, a number of observatories such as KAGRA [36], Advanced VIRGO [37] are trying to detect them. The target frequencies of GWs correspond to those from astronomical phenomena such as the binary of neutron stars, black holes, etc.. Once the GWs are detected in the near future, the era of GW astronomy will come true. Spectroscopy of GWs will make it possible to explore phenomena at the very early stage of the Universe, such as a strongly 1stOPT, cosmic inflation, topological defects like cosmic strings, domain wall, etc.

GWs originated from the strongly 1stOPT have been discussed in a model independent way in Refs. [38,40–42,44]. In the effective theory approach with higher order operators the possibility of detecting such GWs was studied by Delaunay et al. [46]. Apreda et al. evaluated spectra of GWs from the strongly 1stOPT due to thermal loop effects in the minimal supersymmetric SM (MSSM) [47], although such a scenario was already excluded by the LHC data. Espinosa et al. studied spectra of GWs in extended scalar sectors with the $O(N)$ symmetry [48, 49]. GWs from the non-thermal 1stOPT were investigated in singlet extensions of the SM [50] and the MSSM [47] and in the left-right symmetric model [51].

In this chapter, we discuss the possibility that future detailed observation of GWs is useful not only to test the electroweak 1stOPT but also as a probe of extended scalar sectors and further the physics behind. To this end, we evaluate spectra of GWs from the strongly 1stOPT at the EWSB in a set of extended scalar sectors with additional N isospin-singlet fields as an example of renormalizable theories which can cause the 1stOPT thermally. We find that the relic density of the produced GWs can be so significant that they are detectable at future GW interferometers such as DECIGO [128] and BBO [129]. The spectra depend on N and the mass of the additional scalar fields. We conclude that GWs can be a useful probe of physics behind the Higgs sector. This chapter is based on [130].

9.1 Model

9.1.1 Tree level scalar potential

We consider a set of extensions of the SM with additional N isospin-singlet scalars $\vec{S} = (S_1, S_2, \cdots, S_N)^T$ invariant under an $O(N)$ symmetry,

$$V_0(\Phi, \vec{S}) = V_{\rm SM}(\Phi) + \frac{\mu_S^2}{2}|\vec{S}|^2 + \frac{\lambda_S}{4}|\vec{S}|^4 + \frac{\lambda_{\Phi S}}{2}|\Phi|^2|\vec{S}|^2,$$

where $V_{\rm SM}$ is the Higgs potential of the SM. After the EWSB, the SM Higgs doublet is parametrized as

$$\Phi = \begin{pmatrix} \omega^+ \\ \frac{1}{\sqrt{2}}(v + h + iz) \end{pmatrix}$$

where $\omega^\pm$ and z are Nambu-Goldstone bosons and v ($\simeq 246$ GeV) is the vacuum expectation value (VEV). The $O(N)$ symmetry is assumed not to be spontaneously broken. The mass of h is set as $m_h = 125$ GeV, and the common mass of S_i is given at the tree level by

$$m_S^2 = \mu_S^2 + \frac{\lambda_{\Phi S}}{2}v^2. \tag{9.1}$$

We take m_S, μ_S^2 and λ_S as input free parameters in the scalar sector.

9.1.2 Theoretical constraints

The conditions for vacuum stability are given by

$$\lambda > 0, \quad \lambda_S > 0, \quad \sqrt{2\lambda\lambda_S} + \lambda_{\Phi S} > 0. \tag{9.2}$$

As for the constraint from perturbative unitarity for the S-wave amplitudes of two body elastic scatterings of longitudinally polarized weak bosons and all scalar bosons of the model, we obtain the strongest bound as

$$3\lambda + (N+2)\lambda_S + \sqrt{\{3\lambda - (N+2)\lambda_S\}^2 + 4N\lambda_{\Phi S}^2} < 16\pi. \tag{9.3}$$

For the derivation of the above constraint, see Appendix. C.

9.2 One loop effective potential at zero temperature

9.2.1 Renormalized effective potential

Order parameters are given by

$$\langle\Phi\rangle = \frac{1}{\sqrt{2}}\varphi, \quad \left\langle\vec{S}\right\rangle = 0. \tag{9.4}$$

The one-loop effective potential at zero temperature is given by

$$V_{\rm eff}(\varphi, T=0) = V_0(\varphi) + \Delta V_1(\varphi) + V^{\rm c.t.}(\varphi). \tag{9.5}$$

The tree level potential $V_0(\varphi)$ and the one-loop potential $\Delta V_1(\varphi)$ are given by

$$V_0(\varphi) = -\frac{\mu^2}{2}\varphi^2 + \frac{\lambda}{8}\varphi^4, \quad \Delta V_1(\varphi) = \sum_i \frac{n_i}{64\,\pi^2} M_i^4(\varphi)\left\{\ln\frac{M_i^2(\varphi)}{Q^2} - c_i - \Delta\right\}, \tag{9.6}$$

where c_i=3/2, $\Delta = 1/\epsilon - \gamma + \ln 4\pi$, $M_i(\varphi)$ and n_i are the field-dependent mass and the degrees of freedom for each particles F_i, respectively

$$\begin{aligned} n_{W_L^\pm} &= 4, \quad n_{Z_L} = 2, \quad n_{\gamma_L} = 2, \\ n_{W_T^\pm} &= 2, \quad n_{Z_T} = 1, \quad n_{\gamma_T} = 1, \\ n_t &= -12, \quad n_b = -12, \quad n_S = N, \end{aligned} \tag{9.7}$$

and Q is the renormalization scale. The counter term of the dimension full parameter μ^2 is given by

$$V^{\text{c.t.}}(\varphi) = -\frac{1}{2}\delta\mu^2\varphi^2. \tag{9.8}$$

If we define the renormalized vacuum expectation value v, the renormalized mass of the Higgs boson m_h and the renormalized Higgs self-coupling at the one loop level by the following three conditions ($\overline{\text{DR}}$ renormalization scheme),

$$0 \equiv \left.\frac{\partial V_{\text{eff}}(\varphi, T=0)}{\partial\varphi}\right|_{\varphi=v}, \quad m_h^2 \equiv \left.\frac{\partial^2 V_{\text{eff}}(\varphi, T=0)}{\partial\varphi^2}\right|_{\varphi=v}, \tag{9.9}$$

we obtain

$$\ln Q^2 = \frac{\sum_i n_i \left(\frac{\partial M_i^2(\varphi)}{\partial\varphi}\big|_{\varphi=v}\right)^2 \ln m_i^2}{\sum_i n_i \left(\frac{\partial M_i^2(\varphi)}{\partial\varphi}\big|_{\varphi=v}\right)^2}, \quad \delta\mu^2 = \sum_i \frac{n_i m_i^2}{32\pi^2 v}\left.\frac{\partial M_i^2(\varphi)}{\partial\varphi}\right|_{\varphi=v}\left(\ln\frac{m_i^2}{Q^2} - 1\right), \tag{9.10}$$

where m_i is the physical mass of the i-th particle running in the loop.

Thus, the tree level potential $V_0(\varphi)$ and the renormalized one-loop potential $\Delta V_1(\varphi)$ are obtained as

$$V_0(\varphi) = \frac{m_h^2}{8v^2}(\varphi^2 - v^2)^2, \tag{9.11}$$

$$\begin{aligned} \Delta V_1(\varphi) = &\sum_{i=W^\pm,Z,\gamma,t,b} \frac{n_i}{64\,\pi^2}\left(2m_i^2 M_i^2(\varphi) + M_i^4(\varphi)\left\{\ln\frac{M_i^2(\varphi)}{m_i^2} - \frac{3}{2}\right\} + \{M_i^4(\varphi) - 2m_i^2 M_i^2(\varphi)\}\ln\frac{m_i^2}{Q^2}\right) \\ &+\frac{N}{64\,\pi^2}\left(2m_S^2(M_S^2(\varphi) - \mu_S^2) + M_S^4(\varphi)\left\{\ln\frac{M_S^2(\varphi)}{m_S^2} - \frac{3}{2}\right\} + \{M_S^4(\varphi) - 2m_S^2(M_S^2(\varphi) - \mu_S^2)\}\ln\frac{m_S^2}{Q^2}\right). \end{aligned} \tag{9.12}$$

Here, we have neglected the one loop contribution of the Higgs boson.

9.2.2 Triple Higgs boson coupling

The renormalized triple Higgs boson coupling is calculated at the one loop level in our model as

$$\begin{aligned}\lambda_{hhh} &\equiv \left.\frac{\partial^3 V_{\rm eff}(\varphi, T=0)}{\partial \varphi^3}\right|_{\varphi=v} \\ &= \frac{3m_h^2}{v}\left\{1 - \frac{1}{\pi^2}\frac{m_t^4}{v^2 m_h^2} + \frac{N}{12\pi^2}\frac{m_S^4}{v^2 m_h^2}\left(1 - \frac{\mu_S^2}{m_S^2}\right)^3\right\}. \end{aligned} \tag{9.13}$$

There are two sources for the physical common mass m_S of the scalar fields S_i, as shown in Eq. (9.1). If m_S is large because of a large value of μ_S, the one loop correction in Eq. (9.13) decouples in the large mass limit. Instead, if μ_S is relatively small as v, the one loop contribution does not decouple and a quartic powerlike contribution for the mass remains in λ_{hhh} [75]. On the other hand, the triple Higgs boson coupling at one-loop in SM $\lambda_{hhh}^{\rm SM}$ is approximately given by [75]

$$\lambda_{hhh}^{\rm SM} = \frac{3m_h^2}{v}\left(1 - \frac{m_t^4}{\pi^2 m_h^2 v^2}\right). \tag{9.14}$$

Then, deviation of the triple Higgs boson coupling is defined by

$$\frac{\Delta\lambda_{hhh}}{\lambda_{hhh}^{\rm SM}} = \frac{\lambda_{hhh}}{\lambda_{hhh}^{\rm SM}} - 1. \tag{9.15}$$

9.3 One loop effective potential at finite temperature

9.3.1 Thermal mass

When we consider a ring-improved effective potential by replacing the field-dependent masses in Eq. (9.5) as [78]

$$M_i^2(\varphi) \to M_i^2(\varphi, T) = M_i^2(\varphi) + \Pi_i(T), \tag{9.16}$$

where $\Pi_i(T)$ is the finite temperature contribution to the self-energies, field dependent masses of the gauge bosons in the one-loop contribution at zero temperature are replaced by thermally corrected ones,

$$\Delta V_1(\varphi) \to \Delta V_1(\varphi, T). \tag{9.17}$$

The thermally corrected field-dependent masses of the gauge bosons are explained by

$$M_g^{2(L,T)}(\varphi, T) = \frac{\varphi^2}{4}\begin{pmatrix} g^2 & & & \\ & g^2 & & \\ & & g^2 & gg' \\ & & gg' & g'^2 \end{pmatrix} + a_g^{L,T}T^2\begin{pmatrix} g^2 & & & \\ & g^2 & & \\ & & g^2 & \\ & & & g'^2 \end{pmatrix} \tag{9.18}$$

in the (W^+, W^-, W^3, B) basis with $a_g^L = 11/6$, $a_g^T = 0$. Notice that only the self-energy for the longitudinal modes of the gauge bosons receive thermal corrections. The field-dependent masses of fermions do not receive thermal corrections,

$$M_{t,b}^2(\varphi) = m_{t,b}^2 \frac{\varphi^2}{v^2}. \tag{9.19}$$

The thermally corrected field-dependent mass of the singlet scalars are explained by

$$M_S^2(\varphi, T) = (m_S^2 - \mu_S^2)\frac{\varphi^2}{v^2} + \mu_S^2 + \Pi_S(T), \tag{9.20}$$

where

$$\Pi_S(T) = \frac{T^2}{12v^2}[(N+2)\lambda_S v^2 + 4(m_S^2 - \mu_S^2)]. \tag{9.21}$$

9.3.2 Effective potential at finite temperature

The effective potential at finite temperatures is given at the one-loop level by

$$V_{\rm eff}(\varphi, T) = V_0(\varphi) + \Delta V_1(\varphi, T) + \Delta V_T(\varphi, T). \tag{9.22}$$

The finite-temperature contribution to the effective potential is written as

$$\Delta V_T(\varphi, T) = \frac{T^4}{2\pi^2}\left\{ \sum_{i=W^\pm, Z, \gamma, S} n_i I_{\rm B}(a_i^2) + \sum_{i=t,b} n_i I_{\rm F}(a_i^2) \right\} \tag{9.23}$$

where

$$I_{\rm B,F}(a_i^2) \equiv \int_0^\infty dx\, x^2 \, \ln\left[1 \mp \exp\left(-\sqrt{x^2 + a_i^2}\right)\right], \tag{9.24}$$

with $a_i = M_i(\varphi, T)/T$.

9.3.3 First order electroweak phase transition

We can calculate φ_c/T_c numerically without using high temperature expansion by using the ring-improved finite temperature effective potential in Eq. (9.22). We show the region which satisfies both $\varphi_c/T_c > 1$ and $\Gamma/H^4|_{T=T_t} \simeq 1$ (discussed in Sec. 9.3.4), where EWBG can be viable with the strongly 1stOPT on the plane of N and m_S in Fig. 9.1 (left) and on the plane of $\sqrt{\mu_S^2}$ and m_S in Fig. 9.1 (right). In Fig. 9.1 (left), to obtain maximal non-decoupling effects, we set μ_S^2 to be 0. In Fig. 9.1 (right), we show the results for $N = 12$. We also show contour plots for the deviation in the hhh coupling from the SM prediction.

We find that, as indicated in Ref. [20] in the case of the two Higgs doublet model (2HDM), significant deviations in the hhh coupling appear in the allowed region of the strongly 1stOPT. Notice that the scenario of the 2HDM in Ref. [20] corresponds to $N = 4$ in our model [**?**]. We emphasize that the correlation between the strongly 1stOPT and the large deviation in the hhh coupling is a common feature of the models where the condition of quick sphaleron decoupling is satisfied by the thermal loop effects of additional scalar bosons. This property can be utilized to test scenarios of EWBG by measuring the hhh coupling at the ILC as we already pointed out.

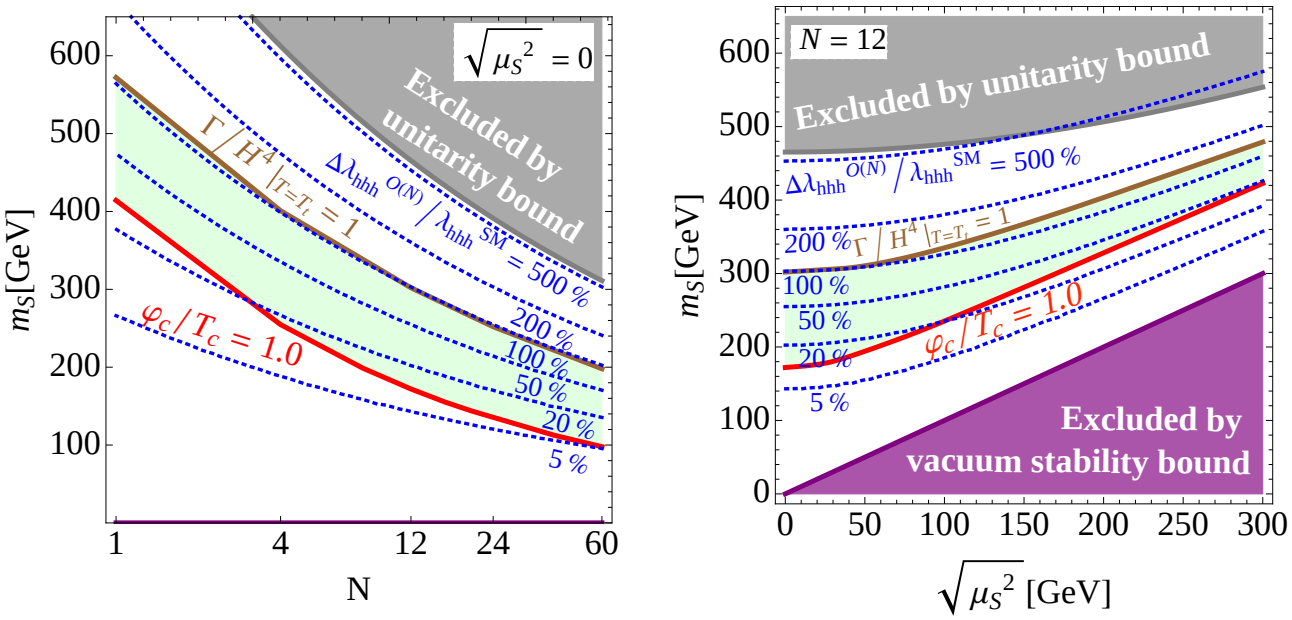

Figure 9.1: The allowed region which satisfies both $\varphi_c/T_c > 1$ and $\Gamma/H^4|_{T=T_t} \simeq 1$, where EWBG can be viable with the strongly 1stOPT on the plane of N and m_S in the left figure and on the plane of $\sqrt{\mu_S^2}$ and m_S in the right figure. We set $\mu_S^2 = 0$ for the left figure, and $N = 12$ for the right figure. Contours for the deviation in the hhh coupling from the SM prediction are also shown in both figures. Bounds from vacuum stability and perturbative unitarity are also shown for $\lambda_S = 0$.

9.3.4 Characteristic parameters of phase transition

On the other hand, characteristic parameters of phase transition can be also calculated from the effective potential in Eq. (9.22). The parameter α is the ratio of the false-vacuum energy density $\epsilon(T)$ and the thermal energy density $\rho_{\rm rad}(T)$ in the symmetric phase by

$$\alpha \equiv \frac{\epsilon(T_t)}{\rho_{\rm rad}(T_t)}$$

and

$$\epsilon(T) \equiv -\Delta V_{\rm eff}(\varphi_B(T), T) + T\frac{\partial \Delta V_{\rm eff}(\varphi_B(T), T)}{\partial T},$$

where $\Delta V_{\rm eff}(\varphi(T), T)$ is the free energy density with respect to that of the symmetric phase, and $\varphi_B(T)$ is the broken phase minimum at T. The radiation energy density is given by $\rho_{\rm rad}(T) = (\pi^2/30)g_*(T)T^4$.

The parameter β is defined as

$$\beta \equiv -\left.\frac{dS_E}{dt}\right|_{t=t_t} \simeq \left.\frac{1}{\Gamma}\frac{d\Gamma}{dt}\right|_{t=t_t},$$

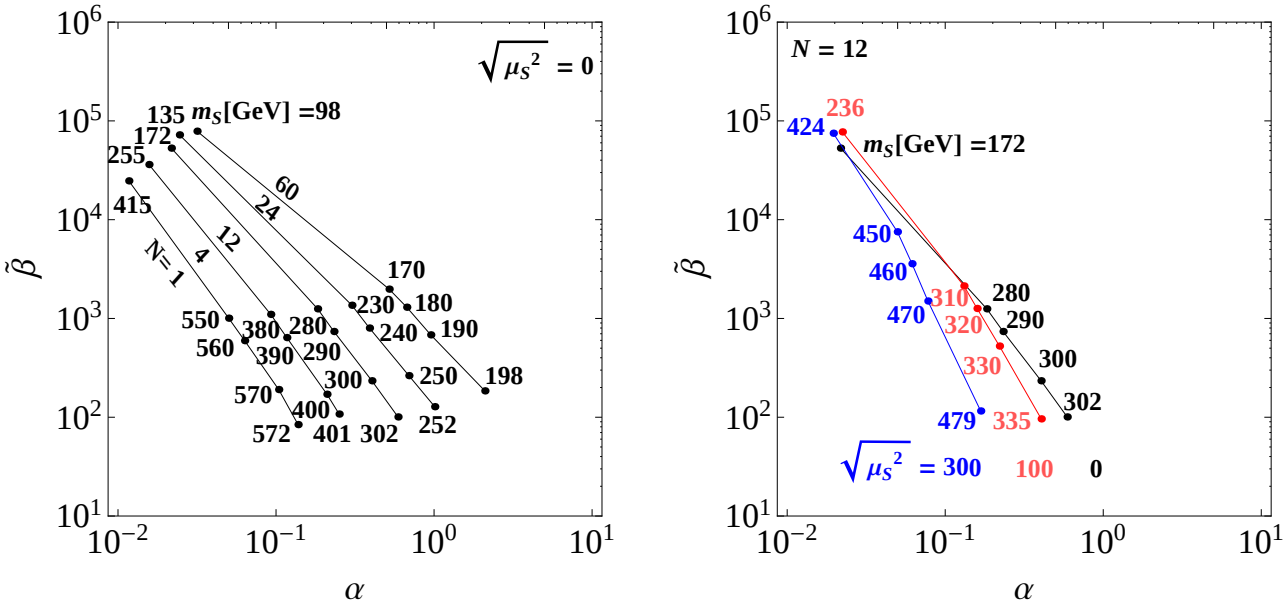

Figure 9.2: The allowed region on $(\alpha,\, \tilde{\beta})$ plane which satisfies both $\varphi_c/T_c > 1$ and $\Gamma/H^4|_{T=T_t} \simeq 1$ in Fig. fig1. We set $\mu_S^2 = 0$ for the left figure, and $N = 12$ for the right figure.

where t_t is the phase transition time, $S_E(T) \simeq S_3(T)/T$ with S_3 being the three dimensional Euclidean action,

$$S_3 \equiv \int d^3r \left[\frac{1}{2}(\vec{\nabla}\varphi)^2 + V_{\rm eff}(\varphi, T)\right],$$

and $\Gamma = \Gamma_0(T)\exp[-S_E(T)]$ is the rate of variation of the bubble nucleation rate with $\Gamma_0(T) \propto T^4$. We then obtain the normalized dimensionless parameter as

$$\tilde{\beta} \equiv \frac{\beta}{H_t} = T_t \frac{d}{dT}\left(\frac{S_3(T)}{T}\right)\bigg|_{T=T_t}.$$

When the phase transition is complete; i.e.,

$$\frac{\Gamma}{H^4}\bigg|_{T=T_t} \simeq 1, \tag{9.25}$$

we obtain $S_3(T_t)/T_t = 4\ln(T_t/H_t) \simeq 140 - 150$.

In Fig. 9.2 (left), the allowed region on $(\alpha,\, \tilde{\beta})$-plane which satisfies both $\varphi_c/T_c > 1$ and $\Gamma/H^4|_{T=T_t} \simeq 1$ in Fig. fig1. We set $\mu_S^2 = 0$ for the left figure, and $N = 12$ for the right figure.

9.4 Gravitational waves from electroweak phase transition

9.4.1 The relic abundance of gravitational waves

The relic abundance of GWs from the electroweak 1stOPT is composed of the contributions from bubble collisions and the turbulence in the plasma as [38]

$$\Omega_{\rm GW}(f)h^2 = \Omega_{\rm coll}(f)h^2 + \Omega_{\rm turb}(f)h^2.$$

If the electroweak phase transition is strongly first order, for instance, the kinetic energy stored in the Higgs field and the bulk motion of the plasma is partially released into gravitational waves. This happens mostly at the end of the phase transition, when collisions break the spherical symmetry of the individual Higgs field bubbles. This possibility was systematically analyzed in papers [33, 39]. In our analysis, we employ the results of Ref. [39] for the bubble collision contribution

$$\Omega_{\rm coll}(f)h^2 = \widetilde{\Omega}_{\rm coll}h^2 \times \begin{cases} \left(\frac{f}{\tilde{f}_{\rm coll}}\right)^{2.8} & (\text{for } f < \tilde{f}_{\rm coll}) \\ \left(\frac{f}{\tilde{f}_{\rm coll}}\right)^{-1} & (\text{for } f > \tilde{f}_{\rm coll}) \end{cases},$$

where the energy density[1] is obtained as

$$\widetilde{\Omega}_{\rm coll}h^2 \simeq 1.1\times 10^{-6}\kappa^2 \left(\frac{H_t}{\beta}\right)^2 \left(\frac{\alpha}{1+\alpha}\right)^2 \left(\frac{v_b^3}{0.24+v_b^3}\right)\left(\frac{100}{g_*^t}\right)^{1/3},$$

at the peak frequency given by

$$\tilde{f}_{\rm coll} \simeq 5.2\times 10^{-3}{\rm mHz}\left(\frac{\beta}{H_t}\right)\left(\frac{T_t}{100{\rm GeV}}\right)\left(\frac{g_*^t}{100}\right)^{1/6}.$$

When bubbles collide, the plasma is stirred up at a length scale comparable to the size of the colliding bubbles. Larger bubbles are more energetic than smaller ones, and indeed it can be

[1] Because β^{-1} is the order of typical time scale, Einstein equation $\Box h^{\mu\nu} = 16\pi G(\rho_{\rm kin}^{\mu\nu} + \cdots)$ gives the relation $\dot{h}^{\mu\nu} \simeq 16\pi G\rho_{\rm kin}^{\mu\nu}/\beta$. Then, the energy density of gravitational waves is written as

$$\rho_{\rm GW}^* \equiv \frac{\dot{h}^2}{32\pi G} \simeq \frac{8\pi G\rho_{\rm kin}^2}{\beta^2}. \tag{9.26}$$

The relic abundance of gravitational waves is

$$\begin{aligned}\Omega_{\rm GW}^* \equiv \frac{\rho_{\rm GW}^*}{\rho_{\rm tot}^*} &= \frac{8\pi G\rho_{\rm kin}^2}{\beta^2}\frac{1}{(\rho_{\rm vac}^* + \rho_{\rm rad}^*)^2}\frac{3H_*^2}{8\pi G} \\ &\simeq \kappa^2\left(\frac{H_*}{\beta}\right)^2\left(\frac{\alpha}{\alpha+1}\right),\end{aligned} \tag{9.27}$$

where we use $3H_*^2/8\pi G = \rho_{\rm rad}^* + \rho_{\rm vac}^* = \rho_{\rm tot}^*$, $\alpha = \rho_{\rm vac}^*/\rho_{rad}^*$, $\kappa = \rho_{\rm kin}/\rho_{\rm vac}$. Exact forma of $\Omega_{\rm GW}^*$ is calculated by numerical calculation.

shown that the most part of the kinetic energy involved in the process is released at the largest length scale in the system, namely the radius of the largest bubbles at the end of the transition. Once the large eddies have formed, after a few revolutions they decay into smaller ones, thus giving rise to the usual turbulent energy cascade. For such the plasma turbulence contribution, we use [131]

$$\Omega_{\rm turb}(f)h^2 = \widetilde{\Omega}_{\rm turb}h^2 \times \begin{cases} \left(\frac{f}{\tilde{f}_{\rm turb}}\right)^2 & (\text{for } f < \tilde{f}_{\rm turb}) \\ \left(\frac{f}{\tilde{f}_{\rm turb}}\right)^{-3.5} & (\text{for } f > \tilde{f}_{\rm turb}) \end{cases},$$

where the energy density is evaluated as

$$\widetilde{\Omega}_{\rm turb}h^2 \simeq 1.4 \times 10^{-4} u_s^5 v_b^2 \left(\frac{H_t}{\beta}\right)^2 \left(\frac{100}{g_*^t}\right)^{1/3},$$

at the peak frequency given by

$$\tilde{f}_{\rm turb} \simeq 3.4 \times 10^{-3}{\rm mHz}\frac{u_s}{v_b}\left(\frac{\beta}{H_t}\right)\left(\frac{T_t}{100{\rm GeV}}\right)\left(\frac{g_*^t}{100}\right)^{1/6}.$$

The bubble wall velocity $v_b(\alpha)$, the turbulent fluid velocity $u_s(\alpha)$ and the efficiency factor $\kappa(\alpha)$ are given in Ref. [33], and g_*^t $(= g_*(T_t))$ is the total number of effective degree of freedom at the transition temperature T_t. H_t is the Hubble parameter at T_t in the radiation dominant Universe.

9.4.2 Predicted spectra of gravitational waves

In Fig. 9.3 (left), the predicted spectra of GWs are shown as a function of the frequency for $N = 1$, 4, 12, 24 and 60 with $\sqrt{\mu_s^2} = 0$ in the $O(N)$ singlet model. For each N, m_S is taken its maximal value under the condition of the complete phase transition given in Eq. (9.25). These sets of (N, m_S) are all in the allowed region shown in Fig. 9.1, where EWBG is possible. Curves of expected experimental sensitivities for GWs at eLISA, DECIGO/BBO and Ultimate-DECIGO are also shown [132, 133]. Estimated foreground noise from white dwarf binaries in Ref. [134] are also shown. One can see that for larger N the strength of GWs is more significant and the spectra are within the observable reach of DECIGO/BBO. Even for smaller values of m_S or for the case of $N = 1$, the spectra may be able to be observed at Ultimate-DECIGO. There is a strong correlation between the strength of the GWs and the value of φ_c/T_c (hence, $\Delta\lambda_{hhh}^{O(N)}/\lambda_{hhh}^{\rm SM}$).

In Fig. 9.3 (right), we show the predictions of the model for $N = 1$, 4, 12, 24 and 60 with various m_S with $\sqrt{\mu_s^2} = 0$ on the $(\alpha, \tilde{\beta})$ plane under the conditions of $\varphi_c/T_c > 1$ and the complete phase transition. We set $T_t = 100$ GeV, as the result is not very sensitive to T_t. Regions of expected experimental sensitivity at eLISA, DECIGO/BBO and Ultimate-DECIGO are also shown. One can see that different sets of (N, m_S) corresponds to different points on the $(\alpha, \tilde{\beta})$ plane. Therefore, future GW observation experiments can be a probe of distinguishing various models of the electroweak 1stOPT.

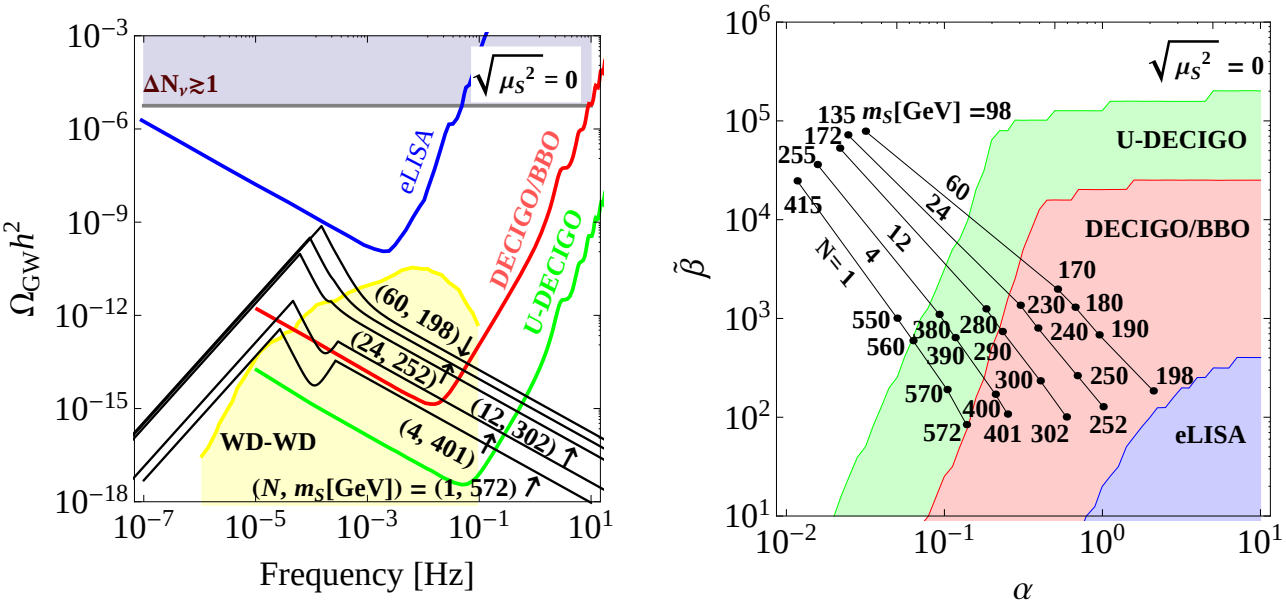

Figure 9.3: (Left) Spectra of GWs in the $O(N)$ singlet model with expected experimental sensitivities at the future GW interferometers, eLISA, DECIGO/BBO and Ultimate-DECIGO (U-DECIGO) are shown for $\sqrt{\mu_S^2} = 0$. The bound from non-observation of the energy density of extra radiation is indicated by $\Delta N_\nu \gtrsim 1$ [135, 136], and the estimated foreground noise from the white dwarf binaries is also shown. (Right) Predictions of the model on the $(\alpha, \tilde{\beta})$ plane with various N and m_S assuming $\sqrt{\mu_S^2} = 0$ and $T_t = 100$ GeV are shown with regions of expected experimental sensitivity at the future GW interferometers.

9.5 Conclusion

We have investigated spectra of GWs which come from the strongly electroweak 1stOPT, which is required for a successful scenario of EWBG in a set of extended scalar sectors with additional N isospin-singlet fields as a concrete example of renormalizable theories. The hhh coupling also has been evaluated at the one loop level in these models. The produced GWs can be significant, so that they are detectable at future GW interferometers such as DECIGO and BBO. Furthermore, since the spectra strongly depend on N and m_S, we conclude that future detailed observation of GWs can be generally useful as a probe of extended scalar sectors with the 1stOPT.

Part VI
Summary of this thesis

In Part III, we have discussed two radiation seesaw models that can explain tiny neutrino masses and DM at the same time. First, we have presented a simple extension of the νTHDM by introducing the third $SU(2)_L$-doublet scalar field η and two neutral $SU(2)_L$ singlet fields (s_1^0 and s_2^0). Although the global $U(1)_X$ is broken by a VEV of s_1^0, there remains a residual Z_2 symmetry under which η and s_2^0 are Z_2-odd particles. These Z_2-odd particles provide a dark matter candidate. The v_ν for neutrino masses can be suppressed without requiring very heavy particles because the VEV is generated at the one-loop level. Second, we have improved the model in Ref. [100] by considering anomaly cancellation of the $U(1)_{B-L}$ gauge symmetry. We have shown that there are four anomaly-free cases of B−L charge assignment, and three of them have an unbroken global $U(1)_{DM}$ symmetry. The $U(1)_{DM}$ guarantees that the lightest $U(1)_{DM}$-charged particle is stable such that it can be regarded as a DM candidate. The spontaneous breaking of the $U(1)_{B-L}$ symmetry generates the Majorana mass term of ν_R and masses of new fermions ψ. In addition, the Dirac mass term of neutrinos is generated at the one-loop level where the DM candidate involved in the loop. Tiny neutrino masses are obtained at the two-loop level.

In Part IV, we have investigated a simple model to explain inflation, neutrino masses and DM simultaneously. We have shown that this scenario would be testable at the ILC by measuring the energy distribution of the inert scalar pair production.

In Part V, we have discussed spectra of GWs which are originated by the strongly first order phase transition at the electroweak symmetry breaking, which is required for a successful scenario of electroweak baryogenesis. We have shown the produced GWs can be significant. we conclude that future detailed observation of GWs can be generally useful as a probe of extended scalar sectors with the 1stOPT.

In this thesis, we have discussed particle phenomenology, in particular in the field where Higgs physics is related to beyond the standard model. We have investigated new physics models which can solve beyond the SM phenomena such as neutrino oscillation, DM, BAU and cosmic inflation. We have considered testability of particle theory by using space experiments such as observations of GWs, observations of the CMB, direct detection of DM, etc. in addition to future collider experiments. The new physics may be described by introducing an extended Higgs sector. In this case, by exploring the Higgs sector, it is possible to approach not only the nature of electroweak symmetry breaking but also new physics.

Appendix

Appendix A

Neutrinophilic two Higgs doublet model

A.1 Scalar Potential

The scalar potential V is given by

$$
\begin{aligned}
V &= V_2 + V_3 + V_4, && \text{(A.1)}\\
V_2 &= -\mu_{s1}^2|s_1^0|^2 + \mu_{s2}^2|s_2^0|^2 - \mu_{\Phi 1}^2\Phi^\dagger\Phi + \mu_{\Phi 2}^2\Phi_\nu^\dagger\Phi_\nu + \mu_\eta^2\eta^\dagger\eta, && \text{(A.2)}\\
V_3 &= -\mu\, s_1^{0*}(s_2^0)^2 + \text{h.c.}, && \text{(A.3)}\\
V_4 &= \lambda_{s1}|s_1^0|^4 + \lambda_{s2}|s_2^0|^4 + \lambda_{s12}|s_1^0|^2|s_2^0|^2 \\
&\quad + \lambda_{\Phi 1}(\Phi^\dagger\Phi)^2 + \lambda_{\Phi 2}(\Phi_\nu^\dagger\Phi_\nu)^2 + \lambda_\eta(\eta^\dagger\eta)^2 \\
&\quad + \lambda_{\Phi 12}(\Phi^\dagger\Phi)(\Phi_\nu^\dagger\Phi_\nu) + \lambda_{\Phi 1\eta}(\Phi^\dagger\Phi)(\eta^\dagger\eta) + \lambda_{\Phi 2\eta}(\Phi_\nu^\dagger\Phi_\nu)(\eta^\dagger\eta) \\
&\quad + \lambda'_{\Phi 12}(\Phi^\dagger\Phi_\nu)(\Phi_\nu^\dagger\Phi) + \lambda'_{\Phi 1\eta}(\Phi^\dagger\eta)(\eta^\dagger\Phi) + \lambda'_{\Phi 2\eta}(\Phi_\nu^\dagger\eta)(\eta^\dagger\Phi_\nu) \\
&\quad + \left(\lambda_{\Phi 12\eta}(\Phi_\nu^\dagger\eta)(\Phi^\dagger\eta) + \text{h.c.}\right) \\
&\quad + \lambda_{s1\Phi 1}|s_1^0|^2(\Phi^\dagger\Phi) + \lambda_{s1\Phi 2}|s_1^0|^2(\Phi_\nu^\dagger\Phi_\nu) + \lambda_{s1\eta}|s_1^0|^2(\eta^\dagger\eta) \\
&\quad + \lambda_{s2\Phi 1}|s_2^0|^2(\Phi^\dagger\Phi) + \lambda_{s2\Phi 2}|s_2^0|^2(\Phi_\nu^\dagger\Phi_\nu) + \lambda_{s2\eta}|s_2^0|^2(\eta^\dagger\eta) \\
&\quad + \left(\lambda_{s\Phi 1\eta}\, s_1^{0*}(s_2^0)^*\Phi^\dagger\eta + \text{h.c.}\right) + \left(\lambda_{s\Phi 2\eta}\, s_1^0 s_2^0\Phi_\nu^\dagger\eta + \text{h.c.}\right). && \text{(A.4)}
\end{aligned}
$$

Actually, the following simplified V_4 is sufficient for our discussion:

$$
\begin{aligned}
V_4(\text{simplified}) &= \lambda_{\Phi 1}(\Phi^\dagger\Phi)^2 + \lambda_{s2}|s_2^0|^4 + \lambda_{s2\Phi 1}|s_2^0|^2(\Phi^\dagger\Phi) \\
&\quad + \lambda_\eta(\eta^\dagger\eta)^2 + \lambda_{\Phi 1\eta}(\Phi^\dagger\Phi)(\eta^\dagger\eta) + \lambda_{\Phi 2\eta}(\Phi^\dagger\eta)(\eta^\dagger\Phi) \\
&\quad + \lambda_{s1}|s_1^0|^4 + \lambda_{\Phi 2}(\Phi_\nu^\dagger\Phi_\nu)^2 \\
&\quad + \left(\lambda_{s\Phi 1\eta}\, s_1^{0*}(s_2^0)^*\Phi^\dagger\eta + \text{h.c.}\right) + \left(\lambda_{s\Phi 2\eta}\, s_1^0 s_2^0\Phi_\nu^\dagger\eta + \text{h.c.}\right). && \text{(A.5)}
\end{aligned}
$$

A.2 Masses of Scalar Bosons

Scalar fields are decomposed as follows: $\phi^0 = (v + \phi_r^0 + i\phi_i^0)$, $\phi_\nu^0 = \frac{1}{\sqrt{2}}(v_\nu + \phi_{\nu r}^0 + i\phi_{\nu i}^0)/\sqrt{2}$, $s_1^0 = (v_s + s_{1r}^0 + is_{1i}^0)/\sqrt{2}$, $\eta^0 = (\eta_r^0 + i\eta_i^0)/\sqrt{2}$, $s_2^0 = (s_{2r}^0 + is_{2i}^0)/\sqrt{2}$. We ignore v_ν in the following formulae.

The mass matrix for (s^0_{2r}, η^0_r) is obtained as

$$M^2_{\mathcal{H}} = \begin{pmatrix} m^2_{s2} - \sqrt{2}\,\mu v_s & \dfrac{1}{2}\lambda_{s\Phi 1\eta}\, v\, v_s \\ \dfrac{1}{2}\lambda_{s\Phi 1\eta}\, v\, v_s & m^2_\eta \end{pmatrix}, \tag{A.6}$$

where $m^2_{s2} \equiv \mu^2_{s2} + (\lambda_{s2\Phi 1} v^2 + \lambda_{s12} v_s^2)/2$ and $m^2_\eta \equiv \mu^2_\eta + \left\{ \left(\lambda_{\Phi 1\eta} + \lambda'_{\Phi 1\eta}\right) v^2 + \lambda_{s1\eta} v_s^2 \right\}/2$. On the other hand, The mass matrix for (s^0_{2i}, η^0_i) results in

$$M^2_{\mathcal{A}} = \begin{pmatrix} m^2_{s2} + \sqrt{2}\,\mu v_s & \dfrac{1}{2}\lambda_{s\Phi 1\eta}\, v\, v_s \\ \dfrac{1}{2}\lambda_{s\Phi 1\eta}\, v\, v_s & m^2_\eta \end{pmatrix}. \tag{A.7}$$

Notice that the difference between $M^2_{\mathcal{H}}$ and $M^2_{\mathcal{A}}$ exists only in the $(1,1)$ element as $(M^2_{\mathcal{A}})_{11} = (M^2_{\mathcal{H}})_{11} + 2\sqrt{2}\,\mu v_s$. Mass eigenstates ($\mathcal{H}^0_1$ and $\mathcal{H}^0_2$) of Z_2-odd CP-even scalar bosons are given by

$$\begin{pmatrix} \mathcal{H}^0_1 \\ \mathcal{H}^0_2 \end{pmatrix} = \begin{pmatrix} \cos\theta'_0 & -\sin\theta'_0 \\ \sin\theta'_0 & \cos\theta'_0 \end{pmatrix} \begin{pmatrix} s^0_{2r} \\ \eta^0_r \end{pmatrix}, \quad \tan(2\theta'_0) = \frac{\lambda_{s\Phi 1\eta}\, v\, v_s}{m^2_\eta - m^2_{s2} + \sqrt{2}\,\mu v_s}, \tag{A.8}$$

while mass eigenstates ($\mathcal{H}^0_1$ and $\mathcal{H}^0_2$) of Z_2-odd CP-odd scalar bosons are obtained as

$$\begin{pmatrix} \mathcal{A}^0_1 \\ \mathcal{A}^0_2 \end{pmatrix} = \begin{pmatrix} \cos\theta'_A & -\sin\theta'_A \\ \sin\theta'_A & \cos\theta'_A \end{pmatrix} \begin{pmatrix} s^0_{2i} \\ \eta^0_i \end{pmatrix}, \quad \tan(2\theta'_A) = \frac{\lambda_{s\Phi 1\eta}\, v\, v_s}{m^2_\eta - m^2_{s2} - \sqrt{2}\,\mu v_s}. \tag{A.9}$$

The mass eigenstate $\mathcal{H}^\pm$ of Z_2-odd charged scalar boson is identical to $\eta^\pm$:

$$\mathcal{H}^\pm = \eta^\pm. \tag{A.10}$$

Masses of these Z_2-odd scalar bosons are calculated as

$$m^2_{\mathcal{H}^0_1} = \frac{1}{2}\left\{ m^2_\eta + m^2_{s2} - \sqrt{2}\,\mu v_s - \sqrt{\left(m^2_\eta - m^2_{s2} + \sqrt{2}\,\mu v_s\right)^2 + \lambda^2_{s\Phi 1\eta}\, v^2 v_s^2} \right\}, \tag{A.11}$$

$$m^2_{\mathcal{H}^0_2} = \frac{1}{2}\left\{ m^2_\eta + m^2_{s2} - \sqrt{2}\,\mu v_s + \sqrt{\left(m^2_\eta - m^2_{s2} + \sqrt{2}\,\mu v_s\right)^2 + \lambda^2_{s\Phi 1\eta}\, v^2 v_s^2} \right\}, \tag{A.12}$$

$$m^2_{\mathcal{A}^0_1} = \frac{1}{2}\left\{ m^2_\eta + m^2_{s2} + \sqrt{2}\,\mu v_s - \sqrt{\left(m^2_\eta - m^2_{s2} - \sqrt{2}\,\mu v_s\right)^2 + \lambda^2_{s\Phi 1\eta}\, v^2 v_s^2} \right\}, \tag{A.13}$$

$$m^2_{\mathcal{A}^0_2} = \frac{1}{2}\left\{ m^2_\eta + m^2_{s2} + \sqrt{2}\,\mu v_s + \sqrt{\left(m^2_\eta - m^2_{s2} - \sqrt{2}\,\mu v_s\right)^2 + \lambda^2_{s\Phi 1\eta}\, v^2 v_s^2} \right\}, \tag{A.14}$$

$$m^2_{\mathcal{H}^\pm} = m^2_\eta - \frac{1}{2}\lambda'_{\Phi 1\eta} v^2. \tag{A.15}$$

Next, the mass matrix for (ϕ^0_r, s^0_{1r}) is given by

$$M^2_H = \begin{pmatrix} 2\lambda_{\Phi 1} v^2 & \lambda_{s1\Phi 1}\, v\, v_s \\ \lambda_{s1\Phi 1}\, v\, v_s & 2\lambda_{s1} v_s^2 \end{pmatrix}. \tag{A.16}$$

Notice that $\phi^0_{\nu r}$ does not mix with them when we ignore v_ν. Mass eigenstates (h^0, H^0, and H^0_ν) of Z_2-even CP-even scalar bosons are given by

$$\begin{pmatrix} h^0 \\ H^0 \end{pmatrix} = \begin{pmatrix} \cos\theta_0 & -\sin\theta_0 \\ \sin\theta_0 & \cos\theta_0 \end{pmatrix} \begin{pmatrix} \phi^0_r \\ s^0_{1r} \end{pmatrix}, \quad \tan(2\theta_0) = \frac{\lambda_{s1\Phi1}\, v\, v_s}{\lambda_{s1} v_s^2 - \lambda_{\Phi1} v^2}, \tag{A.17}$$

$$H^0_\nu = \phi^0_{\nu r}. \tag{A.18}$$

The Nambu-Goldstone boson z^0_2 for the U(1)$_X$ breaking, a Z_2-even CP-odd scalar boson A^0_ν, and the Z_2-even charged scalar boson $H^\pm_\nu$ are defined as follows:

$$z^0_2 = s^0_{1i}, \quad A^0_\nu = \phi^0_{\nu i}, \quad H^\pm_\nu = \phi^\pm_\nu. \tag{A.19}$$

Masses of these Z_2-even scalar bosons are calculated as

$$m^2_{h^0} = \lambda_{s1} v_s^2 + \lambda_{\Phi1} v^2 - \sqrt{\left\{\lambda_{s1} v_s^2 - \lambda_{\Phi1} v^2\right\}^2 + \lambda^2_{s1\Phi1}\, v^2\, v_s^2}, \tag{A.20}$$

$$m^2_{H^0} = \lambda_{s1} v_s^2 + \lambda_{\Phi1} v^2 + \sqrt{\left\{\lambda_{s1} v_s^2 - \lambda_{\Phi1} v^2\right\}^2 + \lambda^2_{s1\Phi1}\, v^2\, v_s^2}, \tag{A.21}$$

$$m^2_{z^0_2} = 0, \tag{A.22}$$

$$m^2_{H^0_\nu} = m^2_{A^0_\nu} = \mu^2_{\Phi2} + \frac{1}{2}\Big\{(\lambda_{\Phi12} + \lambda'_{\Phi12}) v^2 + \lambda_{s1\Phi2} v_s^2\Big\}, \tag{A.23}$$

$$m^2_{H^\pm_\nu} = \mu^2_{\Phi2} + \frac{1}{2}\left\{\lambda_{\Phi12} v^2 + \lambda_{s1\Phi2} v_s^2\right\}. \tag{A.24}$$

Appendix B

Neutrino mass and dark matter from gauged $U(1)_{B-L}$ breaking

B.1 Loop Integration

A loop function $(I_1)_{ija}$ in eq. (7.7) can be expressed as

$$\begin{aligned}(I_1)_{ija} &\equiv -\frac{(8\pi^2 \sin 2\theta_0')^2 m_{\psi_i} m_{\psi_j}}{(m_R)_a^2}\left[\int \frac{d^4p}{(2\pi)^4}\frac{1}{p^2-m_{\psi_i}^2}\left\{\frac{1}{p^2-m_{\mathcal{H}_1^0}^2}-\frac{1}{p^2-m_{\mathcal{H}_2^0}^2}\right\}\right] \\ &\qquad \times\left[\int \frac{d^4q}{(2\pi)^4}\frac{1}{q^2-m_{\psi_j}^2}\left\{\frac{1}{q^2-m_{\mathcal{H}_1^0}^2}-\frac{1}{q^2-m_{\mathcal{H}_2^0}^2}\right\}\right] \\ &= \frac{m_{\psi_i} m_{\psi_j}(m_{\mathcal{H}_1^0}^2-m_{\mathcal{H}_2^0}^2)^2 \sin^2 2\theta_0'}{4(m_R)_a^2}\Big\{C_0(0,0,m_{\psi_i},m_{\mathcal{H}_1^0}^2,m_{\mathcal{H}_2^0}^2) \\ &\qquad \times C_0(0,0,m_{\psi_j},m_{\mathcal{H}_1^0}^2,m_{\mathcal{H}_2^0}^2)\Big\}, \end{aligned} \tag{B.1}$$

where the C_0 function [137] is given by

$$\begin{aligned}&C_0(0,0,m_0^2,m_1^2,m_2^2) \\ &\quad \equiv \frac{1}{(m_0^2-m_1^2)(m_1^2-m_2^2)(m_2^2-m_0^2)}\Big\{m_0^2 m_1^2 \ln\frac{m_0^2}{m_1^2}+m_1^2 m_2^2 \ln\frac{m_1^2}{m_2^2}+m_2^2 m_0^2 \ln\frac{m_2^2}{m_0^2}\Big\}. \end{aligned} \tag{B.2}$$

On the other hand, another loop function $(I_2)_{ija}$ in eq. (7.7) is given by

$$\begin{aligned}(I_2)_{ija} &\equiv (8\pi^2 \sin 2\theta_0')^2 m_{\psi_i} m_{\psi_j} \\ &\qquad \times \iint \frac{d^4p}{(2\pi)^4}\frac{d^4q}{(2\pi)^4}\left\{\frac{1}{p^2-m_{\mathcal{H}_1^0}^2}-\frac{1}{p^2-m_{\mathcal{H}_2^0}^2}\right\}\frac{1}{p^2-m_{\psi_i}^2} \\ &\qquad \times \frac{1}{(p+q)^2-(m_R)_a^2}\left\{\frac{1}{q^2-m_{\mathcal{H}_1^0}^2}-\frac{1}{q^2-m_{\mathcal{H}_2^0}^2}\right\}\frac{1}{q^2-m_{\psi_j}^2} \\ &= (8\pi^2 \sin 2\theta_0')^2 m_{\psi_i} m_{\psi_j} \\ &\qquad \times\Big[I(m_{\mathcal{H}_1^0},m_{\psi_i}|m_{\mathcal{H}_1^0},m_{\psi_j}|(m_R)_a)-I(m_{\mathcal{H}_1^0},m_{\psi_i}|m_{\mathcal{H}_2^0},m_{\psi_j}|(m_R)_a) \\ &\qquad\quad -I(m_{\mathcal{H}_2^0},m_{\psi_i}|m_{\mathcal{H}_1^0},m_{\psi_j}|(m_R)_a)+I(m_{\mathcal{H}_2^0},m_{\psi_i}|m_{\mathcal{H}_2^0},m_{\psi_j}|(m_R)_a)\Big], \end{aligned} \tag{B.3}$$

where

$$I(m_{11},m_{12},\cdots,m_{1n_1}|m_{21},m_{22},\cdots,m_{2n_2}|m_{31},m_{32},\cdots,m_{3n_3}) \equiv \int\frac{d^4p_E}{(2\pi)^4}\int\frac{d^4q_E}{(2\pi)^4}\prod_{i=1}^{n_1}\prod_{j=1}^{n_2}\prod_{k=1}^{n_3}\frac{1}{p_E^2+m_{1i}^2}\,\frac{1}{q_E^2+m_{2j}^2}\,\frac{1}{(p_E+q_E)^2+m_{3k}^2}. \quad (B.4)$$

We can use the following results [**?**]:

$$I(m_{11},m_{12}|m_{21},m_{22}|m_3) = \frac{I(m_{12}|m_{22}|m_3)-I(m_{11}|m_{22}|m_3)-I(m_{12}|m_{21}|m_3)+I(m_{11}|m_{21}|m_3)}{(16\pi^2)^2(m_{11}^2-m_{12}^2)(m_{21}^2-m_{22}^2)}, \quad (B.5)$$

$$I(m_1|m_2|m_3) = -m_1^2\,f\!\left(\frac{m_2^2}{m_1^2},\frac{m_3^2}{m_1^2}\right)-m_2^2\,f\!\left(\frac{m_1^2}{m_2^2},\frac{m_3^2}{m_2^2}\right)-m_3^2\,f\!\left(\frac{m_1^2}{m_3^2},\frac{m_2^2}{m_3^2}\right), \quad (B.6)$$

where

$$\begin{aligned} f(x,y) \equiv\ & -\frac{1}{2}(\ln x)(\ln y)-\frac{1}{2}\left(\frac{x+y-1}{D}\right) \\ & \times\Big\{\mathrm{Li}_2\!\left(\frac{-x_-}{y_+}\right)+\mathrm{Li}_2\!\left(\frac{-y_-}{x_+}\right)-\mathrm{Li}_2\!\left(\frac{-x_+}{y_-}\right)-\mathrm{Li}_2\!\left(\frac{-y_+}{x_-}\right) \\ & +\mathrm{Li}_2\!\left(\frac{y-x}{x_-}\right)+\mathrm{Li}_2\!\left(\frac{x-y}{y_-}\right)-\mathrm{Li}_2\!\left(\frac{y-x}{x_+}\right)-\mathrm{Li}_2\!\left(\frac{x-y}{y_+}\right)\Big\}, \end{aligned} \quad (B.7)$$

and

$$D \equiv \sqrt{1-2(x+y)+(x-y)^2}, \quad (B.8)$$

$$x_\pm \equiv \frac{1}{2}\left(1-x+y\pm D\right), \qquad y_\pm \equiv \frac{1}{2}\left(1+x-y\pm D\right), \quad (B.9)$$

and the dilog function $\mathrm{Li}_2(x)$ is defined as

$$\mathrm{Li}_2(x) \equiv -\int_0^x dt\,\frac{\ln(1-t)}{t}. \quad (B.10)$$

B.2 Ansatz for benchmark point

In eq. (7.7), let us define the following symmetric matrix as

$$A_{ij} \equiv \sum_a h_{ia}(m_R)_a(h^T)_{aj}\Big\{(I_1)_{ija}+(I_2)_{ija}\Big\}. \quad (B.11)$$

We can diagonalize A_{ij} by an orthogonal matrix X as

$$XAX^T = \mathrm{diag}(a_1,a_2,a_3,a_4). \quad (B.12)$$

It is clear that a Yukawa matrix $f_{\ell i}$ of the following structure satisfies constraints from neutrino oscillation data:

$$f = 16\pi^2\, U_{\rm MNS} \begin{pmatrix} \sqrt{\frac{m_1}{|a_1|}} & 0 & 0 & 0 \\ 0 & \sqrt{\frac{m_2}{|a_2|}} & 0 & 0 \\ 0 & 0 & \sqrt{\frac{m_3}{|a_3|}} & 0 \end{pmatrix} X, \tag{B.13}$$

where Majorana phases are given by $\alpha_i = \arg(a_i)$. We used

$$X = \begin{pmatrix} 0.520 & -0.520 & -0.474 & 0.484 \\ -0.712 & -0.284 & 0.165 & 0.621 \\ -0.425 & -0.476 & -0.522 & -0.566 \\ 0.206 & -0.650 & 0.689 & -0.244 \end{pmatrix}, \tag{B.14}$$

where $0 < a_4 < a_1 < a_2 < a_3$. The ordering of eigenvalues a_i is preferred to suppress $y_{\ell i}$ (in order to satisfy a constraint from $\mu \to e\gamma$ search) for the normal mass ordering for neutrinos ($m_1 < m_2 < m_3$). With this ansatz, small neutrino masses are preferred to suppress BR($\mu \to e\gamma$).

Appendix C

$O(N)$ scalar singlet model

C.1 Vacuum stability

Due to the $SU(2)_L \times U(1)_Y$ and O(N) symmetries, one can parametrize the modulus space as

$$\langle \Phi \rangle = \frac{1}{\sqrt{2}} \begin{pmatrix} 0 \\ \phi \end{pmatrix}, \quad \langle S \rangle = \begin{pmatrix} 0 \\ \vdots \\ \phi_S \end{pmatrix}. \tag{C.1}$$

whithout loss of generality. Then we obtain

$$V_0[\phi, \phi_S] = -\frac{\mu^2}{2}\phi^2 + \frac{\mu_S^2}{2}\phi_S^2 + \frac{\lambda}{8}\phi^4 + \frac{\lambda_S}{4}\phi_S^4 + \frac{\lambda_{\Phi S}}{4}\phi^2\phi_S^2. \tag{C.2}$$

Necessary conditions to avoid a potential unbounded from below are

$$\lambda > 0, \quad \lambda_S > 0. \tag{C.3}$$

Then the scalar potential is written as

$$\begin{aligned} V_0[\phi, \phi_S] = &-\frac{\mu^2}{2}\phi^2 + \frac{\mu_S^2}{2}\phi_S^2 \\ &+ \left(\sqrt{\frac{\lambda}{8}}\phi^2 + \sqrt{\frac{8}{\lambda}}\frac{\lambda_{\Phi S}}{4}\phi_S^2 \right)^2 + \left(\frac{\lambda_S}{4} - \frac{\lambda_{\Phi S}^2}{2\lambda} \right) \phi_S^4. \end{aligned} \tag{C.4}$$

For vacuum stability, we must require

$$\sqrt{2\lambda\lambda_S} + \lambda_{\Phi S} > 0. \tag{C.5}$$

C.2 Perturbative unitarity

In the basis of

$$u = \frac{1}{\sqrt{2}}(\sqrt{2}w^+w^-, zz, hh, S_1S_1, S_2S_2, S_3S_3, \cdots), \tag{C.6}$$

the transition matrix of the s-wave amplitude in the high energy limit ($s \gg m_h, m_S$) is given by

$$t_0 = -\frac{1}{32\pi}\begin{pmatrix} 4\lambda & \sqrt{2}\lambda & \sqrt{2}\lambda & \sqrt{2}\lambda_{\Phi S} & \sqrt{2}\lambda_{\Phi S} & \sqrt{2}\lambda_{\Phi S} & \cdots \\ \sqrt{2}\lambda & 3\lambda & \lambda & \lambda_{\Phi S} & \lambda_{\Phi S} & \lambda_{\Phi S} & \cdots \\ \sqrt{2}\lambda & \lambda & 3\lambda & \lambda_{\Phi S} & \lambda_{\Phi S} & \lambda_{\Phi S} & \cdots \\ \sqrt{2}\lambda_{\Phi S} & \lambda_{\Phi S} & \lambda_{\Phi S} & 6\lambda_S & 2\lambda_S & 2\lambda_S & \cdots \\ \sqrt{2}\lambda_{\Phi S} & \lambda_{\Phi S} & \lambda_{\Phi S} & 2\lambda_S & 6\lambda_S & 2\lambda_S & \cdots \\ \sqrt{2}\lambda_{\Phi S} & \lambda_{\Phi S} & \lambda_{\Phi S} & 2\lambda_S & 2\lambda_S & 6\lambda_S & \cdots \\ \vdots & \vdots & \vdots & \vdots & \vdots & \vdots & \ddots \end{pmatrix}. \tag{C.7}$$

The eigenvalues of the above matrix are

$$a_i = -\frac{\lambda}{16\pi}, -\frac{\lambda_S}{8\pi}, -\frac{\lambda_{\Phi S}}{16\pi}, -\frac{1}{32\pi}\left[\{3\lambda + (N+2)\lambda_S\} \mp \sqrt{\{3\lambda - (N+2)\lambda_S\}^2 + 4N\lambda_{\Phi S}^2}\right]. \tag{C.8}$$

In order keep perturbativity, we require that the absolute value of the eigenvalues of the s-wave amplitudes are at most of the order of the unity:

$$|a_i| < a_{\max}. \tag{C.9}$$

We take $a_{\max} = 1/2$ in our analysis.

Bibliography

[1] G. Aad *et al.* [ATLAS Collaboration], Phys. Lett. B **716**, 1 (2012).

[2] S. Chatrchyan *et al.* [CMS Collaboration], Phys. Lett. B **716**, 30 (2012).

[3] G. Hinshaw *et al.* [WMAP Collaboration], Astrophys. J. Suppl. **208**, 19 (2013).

[4] P. A. R. Ade *et al.* [Planck Collaboration], arXiv:1502.02114 [astro-ph.CO].

[5] B. T. Cleveland *et al.*, Astrophys. J. **496**, 505 (1998); W. Hampel *et al.* [GALLEX Collaboration], Phys. Lett. B **447**, 127 (1999); J. N. Abdurashitov *et al.* [SAGE Collaboration], Phys. Rev. C **80**, 015807 (2009); K. Abe *et al.* [Super-Kamiokande Collaboration], Phys. Rev. D **83**, 052010 (2011); G. Bellini *et al.* [Borexino Collaboration], Phys. Rev. D **89**, no. 11, 112007 (2014).

[6] B. Aharmim *et al.* [SNO Collaboration], Phys. Rev. C **88**, no. 2, 025501 (2013).

[7] R. Wendell *et al.* [Super-Kamiokande Collaboration], Phys. Rev. D **81**, 092004 (2010).

[8] M. H. Ahn *et al.* [K2K Collaboration], Phys. Rev. D **74**, 072003 (2006); P. Adamson *et al.* [MINOS Collaboration], Phys. Rev. Lett. **112**, 191801 (2014).

[9] K. Abe *et al.* [T2K Collaboration], Phys. Rev. Lett. **112**, 181801 (2014).

[10] P. Adamson *et al.* [MINOS Collaboration], Phys. Rev. Lett. **107**, 181802 (2011); K. Abe *et al.* [T2K Collaboration], Phys. Rev. Lett. **112**, 061802 (2014).

[11] M. Apollonio *et al.* [CHOOZ Collaboration], Eur. Phys. J. C **27**, 331 (2003); J. K. Ahn *et al.* [RENO Collaboration], Phys. Rev. Lett. **108**, 191802 (2012); Y. Abe *et al.* [Double Chooz Collaboration], arXiv:1401.5981 [hep-ex].

[12] F. P. An *et al.* [Daya Bay Collaboration], Phys. Rev. Lett. **112**, 061801 (2014).

[13] A. Gando *et al.* [KamLAND Collaboration], Phys. Rev. D **83**, 052002 (2011).

[14] A. H. Guth, Phys. Rev. D **23**, 347 (1981); K. Sato, Mon. Not. Roy. Astron. Soc. **195**, 467 (1981).

[15] A. D. Sakharov, Pisma Zh. Eksp. Teor. Fiz. **5**, 32 (1967).

[16] R. H. Cyburt, B. D. Fields and K. A. Olive, JCAP **0811**, 012 (2008).

[17] A. D. Linde, Phys. Lett. B **108**, 389 (1982); A. Albrecht and P. J. Steinhardt, Phys. Rev. Lett. **48**, 1220 (1982).

[18] F. L. Bezrukov and M. Shaposhnikov, Phys. Lett. B **659**, 703 (2008).

[19] V. A. Kuzmin, V. A. Rubakov and M. E. Shaposhnikov, Phys. Lett. B **155**, 36 (1985).

[20] S. Kanemura, Y. Okada and E. Senaha, Phys. Lett. B **606**, 361 (2005).

[21] D. M. Asner *et al.*, arXiv:1310.0763 [hep-ph].

[22] T. Yanagida, in Proceedings of the *"Workshop on the Unified Theory and the Baryon Number in the Universe"*, Tsukuba, Japan, Feb. 13-14, 1979, edited by O. Sawada and A. Sugamoto, KEK report KEK-79-18, p. 95; Prog. Theor. Phys. **64**, 1103 (1980); M. Gell-Mann, P. Ramond and R. Slansky, in *"Supergravity" eds.* D. Z. Freedom and P. van Nieuwenhuizen, (North-Holland, Amsterdam, 1979); R. N. Mohapatra and G. Senjanovic, Phys. Rev. Lett. **44**, 912 (1980).

[23] T. P. Cheng and L. F. Li, Phys. Rev. D **22**, 2860 (1980); J. Schechter and J. W. F. Valle, Phys. Rev. D **22**, 2227 (1980); G. Lazarides, Q. Shafi and C. Wetterich, Nucl. Phys. B **181**, 287 (1981); R. N. Mohapatra and G. Senjanovic, Phys. Rev. D **23**, 165 (1981); M. Magg and C. Wetterich, Phys. Lett. B **94**, 61 (1980).

[24] R. Foot, H. Lew, X. G. He and G. C. Joshi, Z. Phys. C **44**, 441 (1989).

[25] L. M. Krauss, S. Nasri and M. Trodden, Phys. Rev. D **67**, 085002 (2003); K. Cheung and O. Seto, Phys. Rev. D **69**, 113009 (2004); A. Ahriche and S. Nasri, JCAP **1307**, 035 (2013).

[26] E. Ma, Phys. Rev. D **73**, 077301 (2006); Phys. Lett. B **662**, 49 (2008); J. Kubo, E. Ma and D. Suematsu, Phys. Lett. B **642**, 18 (2006); T. Hambye, K. Kannike, E. Ma and M. Raidal, Phys. Rev. D **75**, 095003 (2007); E. Ma and D. Suematsu, Mod. Phys. Lett. A **24**, 583 (2009).

[27] M. Aoki, S. Kanemura and O. Seto, Phys. Rev. Lett. **102**, 051805 (2009); Phys. Rev. D **80** 033007 (2009); M. Aoki, S. Kanemura and K. Yagyu, Phys. Rev. D **83**, 075016 (2011); Phys. Lett. B **702**, 355 (2011).

[28] A. De Simone, M. P. Hertzberg and F. Wilczek, Phys. Lett. B **678**, 1 (2009); F. Bezrukov and M. Shaposhnikov, JHEP **0907**, 089 (2009); J. Elias-Miro, J. R. Espinosa, G. F. Giudice, G. Isidori, A. Riotto and A. Strumia, Phys. Lett. B **709**, 222 (2012); G. Degrassi, S. Di Vita, J. Elias-Miro, J. R. Espinosa, G. F. Giudice, G. Isidori and A. Strumia, JHEP **1208**, 098 (2012).

[29] N. G. Deshpande and E. Ma, Phys. Rev. D **18**, 2574 (1978).

[30] S. Nie and M. Sher, Phys. Lett. B **449**, 89 (1999); S. Kanemura, T. Kasai and Y. Okada, Phys. Lett. B **471**, 182 (1999).

[31] C. P. Burgess, H. M. Lee and M. Trott, JHEP **0909**, 103 (2009); JHEP **1007**, 007 (2010); J. L. F. Barbon and J. R. Espinosa, Phys. Rev. D **79**, 081302 (2009); M. P. Hertzberg, JHEP **1011**, 023 (2010).

[32] G. F. Giudice and H. M. Lee, Phys. Lett. B **694**, 294 (2011).

[33] M. Kamionkowski, A. Kosowsky and M. S. Turner, Phys. Rev. D **49**, 2837 (1994).

[34] G. M. Harry, Class. Quant. Grav. **27**, 084006 (2010).

[35] B. P. Abbott *et al.* [LIGO Scientific and Virgo Collaborations], Phys. Rev. Lett. **116**, no. 6, 061102 (2016).

[36] K. Somiya, Class. Quant. Grav. **29**, 124007 (2012).

[37] T. Accadia *et al.*, Proceedings of *12th Marcel Grossmann Meeting on General Relativity*, pp. 1738–1742 (2009).

[38] C. Grojean and G. Servant, Phys. Rev. D **75**, 043507 (2007).

[39] S. J. Huber and T. Konstandin, JCAP **0809**, 022 (2008).

[40] Y. Kikuta, K. Kohri and E. So, arXiv:1405.4166 [hep-ph].

[41] J. R. Espinosa, T. Konstandin, J. M. No and G. Servant, JCAP **1006**, 028 (2010).

[42] J. M. No, Phys. Rev. D **84**, 124025 (2011).

[43] M. Hindmarsh, S. J. Huber, K. Rummukainen and D. J. Weir, Phys. Rev. Lett. **112**, 041301 (2014).

[44] M. Hindmarsh, S. J. Huber, K. Rummukainen and D. J. Weir, Phys. Rev. D **92**, no. 12, 123009 (2015).

[45] C. Caprini *et al.*, arXiv:1512.06239 [astro-ph.CO].

[46] C. Delaunay, C. Grojean and J. D. Wells, JHEP **0804**, 029 (2008).

[47] R. Apreda, *et al.*, Nucl. Phys. B **631**, 342 (2002).

[48] J. R. Espinosa and M. Quiros, Phys. Rev. D **76**, 076004 (2007).

[49] J. R. Espinosa, T. Konstandin, J. M. No and M. Quiros, Phys. Rev. D **78**, 123528 (2008).

[50] A. Ashoorioon and T. Konstandin, JHEP **0907**, 086 (2009).

[51] L. Sagunski, DESY-THESIS-2013-011.

[52] K. Inoue, A. Kakuto and Y. Nakano, Prog. Theor. Phys. **63**, 234 (1980); H. Komatsu, Prog. Theor. Phys. **67**, 1177 (1982); A. Goudelis, B. Herrmann, O. Stål, JHEP **09**, 106 (2013).

[53] F. Capela, M. Pshirkov and P. Tinyakov, Phys. Rev. D **87**, no. 2, 023507 (2013).

[54] K. Griest, A. M. Cieplak and M. J. Lehner, Astrophys. J. **786**, no. 2, 158 (2014).

[55] E.W.Kolb and M.S.Turner, "The Early Universe," Westview Press (1994).

[56] K. Griest and D. Seckel, Phys. Rev. D **43**, 3191 (1991).

[57] P. Gondolo and G. Gelmini, Nucl. Phys. B **360**, 145 (1991).

[58] J. Edsjo and P. Gondolo, Phys. Rev. D **56**, 1879 (1997).

[59] P. Minkowski, Phys. Lett. B **67**, 421 (1977); T. Yanagida, Conf. Proc. C **7902131**, 95 (1979); Prog. Theor. Phys. **64**, 1103 (1980); M. Gell-Mann, P. Ramond and R. Slansky, Conf. Proc. C **790927**, 315 (1979); R. N. Mohapatra and G. Senjanovic, Phys. Rev. Lett. **44**, 912 (1980).

[60] E. Ma, Phys. Rev. Lett. **86**, 2502 (2001);

[61] E. Ma and M. Raidal, Phys. Rev. Lett. **87**, 011802 (2001) [Erratum-ibid. **87**, 159901 (2001)]; N. Haba and M. Hirotsu, Eur. Phys. J. C **69**, 481 (2010); N. Haba, O. Seto and O. Seto, Prog. Theor. Phys. **125**, 1155 (2011); N. Haba and K. Tsumura, JHEP **1106**, 068 (2011).

[62] N. Haba and T. Horita, Phys. Lett. B **705**, 98 (2011).

[63] F. Wang, W. Wang and J. M. Yang, Europhys. Lett. **76**, 388 (2006); S. Gabriel and S. Nandi, Phys. Lett. B **655**, 141 (2007).

[64] S. M. Davidson and H. E. Logan, Phys. Rev. D **80**, 095008 (2009).

[65] Z. Maki, M. Nakagawa and S. Sakata, Prog. Theor. Phys. **28**, 870 (1962).

[66] T. Morozumi, H. Takata and K. Tamai, Phys. Rev. D **85**, 055002 (2012).

[67] S. Kanemura and T. Ota, Phys. Lett. B **694**, 233 (2011).

[68] J. Beringer *et al.* [Particle Data Group Collaboration], Phys. Rev. D **86**, 010001 (2012).

[69] M. Fukugita and T. Yanagida, Phys. Lett. B **174**, 45 (1986).

[70] S. Davidson, E. Nardi and Y. Nir, Phys. Rept. **466**, 105 (2008).

[71] K. Funakubo, Prog. Theor. Phys. **96**, 475 (1996).

[72] P. Arnold and L. D. McLerran, Phys. Rev. D **36**, 581 (1987).

[73] K. Funakubo and E. Senaha, Phys. Rev. D **79**, 115024 (2009).

[74] K. Fuyuto and E. Senaha, Phys. Rev. D **90**, no. 1, 015015 (2014).

[75] S. Kanemura, S. Kiyoura, Y. Okada, E. Senaha and C. P. Yuan, Phys. Lett. B **558**, 157 (2003).

[76] S. Kanemura, Y. Okada, E. Senaha and C.-P. Yuan, Phys. Rev. D **70**, 115002 (2004).

[77] S. Kanemura, Y. Okada and E. Senaha, eConf C **050318**, 0704 (2005).

[78] M. E. Carrington, Phys. Rev. D **45**, 2933 (1992).

[79] S. M. Davidson and H. E. Logan, Phys. Rev. D **82**, 115031 (2010).

[80] M. Gustafsson, J. M. No and M. A. Rivera, Phys. Rev. Lett. **110**, 211802 (2013).

[81] M. Aoki, S. Kanemura and K. Yagyu, Phys. Lett. B **702**, 355 (2011).

[82] S. Kanemura and T. Ota, Phys. Lett. B **694**, 233 (2010); F. Bonnet, M. Hirsch, T. Ota and W. Winter, JHEP **1207**, 153 (2012).

[83] P. H. Gu and U. Sarkar, Phys. Rev. D **77**, 105031 (2008).

[84] S. Kanemura, T. Nabeshima and H. Sugiyama, Phys. Rev. D **85**, 033004 (2012); Phys. Rev. D **87**, 015009 (2013).

[85] Y. Kajiyama, H. Okada and K. Yagyu, Nucl. Phys. B **874**, 198 (2013).

[86] S. Kanemura and H. Sugiyama, Phys. Rev. D **86**, 073006 (2012).

[87] D. Chang and R. N. Mohapatra, Phys. Rev. Lett. **58**, 1600 (1987).

[88] S. Kanemura, T. Matsui and H. Sugiyama, Phys. Lett. B **727**, 151 (2013).

[89] Y. Chikashige, R. N. Mohapatra and R. D. Peccei, Phys. Lett. B **98**, 265 (1981).

[90] J. Adam *et al.* [MEG Collaboration], Phys. Rev. Lett. **110**, 201801 (2013).

[91] V. Silveira and A. Zee, Phys. Lett. B **161**, 136 (1985).

[92] C. P. Burgess, M. Pospelov and T. ter Veldhuis, Nucl. Phys. B **619**, 709 (2001); K. Cheung, Y. -L. S. Tsai, P. -Y. Tseng, T. -C. Yuan and A. Zee, JCAP **1210**, 042 (2012); J. M. Cline, K. Kainulainen, P. Scott and C. Weniger, arXiv:1306.4710 [hep-ph].

[93] R. Barbieri, L. J. Hall and V. S. Rychkov, Phys. Rev. D **74**, 015007 (2006).

[94] L. Lopez Honorez, E. Nezri, J. F. Oliver and M. H. G. Tytgat, JCAP **0702**, 028 (2007); A. Pierce and J. Thaler, JHEP **0708**, 026 (2007); E. Lundstrom, M. Gustafsson and J. Edsjo, Phys. Rev. D **79**, 035013 (2009); E. M. Dolle and S. Su, Phys. Rev. D **80**, 055012 (2009); M. Gustafsson, S. Rydbeck, L. Lopez-Honorez and E. Lundstrom, Phys. Rev. D **86**, 075019 (2012); M. Krawczyk, D. Sokolowska, P. Swaczyna and B. Swiezewska, JHEP **1309**, 055 (2013).

[95] M. Gustafsson, PoS CHARGED **2010**, 030 (2010).

[96] R. Bonciani, S. Catani, M. L. Mangano and P. Nason, Nucl. Phys. B **529**, 424 (1998) [Erratum-ibid. B **803**, 234 (2008)].

[97] J. M. Campbell and R. K. Ellis, Phys. Rev. D **60**, 113006 (1999).

[98] N. Kidonakis, Phys. Rev. D **81**, 054028 (2010).

[99] T. Yanagida, Conf. Proc. C **7902131**, 95 (1979); Prog. Theor. Phys. **64**, 1103 (1980).

[100] S. Kanemura, T. Nabeshima and H. Sugiyama, Phys. Rev. D **85**, 033004 (2012); Phys. Rev. D **87**, 015009 (2013).

[101] S. Kanemura, T. Matsui and H. Sugiyama, Phys. Rev. D **90**, 013001 (2014).

[102] J. Hisano, T. Moroi, K. Tobe and M. Yamaguchi, Phys. Rev. D **53**, 2442 (1996).

[103] J. Adam *et al.* [MEG Collaboration], Phys. Rev. Lett. **110**, no. 20, 201801 (2013).

[104] N. Okada and O. Seto, Phys. Rev. D **82**, 023507 (2010); S. Kanemura, O. Seto and T. Shimomura, Phys. Rev. D **84**, 016004 (2011); T. Basak and T. Mondal, Phys. Rev. D **89**, 063527 (2014).

[105] D. S. Akerib *et al.* [LUX Collaboration], Nucl. Instrum. Meth. A **704**, 111 (2013).

[106] S. Kanemura, S. Matsumoto, T. Nabeshima and N. Okada, Phys. Rev. D **82**, 055026 (2010).

[107] J. M. Cline, K. Kainulainen, P. Scott and C. Weniger, Phys. Rev. D **88**, 055025 (2013).

[108] M. S. Carena, A. Daleo, B. A. Dobrescu and T. M. P. Tait, Phys. Rev. D **70**, 093009 (2004); G. Cacciapaglia, C. Csaki, G. Marandella and A. Strumia, Phys. Rev. D **74**, 033011 (2006).

[109] L. Basso, arXiv:1106.4462 [hep-ph].

[110] ATLAS Collaboration, ATLAS-CONF-2013-017; CMS Collaboration, CMS-PAS-EXO-12-061.

[111] S. Kanemura, T. Matsui and T. Nabeshima, Phys. Lett. B **723**, 126 (2013).

[112] S. K. Kang and J. Park, JHEP **1504**, 009 (2015).

[113] L. Lopez Honorez, E. Nezri, J. F. Oliver and M. H. G. Tytgat, JCAP **0702**, 028 (2007).

[114] S. Kanemura, S. Matsumoto, T. Nabeshima and N. Okada, Phys. Rev. D **82** 055026 (2010).

[115] H. Ohki *et al.*, Phys. Rev. D **78**, 054502 (2008); PoS **LAT2009**, 124 (2009).

[116] R. J. Crewther, Phys. Rev. Lett. **28**, 1421 (1972); M. S. Chanowitz and J. R. Ellis, Phys. Lett. B **40**, 397 (1972); Phys. Rev. D **7**, 2490 (1973); J. C. Collins, A. Duncan and S. D. Joglekar, Phys. Rev. D **16**, 438 (1977); M. A. Shifman, A. I. Vainshtein and V. I. Zakharov, Phys. Lett. B **78**, 443 (1978).

[117] E. Aprile *et al.* [XENON100 Collaboration], Phys. Rev. Lett. **109**, 181301 (2012).

[118] D. S. Akerib *et al.* [LUX Collaboration], arXiv:1310.8214 [astro-ph.CO].

[119] A. Djouadi, O. Lebedev, Y. Mambrini and J. Quevillon, Phys. Lett. B **709**, 65 (2012) .

[120] M. Gustafsson, S. Rydbeck, L. Lopez-Honorez and E. Lundstrom, Phys. Rev. D **86**, 075019 (2012) .

[121] J. R. Espinosa, C. Grojean, M. Muhlleitner and M. Trott, JHEP **1212**, 045 (2012) .

[122] G. Abbiendi *et al.* [OPAL Collaboration], Eur. Phys. J. C **35**, 1 (2004) ; Eur. Phys. J. C **32**, 453 (2004) ; M. Acciarri *et al.* [L3 Collaboration], Phys. Lett. B **472**, 420 (2000) .

[123] A. Pierce and J. Thaler, JHEP **0708**, 026 (2007) .

[124] E. Lundstrom, M. Gustafsson and J. Edsjo, Phys. Rev. D **79**. 035013 (2009) .

[125] E. Dolle, X. Miao, S. Su and B. Thomas, Phys. Rev. D **81**, 035003 (2010) .

[126] A. Pukhov, hep-ph/0412191.

[127] M. Aoki and S. Kanemura, Phys. Lett. B **689**, 28 (2010) . M. Aoki, S. Kanemura and H. Yokoya, Phys. Lett. B **725**, 302 (2013) .

[128] N. Seto, S. Kawamura and T. Nakamura, Phys. Rev. Lett. **87**, 221103 (2001).

[129] V. Corbin and N. J. Cornish, Class. Quant. Grav. **23**, 2435 (2006).

[130] M. Kakizaki, S. Kanemura and T. Matsui, Phys. Rev. D **92**, no. 11, 115007 (2015).

[131] A. Nicolis, Class. Quant. Grav. **21**, L27 (2004).

[132] P. A. Seoane *et al.*, arXiv:1305.5720 [astro-ph.CO].

[133] H. Kudoh, *et al.*, Phys. Rev. D **73**, 064006 (2006).

[134] R. Schneider, S. Marassi and V. Ferrari, Class. Quant. Grav. **27**, 194007 (2010).

[135] K. A. Olive *et al.*, Chin. Phys. C **38**, 090001 (2014).

[136] P. A. R. Ade *et al.*, arXiv:1502.01589 [astro-ph.CO].

[137] G. Passarino and M. J. G. Veltman, Nucl. Phys. B **160**, 151 (1979).